2026-3 | International Shoulder Group (ISG) Congress 2026
2-3 June 2026, Lyon, France

Multidisciplinary Biomechanics Journal

Statistical Parameter Mapping Analysis of Trunk, Shoulder Girdle, and Shoulder Kinematic Alterations Associated with Body Armor

Bryan L. Riemann[a, b]*, Sandra John[a, b], Emma N. Williams[a, b], Joseph R. Kardouni[a, b]

a Biodynamics and Human Performance Center, Georgia Southern University-Armstrong, Savannah, GA, USA
b Tactical and Occupational Performance Institute, Georgia Southern University-Armstrong, Savannah, GA, USA
* **Corresponding author:** briemann@georgiasouthern.edu

Received date: 16/01/2026
Accepted date: 16/03/2026
Publication date: 02/06/2026

Keywords: scapula, clavicular, glenohumeral, tactical athlete, military

1. Introduction

Body armor (BA) is an essential part of the protective equipment worn by warfighters and law enforcement personnel to mitigate the risk of penetrating trauma to the torso during tactical engagements. During upper extremity movements, wearing BA may prompt deviation from normal upper extremity and trunk kinematics due to the added mass over the shoulder girdle and trunk. In contrast to comparing discrete points during a task, statistical parameter mapping (SPM) provides for examination of differences across an entire movement trajectory (Pataky et al., 2015). Thus, the purpose of this investigation was to examine trunk, shoulder girdle, and shoulder kinematic alterations associated with BA during upper extremity elevation (UEE) and a functional lifting task using SPM.

2. Methods

2.1 Participants

Healthy physically active(Ozemek et al., 2026), military aged participants (range 18-37 yrs) performed two tasks while wearing BA and without BA. Participants had no history of shoulder injury or surgery and tested negative for subacromial impingement during screening.

2.2 Procedures

The BA used was a military-grade Improved Outer Tactical Vest with soft armor panels and two hard ceramic ballistic plates (front, back). Four sizes ranging from 7kg (extra-small) to 9kg (large) ensured proper and comfortable fit between participants. For the first task (n=40, 21 males, 72.1±21.2kg, 1.67±0.28m), participants performed bilateral UEE in the scapular plane while holding a dumbbell (1.36kg for participants with mass <68kg; 2.27kg for participants with mass ≥68kg)(Kardouni et al., 2015). The second task (n=35, 20 males, 73.7±21.4kg, 1.67±0.30m) involved an ammunition can (12.5kg) lift (ACL) from the floor (Lenton et al., 2016) and placing it on a shelf set to clavicular height. Five repetitions of each task were completed. Trunk, scapular, and humeral, kinematics were measured using an electromagnetic (EM) tracking system (100 Hz) with receivers secured on the skin over the 7th cervical vertebra, humerus, and acromion process, duplicating the process that was validated with bone pins(Karduna et al., 2001). Digitization of bony landmarks and computation of trunk, scapular and humeral kinematics followed the International Society of Biomechanics recommendations(Wu et al., 2005).

2.3 Data reduction and statistical analysis

Following time-normalization (0-100% of the task) and ensemble averaging across the five repetitions, trunk extension and dominant limb scapular upward rotation, scapular posterior tilt, scapular internal rotation, clavicular elevation, clavicular protraction, and humeral elevation were compared with paired-sample SPM{t} tests (2-tailed, α=.05) using SPM1d version M.0.4.50 (Pataky et al., 2015).

To cite this article: Bryan L. Riemann, Sandra John, Emma N. Williams, Joseph R. Kardouni, Statistical Parameter Mapping Analysis of Trunk, Shoulder Girdle, and Shoulder Kinematic Alterations Associated with Body Armor, *Multidisciplinary Biomechanics Journal*, 2026, vol. 3, p. 13–15, DOI: 10.46298/mbj.17929.

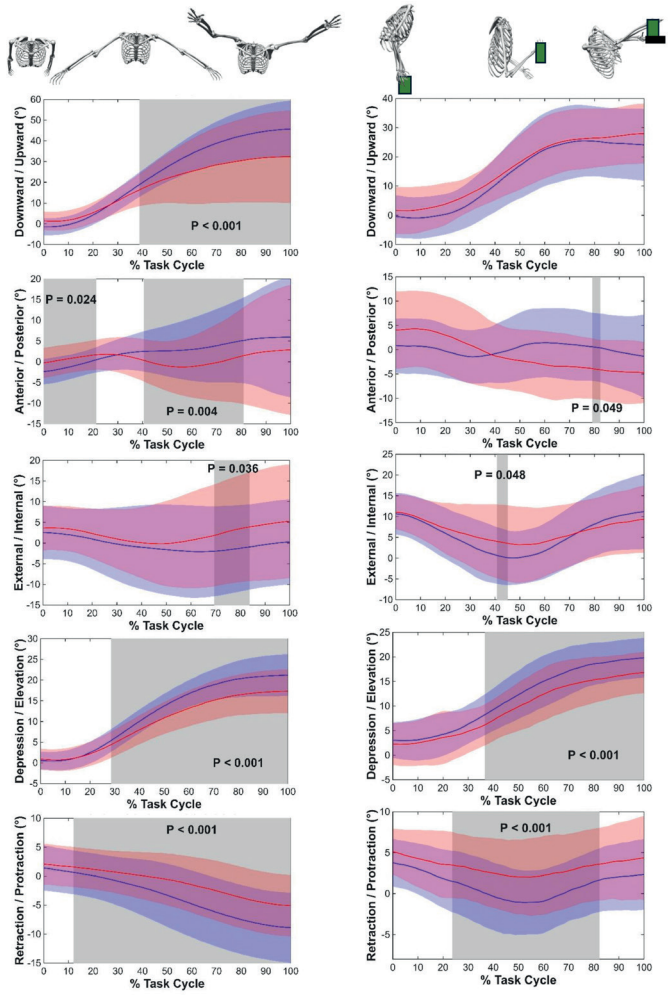

Figure 1. The results of statistical parameter mapping for scapular (upward rotation, posterior tilt and internal rotation) and clavicular (elevation and protraction) kinematics. Comparisons are shown between wearing body armor (red) and without body armor (blue) during upper extremity elevation (left panel) and ammunition can lifting (right panel). Gray shaded regions indicate a statistical difference between conditions (P<0.05); shaded bands around the mean lines represent ± one standard deviation.

3. Results and Discussion

The SPM analysis yielded several significant effects of BA during both tasks (Figure 1). During UEE, wearing BA resulted in a significant decrease in scapular upward rotation beginning mid-cycle through the end of the movement. Wearing BA elicited significantly greater scapular posterior tilt during the initial phase of the movement (0 to 18%), followed by a significant increase in anterior tilt mid-cycle (40 to 80%). In contrast, wearing BA did not significantly alter scapular upward rotation during the ACL task and elicited significantly greater anterior scapular tilt only during a brief interval (79 to 82%). Wearing BA resulted in very short durations (UEE: 69 to 84%, ACL:41 to 45%) of significantly greater scapular internal rotation during both tasks. These kinematic differences between tasks likely stem from the ACL task's heavier load and its movement pattern, which favored pure flexion over the broader humeral elevation seen in the UEE task. Wearing BA altered clavicular kinematics markedly in both the UEE and ACL tasks. After the initial third of the movement, clavicular elevation was significantly reduced for the remainder of both tasks while wearing BA. Furthermore, wearing BA induced significantly greater clavicular protraction throughout most of both tasks. The more pronounced impact of BA on clavicular kinematics, relative to the scapula, is likely due to the direct point of application of the armor over the clavicle. Wearing BA significantly increased HE during the onset of the UEE task (0–23%, P=0.002), followed by a significant reduction during the terminal stage of the motion (59–100%, P=0.003). In contrast to the UEE task, humeral elevation was statistically similar across the BA conditions during the ACL task. While BA application significantly increased trunk flexion during the mid-phase of the ACL task (38–52%, $P < 0.025$), it did not significantly affect trunk extension during the UEE task. The change in trunk flexion during the ACL task may serve as a compensatory strategy to stabilize the BA center of mass, minimizing trunk movement away from the base of support.

4. Conclusions

Wearing body armor resulted in significantly altered trunk, shoulder girdle and shoulder kinematics, though the magnitude and timing of the effects are task dependent. Across the two tasks, the most consistent finding was marked alteration of clavicular elevation and protraction. These findings suggest that evaluating protective gear requires a comprehensive evaluation of the entire shoulder complex. Future studies should evaluate experienced tactical operators to determine if these kinematic shifts increase injury risk and whether muscle strength serves as a protective factor against the effects of BA.

Acknowledgements

The authors thank Kasey Comey for her assistance with data collection.

Conflict of Interest Statement

None.

Contributor Roles

BLR: Conceptualization, Supervision, Methodology, Formal analysis, Software, Visualization, Writing original draft; SJ: Methodology, Data collection, Writing – review & editing, Project administration; ENW: Methodology, Data collection, Writing – review & editing, Project administration JRK: Conceptualization, Supervision, Methodology, Writing – review & editing, Project administration.

Funding

None.

Data, software, code availability

SPM1d version M.0.4.50 (https://www.spm1d.org).

References

Kardouni, J. R., Pidcoe, P. E., Shaffer, S. W., Finucane, S. D., Cheatham, S. A., Sousa, C. O., & Michener, L. A. (2015). Thoracic spine manipulation in individuals with subacromial impingement syndrome does not immediately alter thoracic spine kinematics, thoracic excursion, or scapular kinematics: A randomized controlled trial. *J Orthop Sports Phys Ther, 45*(7), 527–538. https://doi.org/10.2519/jospt.2015.5647

Karduna, A. R., McClure, P. W., Michener, L. A., & Sennett, B. (2001). Dynamic measurements of three-dimensional scapular kinematics: a validation study. *J Biomech Eng, 123*(2), 184–190. https://doi.org/10.1115/1.1351892

Lenton, G., Aisbett, B., Neesham-Smith, D., Carvajal, A., & Netto, K. (2016). The effects of military body armour on trunk and hip kinematics during performance of manual handling tasks. *Ergonomics, 59*(6), 806–812. https://doi.org/10.1080/00140139.2015.1092589

Ozemek, C., Bonikowske, A. R., Christle, J. W., & Gallo, P. M. (2026). *ACSM's guidelines for exercise testing and prescription* (Twelfth edition. ed.). Wolters Kluwer.

Pataky, T., Robinson, M., & Vanrenterghem, J. (2015). Corrigendum. *Journal of Biomechanics, 48*(1), 190–192. https://doi.org/10.1016/j.jbiomech.2014.09.025

Wu, G., van der Helm, F. C., Veeger, H. E., Makhsous, M., Van Roy, P., Anglin, C., Nagels, J., Karduna, A. R., McQuade, K., Wang, X., Werner, F. W., & Buchholz, B. (2005). ISB recommendation on definitions of joint coordinate systems of various joints for the reporting of human joint motion – Part II: shoulder, elbow, wrist and hand. *J Biomech, 38*(5), 981–992. https://doi.org/10.1016/j.jbiomech.2004.05.042

2026-3 | International Shoulder Group (ISG) Congress 2026
2-3 June 2026, Lyon, France

A Unified Human-Robot Simulation Enables Modulation of Supraspinatus Muscle Activation

Pierre Schegg[a*], Pierre Puchaud[b], François Bailly[a]

a CAMIN, Inria, Univ Montpellier, Montpellier, France
b AUCTUS, Inria, Bordeaux, France
* Corresponding author: pierre.schegg@inria.fr

Received date: 16/01/2026
Accepted date: 16/03/2026
Publication date: 02/06/2026

Keywords: supraspinatus, optimal control, human-robot interaction, rehabitilition

1. Introduction

Orthopedic rehabilitation can benefit from using robotic devices, however, current robot-assisted physiotherapy methods (e.g. exoskeletons) often only implement impedance control or gravity compensation and do not explicitly include biomechanical information in their control systems (Dalla Gasperina et al., 2021). This abstract presents an automated approach that adjusts the robot's controls to modulate the maximum level of muscle activity with a single parameter $\boldsymbol{R}$, applied to a rotator cuff tendon rehabilitation scenario. Using a unified framework co-simulating a musculoskeletal (MSK) model of the shoulder and elbow and a collaborative robotic arm, we solve an optimal control problem to define assistive robot torque trajectories that achieve a targeted level of muscle activations along a predefined trajectory.

2. Methods

We used an upper limb MSK model from (Bailly et al., 2021) with 3 shoulder (glenohumeral) and 1 elbow rotational degrees of freedom (DoF), incorporating 19 muscles and the Unified Robot Description Format of a 7-DoF Kuka iiwa robot to combine them in a unified format with biobuddy (Charbonneau et al., 2025) and enable their mutual simulation in Bioptim (Michaud et al., 2022), a Python numerical optimal control package for biomechanics. The combined model is displayed in Figure 1a.

In the simulation, both the robot and the human state and control variables are part of a single trajectory optimization problem. This provides a bidirectional sensitivity between the robot and human decision variables (positions, velocities, torques or muscles). As such, constraints and objectives set on the MSK model influence the robot's control law and state, and vice versa. The interaction between the human and the robot was modeled using holonomic constraints (Docquier et al., 2013), transmitting forces between the wrist and robot end-effector.

We prescribed an elliptical trajectory (70 cm × 35 cm) in a plane rotated 30° from the sagittal plane about the anteroposterior axis, which spanned a large part of the combined robot and MSK model workspace, and naturally resulted in maximal Supraspinatus muscle activation during 48% of the trajectory in a simulation without robotic assistance. The simulated movement lasted 1 second and was optimized using direct collocation with 40 intervals. We assume that a human is not able to isolate and control the activation of the Supraspinatus alone, as such we grouped its activation with its synergists involved in the humerus elevation in the sagittal plane: Pectoralis Major clavicular (PMc) and Deltoid Anterior (DA).

The objective function is comprised of two main terms: minimizing the robot joint torques (weight $w_\tau = 1$) and minimizing the humerus elevator muscles' activation (weight w_{he}, applied to Supraspinatus, PMc and DA).

To cite this article: Pierre Schegg, Pierre Puchaud, François Bailly, A Unified Human-Robot Simulation Enables Modulation of Supraspinatus Muscle Activation, *Multidisciplinary Biomechanics Journal*, 2026, vol. 3, p. 17–19, DOI: 10.46298/mbj.17938.

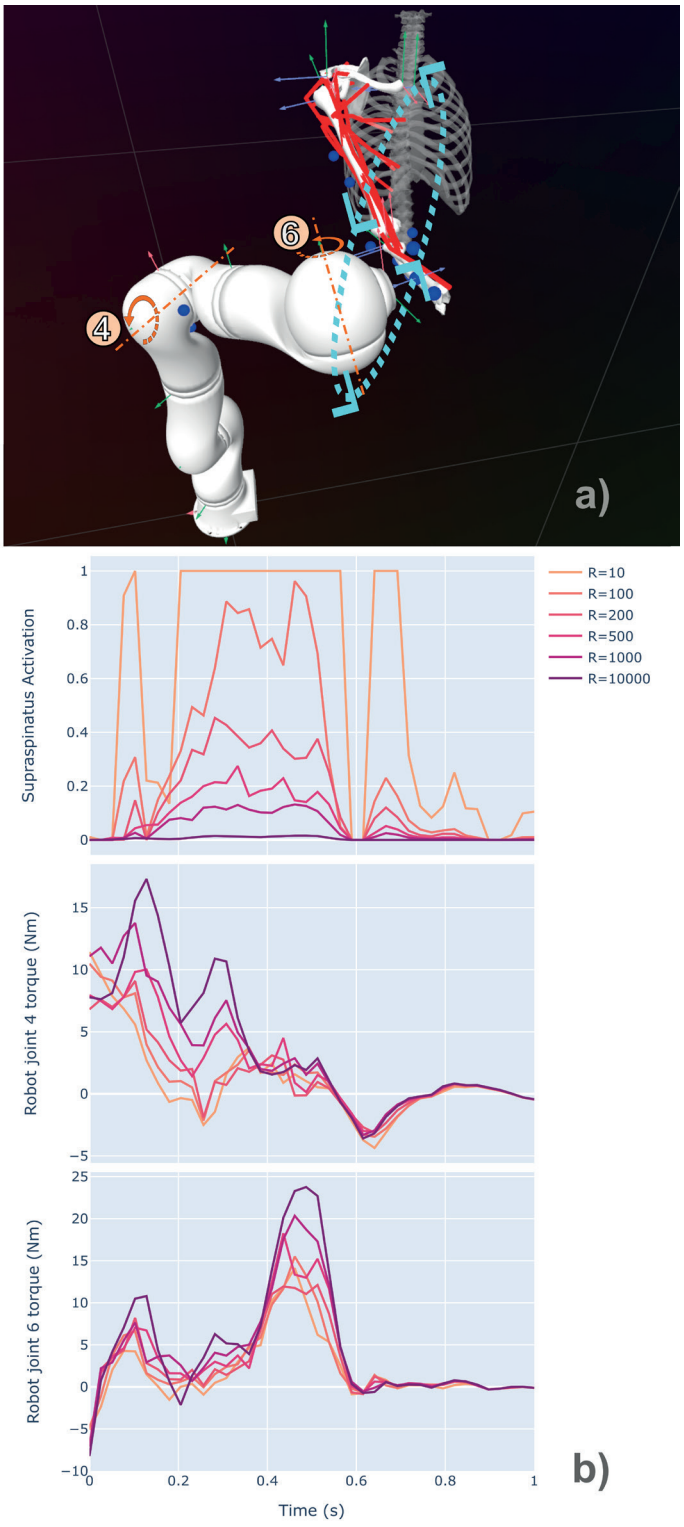

Figure 1. a) Combined MSK and robot model configuration at the tenth interval of the simulation. Prescribed trajectory is represented in blue. b) Supraspinatus activation and robot joint torques (4th and 6th axes) along the trajectory, comparison of six R parameter values.

Their relative importance is tuned by the parameter $\boldsymbol{R}$, defined as $w_{he} \triangleq \boldsymbol{R} \times w_{\tau}$, so that larger values of $\boldsymbol{R}$ correspond to greater assistance (more muscle activation reduction). The three remaining terms track the trajectory, minimize the robot joint velocities and minimize the 16 other muscle activations.

Six simulations are performed with R={10, 100, 200, 500, 1000, 10000}.

Table 1. Six R parameter values and corresponding Supraspinatus Maximum Activation.

Parameter R	Supraspinatus Maximum Activation
10	1.0
100	0.96
200	0.47
500	0.27
1000	0.13
10000	0.02

3. Results and discussion

Simulation convergence time was 17±2 minutes.

Preliminary results demonstrate that our formulation reliably adapts the robot control law to modulate activation of the three muscles, in particular Supraspinatus. Increasing R yields progressively lower activation and non-trivially redistributes the load across the robot joints depending on the trajectory phases (joint 4 handles the first Suprastinatus activation peak around 0.1s and joint 6 the second around 0.5s). Figure 1b illustrates how Supraspinatus activation and torques at robot joints 4 and 6 co-vary with R; analogous activation patterns were observed for PMc and DA. Robot joints 4 and 6 display the most visible changes along the trajectory when modifying R. The correspondance between the R parameter value and obtained maximum Supraspinatus activation is given in Table 1.

While the elliptical trajectory chosen to illustrate this abstract was designed to span the workspace and strongly activate target muscles, it does not reflect motions typically used in physical therapy. However, modifying the trajectory is straightforward and can be adapted for specific applications.

Additionally, this study is purely simulation-based. As such, we cannot confirm whether the predicted muscle

activations accurately reflect those observed in real-world scenarios when applying the robot control laws. Experiments including electromyography measurements are required and planned as future validation work.

4. Conclusions

We demonstrated that a single optimal control program can be used to integrate biomechanics constraints into the computation of a robot's control law in the context of human-robot interaction, exemplified here in rotator cuff tendon rehabilitation.

An extension of this work lies in movement assistance applications (e.g. muscle dystrophy or hemiplegia), where robotic devices could provide individualized support based on a personalized MSK model and optimal control strategies.

Acknowledgements

The authors thank Benjamin Michaud, Eve Charbonneau and Mickaël Begon for their assistance and guidance in using the Bioptim software.

Conflict of Interest Statement

None.

Contributor Roles

PS: Conceptualization, Methodology, Software, Validation, Visualization, Writing – original draft, Writing – review & editing. PP: Methodology, Software, Writing – review & editing. FB: Conceptualization, Funding acquisition, Methodology, Supervision, Validation, Writing – review & editing.

Funding

This research was funded by ANR B-IRD (Grant no: ANR-23-CE19-0005).

References

Bailly, F., Ceglia, A., Michaud, B., Rouleau, D. M., & Begon, M. (2021). Real-time and dynamically consistent estimation of muscle forces using a moving horizon emg-marker tracking algorithm—application to upper limb biomechanics. *Frontiers in bioengineering and biotechnology, 9*, 642742. https://doi.org/10.3389/fbioe.2021.642742

Charbonneau, E., Puchaud, P., Caderby, T., Begon, M., & Michaud, B. (2025, October). Bringing the musculoskeletal modeling community together with Biobuddy. In *50e congrès de la Société de Biomécanique*.

Dalla Gasperina, S., Roveda, L., Pedrocchi, A., Braghin, F., & Gandolla, M. (2021). Review on patient-cooperative control strategies for upper-limb rehabilitation exoskeletons. *Frontiers in Robotics and AI, 8*, 745018. https://doi.org/10.3389/frobt.2021.745018

Docquier, N., Poncelet, A., & Fisette, P. (2013). ROBOTRAN: a powerful symbolic gnerator of multibody models. *Mechanical Sciences, 4*(1), 199–219. https://doi.org/10.5194/ms-4-199-2013

Michaud, B., Bailly, F., Charbonneau, E., Ceglia, A., Sanchez, L., & Begon, M. (2022). Bioptim, a python framework for musculoskeletal optimal control in biomechanics. *IEEE Transactions on Systems, Man, and Cybernetics: Systems, 53*(1), 321–332. https://doi.org/10.1109/TSMC.2022.3183831

2026-3 | International Shoulder Group (ISG) Congress 2026
2-3 June 2026, Lyon, France

Multidisciplinary Biomechanics Journal

Patient-Specific Reconstruction of Shoulder Anatomy Driven by Radiographic Anatomical Parameters Using Statistical Shape Modelling

Lisa Mareschal[a*], Jeremy Genter[a], Eleonora Croci[b, c], Dominic Gascho[d], Eva Deininger-Czermak[d, g], Annegret Mündermann[b, e], Ajay Seth[f], Andreas M. Müller[b, c], Daniel Baumgartner[a]

a Institute of Mechanical Systems, Zürich University of Applied Sciences, Switzerland
b Department of Biomedical Engineering, University of Basel, Switzerland
c Department of Orthopaedics and Traumatology, University Hospital of Basel, Switzerland
d Institute of Forensic Medicine, University of Zurich, Switzerland
e Department of Teaching, Research and Development, Schulthess Clinic, Zurich, Switzerland
f Department of Biomechanical Engineering, TU Delft, Netherlands
g Department of Nuclear Medicine, University Hospital Zurich, Zurich, Switzerland
* Corresponding author: lisa.mareschal@zhaw.ch

Received date: 14/01/2026
Accepted date: 16/03/2026
Publication date: 02/06/2026

Keywords: Statistical shape modelling (SSM), anatomical parameters, shoulder reconstruction, scapula, humerus

1. Introduction

The complex anatomy of the shoulder exhibits substantial inter-individual variability, strongly influencing joint biomechanics and muscle mechanics (Silvestros et al. 2024). In clinical practice, shoulder morphology is routinely described using standardized radiographic clinical morphological parameters (CMPs) of bone geometry. However, current musculoskeletal models typically rely on generic anatomies or require time-consuming segmentation and point correspondence from 3D imaging (Cates et al. 2017).

This study aimed to develop and evaluate a statistical shape model (SSM) reconstruction pipeline for patient-specific 3D bone models of scapula and humeral head from a limited set of 2D CMPs.

2. Methods

2.1 Data

The dataset consisted of 128 shoulder shapes, derived from MRI segmentations of the scapula and humerus in healthy subjects and patients with symptomatic or asymptomatic rotator cuff tears (Croci et al. 2026). The study was approved by the regional ethics board (Ethics Committee Northwest Switzerland EKNZ 2024-01940). The SSM was generated using 80% of the dataset, the remaining 20% were used for validation. Key CMPs were obtained on all shapes based on manually labeled anatomical landmarks to provide ground-truth measurements. The model parameters included glenoid version (GV), glenoid inclination (GI), critical shoulder angle (CSA), lateral acromion angle (LAA), acromial slope (AS), acromial index (AI), acromial tilt (AT) and the ratio of the glenoid width over the humeral head radius (GW/HH) (Verhaegen et al. 2021).

2.2 SSM and optimization

Particle-based correspondence across all shapes was established using ShapeWorks (Akhundov et al. 2022). The humerus and scapula were represented by 1024 and 4736 corresponding particles, respectively. Shapes were aligned and scaled using Generalized Procrustes Analysis prior to Principal Component Analysis (PCA) to capture the main modes of anatomical variation.

Patient-specific reconstruction was performed by optimizing the PCA shape coefficients of the MRI-derived SSM using sequential least-squares programming, such that the CMPs of the reconstruction match the CMPs of the ground-truth models.

At each iteration, reconstructed CMPs were updated by tracking the particles corresponding to CMP landmarks defined on the SSM mean shape.

To cite this article: L. Mareschal, J. Genter, E. Croci, D. Gascho, E. Deininger-Czermak, A. Mündermann, A. Seth, A. M. Müller, D. Baumgartner, Patient-Specific Reconstruction of Shoulder Anatomy Driven by Radiographic Anatomical Parameters Using Statistical Shape Modelling, *Multidisciplinary Biomechanics Journal*, 2026, vol. 3, p.23–25, DOI: 10.46298/mbj.17933.

The optimization model minimized the following loss function.

$$L = \sum_i w_i \left(CMP_i^{recon} - CMP_i^{target} \right)^2$$

2.3 Validation

The known CMPs were used as target inputs for the optimization model. Reconstruction performance was quantified by computing the absolute error of radiographic parameters between the original and optimized shapes, the mean Hausdorff distance across all reconstructed shapes, and the root mean square error (RMSE) of particle positions.

3. Results and Discussion

Table 1. CMPs absolute reconstruction error.

CMPs	Mean error ± std	Max error
GV (°)	0.1 ± 0.2	0.7
GI (°)	0.1 ± 0.2	0.8
CSA (°)	<0.1 ± 0.1	0.5
LAA (°)	0.3 ± 0.8	3.1
AS (°)	0.2 ± 0.5	2.4
AI	0.001 ± 0.002	0.009
AT (°)	<0.1 ± 0.2	0.8
GW/HH	0.002 ± 0.006	0.019

Credit: Mareschal.

The mean reconstruction error to the target CMP was ≤0.3±0.8° for all angular parameters and ≤0.002 for AI and GW/HH ratio (Table 1). Across all shapes, we obtained a mean Hausdorff distance of 14.7±6.9mm. Surface-to-surface similarity was lowest in the superior angle of the scapula, along the scapular spine, and at the medial border in most shapes.

Figure 1 shows the spatial heterogeneity of RMSE between particle positions of target and reconstructed shapes. Regions constrained by input parameters, such as the glenoid, acromion and humeral head, exhibited the lowest errors (≤4.2 mm). Higher RMSE values were observed in areas less represented by parameters including the superior angle of the scapula (9.8 mm), the scapular spine (7.3 mm) and the coracoid process (5.6 mm).

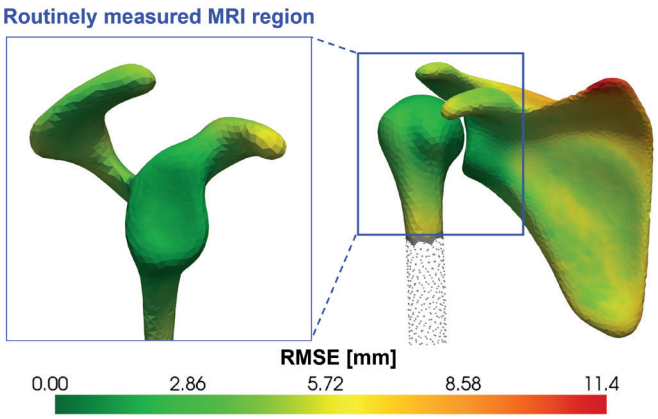

Figure 1. Mean reconstruction RMSE projected onto the 3D mean shape.

Credit: Mareschal.

The reconstruction pipeline effectively reproduced the CMPs in anatomically and biomechanically relevant regions. The low RMSE in the glenoid and acromion corresponded mostly to areas constrained by the CMPs and thus of primary interest. Higher errors in above-mentioned regions reflected the current limitations of CMP-driven reconstruction.

4. Conclusions

We demonstrated that patient-specific shoulder geometries can be accurately reconstructed from a limited set of routinely measured radiographic parameters. Because MRI-derived CMPs are measured in the projected true anteroposterior and scapular Y-view planes, the method should be transferable to standard X-ray projections. The method reliably reproduced the overall shapes, particularly in clinically relevant regions, such as the glenoid and acromion. Areas less represented by parameters, such as superior angle and scapular spine, show larger errors. Although these regions are expected to have limited influence on musculoskeletal simulation outcomes, they may be less suitable for analyses requiring detailed local geometry. For routine modelling applications, 3D reconstructions derived from standard CMPs may suffice without the need for further complex analyses. This reconstruction pipeline will enable integration into computational models for the study of shoulder biomechanics and pathology, with potential applicability in clinically relevant workflows. With further refinement and additional input parameters, the approach will have the potential to support clinicians in patient-specific surgical planning.

Conflict of Interest Statement

None.

Contributor Roles

LM: Methodology, Formal analysis, Visualization, Writing original draft; JG: Conceptualization, Methodology, Visualization, Funding acquisition, Supervision, Project administration, Writing-review & editing; EC: Resources, Conceptualization, Data collection, Writing-review & editing; AM, BD: Conceptualization, Methodology, Funding acquisition, Supervision, Writing-review & editing; DG: Conceptualization, Methodology, Funding acquisition, Writing-review & editing; ECD: Methodology, Funding acquisition, Writing-review & editing; AS&AMM: Conceptualization, Supervision, Writing-review & editing.

Funding

This study used data from the liTrans study (Swiss National Science Foundation, SNF 189082) and was funded by the Digitalization Initiative of the Zurich Higher Education Institutions (DIZH).

References

Akhundov, R., Saxby, D. J., Diamond, L. E., Edwards, S., Clausen, P., Dooley, K., Blyton, S., & Snodgrass, S. J. (2022). Is subject-specific musculoskeletal modelling worth the extra effort or is generic modelling worth the shortcut? *PLOS ONE, 17*(1), e0262936. https://doi.org/10.1371/journal.pone.0262936

Cates, J., Elhabian, S., & Whitaker, R. (2017). Chapter 10—ShapeWorks: Particle-Based Shape Correspondence and Visualization Software. In G. Zheng, S. Li, & G. Székely (Eds.), *Statistical Shape and Deformation Analysis* (pp. 257–298). Academic Press. https://doi.org/10.1016/B978-0-12-810493-4.00012-2

Croci, E., Hess, H., Nüesch, C., Baumgartner, D., Gerber, K., Müller, A. M., & Mündermann, A. (2026). Association between functional scores, radiological parameters, and muscle strength in shoulders with asymptomatic or symptomatic rotator cuff tears and healthy controls. *Journal of Shoulder and Elbow Surgery, 35*(1), 155–166. https://doi.org/10.1016/j.jse.2025.04.004

Silvestros, P., Athwal, G. S., & Giles, J. W. (2024). Scapular morphology variation affects reverse total shoulder arthroplasty biomechanics. A predictive simulation study using statistical and musculoskeletal shoulder models. *Journal of Orthopaedic Research, 42*(7), 1383–1398. https://doi.org/10.1002/jor.25801

Verhaegen, F., Meynen, A., Matthews, H., Claes, P., Debeer, P., & Scheys, L. (2021). Determination of pre-arthropathy scapular anatomy with a statistical shape model: Part I—rotator cuff tear arthropathy. *Journal of Shoulder and Elbow Surgery, 30*(5), 1095–1106. https://doi.org/10.1016/j.jse.2020.07.043

2026-3 | International Shoulder Group (ISG) Congress 2026
2-3 June 2026, Lyon, France

Multidisciplinary Biomechanics Journal

Changes in EMG–Angle Relationships Following Reverse Total Shoulder Arthroplasty

Hugo Francalanci[a], Nicolas Holzer[b], Yosra Cherni[c, d, e], Florent Moissenet[a, f*]

a Biomechanics and Translational Research in Surgery Research Group, Department of Surgery, University of Geneva, Geneva, Switzerland
b Orthopedic Surgery and Musculoskeletal Trauma Care Division, Department of Surgery, Geneva University Hospitals, Geneva, Switzerland
c Laboratoire de neurobiomécanique et neuroréadaptation de la locomotion, Centre de recherche Azrieli du CHU Sainte Justine, Montréal, Canada
d Ecole de kinésiologie et sciences de l'activité physique, Université de Montréal, Montréal, Canada
e Institut de génie biomédical, Université de Montréal, Montréal, Canada
f Kinesiology Laboratory, Geneva University Hospitals and University of Geneva, Geneva, Switzerland
* Corresponding author: florent.moissenet@unige.ch

Received date: 14/01/2026
Accepted date: 16/03/2026
Publication date: 02/06/2026

Keywords: reverse total shoulder arthroplasty, rotator cuff tear, motor control, kinematics, electromyography

1. Introduction

Restoring shoulder function in patients with massive rotator cuff tears (MRCT) partly relies on the motor system's ability to reorganise muscle activation. Reverse total shoulder arthroplasty (rTSA) stabilises the glenohumeral centre, enabling the deltoid to compensate for cuff deficiency, but also induces significant neuromuscular adaptations (Smith et al., 2020). Understanding recovery after rTSA requires more than kinematic analysis alone, as muscle activation patterns reflect compensatory strategies. However, the interaction between shoulder kinematics and electromyography (EMG) remains poorly documented.

This study investigates the change in the relationship between thoracohumeral (TH) elevation and shoulder muscle activations before and after rTSA in comparison to asymptomatic shoulders. We hypothesised that postoperative kinematic improvements would be accompanied by a more stable and functional EMG–angle relationship, indicating a shift towards efficient coordination strategies.

2. Methods

2.1 Data acquisition and preprocessing

Retrospective data were collected from asymptomatic (n = 20; 71.7 ± 9.7 years) and symptomatic (n = 20; 71.8 ± 10.3 years) shoulders assessed preoperatively and 12 months following rTSA. All participants provided written informed consent, and the study was approved by the local ethics committee (CER 2025-00773). Data acquisition was performed during four functional tasks: hand to mouth, hand to head, maximal overhead reach, and hand behind the back, each repeated three times.

EMG signals from the deltoid (DELTA, DELTM, DELTP), trapezius (TRAPM, TRAPS), and serratus (SERRA) were processed using: band-pass filtering (15–475 Hz), full-wave rectification, root mean square (RMS) smoothing (250 ms), and normalisation to submaximal tasks. For each subject and muscle, three cycles per task were time normalised and averaged to obtain a representative EMG cycle.

TH joint elevation angle was computed for the same cycles using a Y-X-Y Euler sequence decomposition (Wu et al., 2005) and averaged similarly. The resulting mean EMG and TH cycles were aligned to allow the analysis of the relationships. All data processing was performed using MATLAB (R2024b, The MathWorks, USA).

2.2 EMG–angle relationships

EMG–angle relationships were quantified at the subject level over the movement cycle using linear regressions,

To cite this article: Hugo Francalanci, Nicolas Holzer, Yosra Cherni, Florent Moissenet, Changes in EMG–angle relationships following reverse total shoulder arthroplasty, *Multidisciplinary Biomechanics Journal*, 2026, vol. 3, p. 27–30, DOI: 10.46298/mbj.17926.

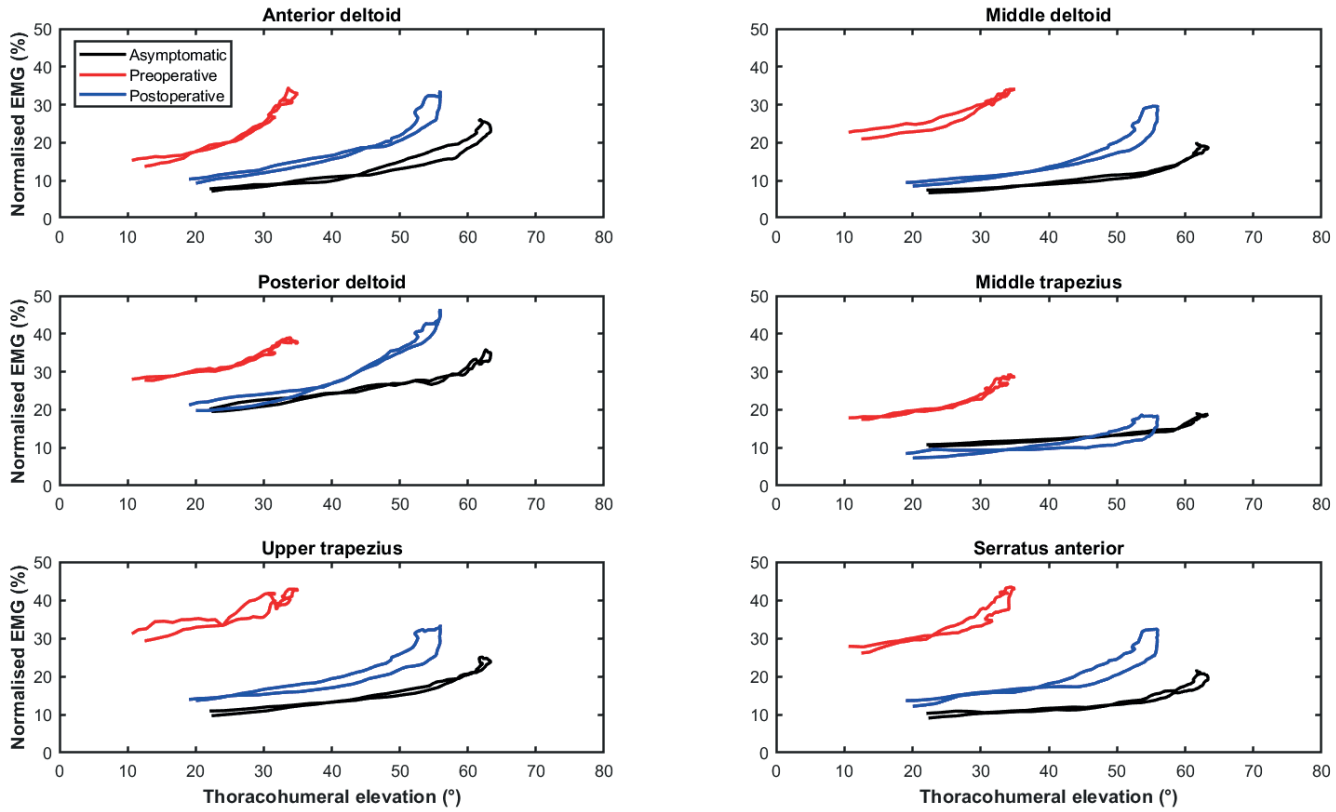

Figure 1. Comparison of normalised shoulder muscle EMG activity across thoracohumeral elevation angles between groups during combined functional tasks. Each plot displays the linear relationship between EMG activity and elevation angle for a single muscle.
Credit: Francalanci.

and metrics were compared across groups. The regression slope indexed muscle activation relative to TH elevation, while the RMS deviation (RMSD) from the group-averaged EMG–angle curve quantified intra-group variability and EMG–angle coupling consistency.

2.3 Statistical analysis

Two-way ANOVAs (Group×Muscle) were performed for regression slopes and RMSD values. When a significant Group×Muscle interaction was detected, separate one-way ANOVAs were conducted for each muscle, followed by post-hoc pairwise t-tests. When no significant interaction was present, post-hoc tests were performed globally across all muscles. Significance was set at $p < 0.05$.

3. Results and discussion

3.1 EMG–angle relationships

Regression slope analysis revealed that changes in EMG–angle relationships (Fig. 1) were primarily driven by clinical status rather than muscle-specific effects (Table 1), indicating a global reorganisation of motor control.

Preoperatively, altered DELTA recruitment was associated with rotator cuff deficiency and pseudoparalysis (Bauer et al., 2022), reflected by reduced TH elevation amplitude compared with asymptomatic shoulders (24.4° vs 43.6°). After rTSA, the EMG–angle relationship of DELTM remained altered, suggesting a modified functional role in restoring elevation (Pietroski et al., 2025), consistent with postoperative recovery of TH elevation (41° vs 43.6°). Differences in DELTP slopes between asymptomatic and postoperative groups indicate an increased contribution of this muscle to postoperative shoulder coordination.

The TRAPM fibres showed altered EMG–angle coupling only preoperatively, consistent with impaired scapular stabilisation in MRCT, with recovery observed after surgery. In contrast, SERRA coupling remained altered postoperatively, suggesting incomplete restoration of coordination or persistent compensatory strategies following rTSA.

Table 1. Statistical comparison of EMG–angle relationships (slopes) and intra-group variability (RMSD) between groups during combined functional tasks [Credit: Francalanci]

			One-way ANOVA Group	Two-way ANOVA Group× Muscle	Post-hoc Asymptomatic vs Preoperative	Post-hoc Asymptomatic vs Postoperative	Post-hoc Preoperative vs Postoperative
EMG-angle relationships (slopes)	Main effects	Group	—	<0.001*	—	—	—
		Muscle	—	0.081	—	—	—
	Interaction effect	GroupxMuscle	—	0.421	—	—	—
	Muscles	DELTA	—	—	0.017*	0.066	0.244
		DELTM	—	—	0.011*	0.049*	0.515
		DELTP	—	—	0.057	0.026*	0.259
		TRAPM	—	—	0.021*	0.912	0.057
		TRAPS	—	—	0.443	0.055	0.597
		SERRA	—	—	0.082	0.006*	0.731
Intra-group variability (RMSD)	Main effects	Group	—	<0.001*	—	—	—
		Muscle	—	<0.001*			
	Interaction effect	GroupxMuscle	—	<0.001*			
	Muscles	DELTA	0.252	—	—	—	—
		DELTM	0.159	—	—	—	—
		DELTP	0.154	—	—	—	—
		TRAPM	0.404	—	—	—	—
		TRAPS	<0.001*	—	<0.001*	0.581	<0.001*
		SERRA	<0.001*	—	<0.001*	0.263	0.005*

DELTA: anterior deltoid; DELTM: middle deltoid; DELTP: posterior deltoid; TRAPM: middle trapezius; *TRAPS: upper trapezius; SERRA: serratus anterior; *: $p < 0.05$.*

3.2 Intra-group variability and coupling consistency

RMSD analysis demonstrated that EMG–angle variability reflected both global motor control changes and muscle-specific behaviour (Table 1). No group differences were observed for the deltoid portions or TRAPM, whereas TRAPS and SERRA showed higher variability preoperatively compared with asymptomatic and postoperative shoulders. This indicates reduced coupling consistency before surgery and a postoperative return towards asymptomatic patterns.

These findings highlight the sensitivity of scapular stabilisers to MRCT-related dysfunction (Hawkes et al., 2012) and their responsiveness to rTSA. Interpretation should be cautious given the limited muscle set and task selection.

4. Conclusions

Clinical status primarily drives global motor control adaptations. Preoperative subjects showed altered recruitment patterns and high variability, particularly in the anterior deltoid and scapular stabilisers, whereas postoperative subjects exhibited more consistent EMG–angle coupling and a reorganisation of coordination strategies, with all three deltoid portions emerging as primary contributors to restoring thoracohumeral elevation, reflecting a shift towards efficient coordination strategies.

Conflict of Interest Statement

None.

Contributor Roles

HF: Conceptualisation, Formal analysis, Methodology, Visualisation, Writing – original draft. NH: Conceptualisation, Writing – review & editing. YC: Conceptualisation, Methodology, Software, Visualisation, Supervision, Writing – review & editing. FM: Conceptualisation, Data collection, Methodology, Visualisation, Supervision, Writing – review & editing.

Funding

No funding was received by the authors for this study.

Data, software, code availability

Code is available at the following GitHub repository: https://github.com/HugoFrancalanci/Changes-in-EMG-angle-relationships-following-reverse-total-shoulder-arthroplasty.git. Data are available upon request to the corresponding author.

References

Bauer, S., Okamoto, T., Babic, S. M., Coward, J. C., Coron, C. M. P. L., & Blakeney, W. G. (2022). Understanding shoulder pseudoparalysis: Part I: Definition to diagnosis. *EFORT Open Reviews, 7*(3), 214–226. https://doi.org/10.1530/EOR-21-0069

Hawkes, D. H., Alizadehkhaiyat, O., Kemp, G. J., Fisher, A. C., Roebuck, M. M., & Frostick, S. P. (2012). Shoulder muscle activation and coordination in patients with a massive rotator cuff tear: an electromyographic study. *Journal of Orthopaedic Research: Official Publication of the Orthopaedic Research Society, 30*(7), 1140–1146. https://doi.org/10.1002/JOR.22051

Pietroski, A., Zhou, Y., Kasto, J., Obinero, C., Zhu, K., Mazeh, M., Chen, C., & Muh, S. (2025). Surface electromyography reveals middle deltoid as the functionally dominant shoulder muscle after reverse total shoulder arthroplasty. *Cureus, 17*(3). https://doi.org/10.7759/CUREUS.80229

Smith, R. A., Woolley, K., Mazzocca, A., Feinn, R., Cote, M., Gomlinski, G., Garbalosa, J., & Myrick, K. M. (2020). Kinematics and EMG activity in reverse total shoulder arthroplasty. *Journal of Orthopaedics, 22*, 165–169. https://doi.org/10.1016/J.JOR.2020.04.017

Wu, G., van der Helm, F. C. T., Veeger, H. E. J., Makhsous, M., van Roy, P., Anglin, C., Nagels, J., Karduna, A. R., McQuade, K., Wang, X., Werner, F. W., & Buchholz, B. (2005). ISB recommendation on definitions of joint coordinate systems of various joints for the reporting of human joint motion—Part II: shoulder, elbow, wrist and hand. *Journal of Biomechanics, 38*(5), 981–992. https://doi.org/10.1016/J.JBIOMECH.2004.05.042

2026-3 | International Shoulder Group (ISG) Congress 2026
2-3 June 2026, Lyon, France

Multidisciplinary Biomechanics Journal

Characterisation of Variability and Investigation of Factors Influencing Maximum Coronal Abduction and Forward Elevation in Post-Operative rTSA Subjects

Eva C. Herbst[a, b*], Maartje van Beurden[a], Heath B. Henninger[c], Stephen J. Ferguson[a], Philipp Moroder[b]

a Institute for Biomechanics, ETH, Zurich, Switzerland
b Schulthess Klinik, Zurich, Switzerland
c Department of Orthopaedics, University of Utah, Salt Lake City, U.S.A.
* Corresponding author: eva.herbst@hest.ethz.ch

Received date: 16/01/2026
Accepted date: 16/03/2026
Publication date: 02/06/2026

Keywords: reverse total shoulder arthroplasty, range of motion, humeral elevation, posture, biplanar fluoroscopy

1. Introduction

The variability in *in vivo* coronal abduction (CA) and forward elevation (FE) capacity in rTSA (reverse total shoulder arthroplasty) subjects, and possible sources of this variability, remain to be explored using gold-standard biplane fluoroscopy. Maximum humeral CA and FE are relevant because they indicate the ability of the patient to perform specific functions requiring interaction with the global space (i.e. reaching a shelf).

Our aims were to:

1. quantify maximum CA and FE in post-operative rTSA patients, including comparison with healthy controls
2. determine whether scapular global posture, age, sex, and humeral starting position correlate with maximum CA and FE in rTSA patients

2. Methods

2.1 Dataset

We analysed 18 rTSA subjects and 20 healthy subjects using an open-source biplanar fluoroscopy dataset (Henninger 2025). One rTSA subject was excluded from CA analysis and one healthy subject from FE analysis due to inability to perform the motion or a recording gap.

2.2 Measurements

Scapular upward rotation (SUR), internal rotation (SIR), and tilt (ST) were measured in a neutral rest position (static trials) using a patient-global coordinate system (Moroder et al. 2022), with the superoinferior axis defined by the global gravity vector and the patient mediolateral and anteroposterior axes defined using thorax and sternum skin markers. Maximum CA was quantified by projecting the humeral shaft long axis (determined by a cylinder fit) into the patient-global-coronal plane. Maximum FE was defined by projecting the humeral long axis into the patient-global-sagittal plane. Postures and maximum CA/FE were projected into subject-global planes to maximize clinical interpretability.

We analysed maximum FE/CA instead of analysing final minus start position because subtracting the starting position may misrepresent the functional reaching capacity of subjects starting with a more abducted arm.

Differences between maximum CA and FE in healthy subjects and rTSA patients were compared using t-tests (for FE, which was normally distributed) and Wilcox rank sum tests (for CA, which was non-normally distributed) with Bonferroni correction. Distribution was assessed with QQ plots. The effects of age, sex, SUR, SIR, ST, and starting humeral elevation on rTSA maximum CA and FE were analysed using a linear model with separate models for FE and CA. Analyses were performed in RStudio (2026, R 4.5.2).

3. Results and discussion

The rTSA population tended to have reduced maximum CA and FE compared to healthy subjects (Fig. 1 a,b,

To cite this article: Eva C. Herbst, Maartje van Beurden, Heath B. Henninger, Stephen J. Ferguson, Philipp Moroder, Characterisation of Variability and Investigation of Factors Influencing Maximum Coronal Abduction and Forward Elevation in Post-Operative rTSA Subjects, *Multidisciplinary Biomechanics Journal*, 2026, vol. 3, p. 31–33, DOI: 10.46298/mbj.17922.

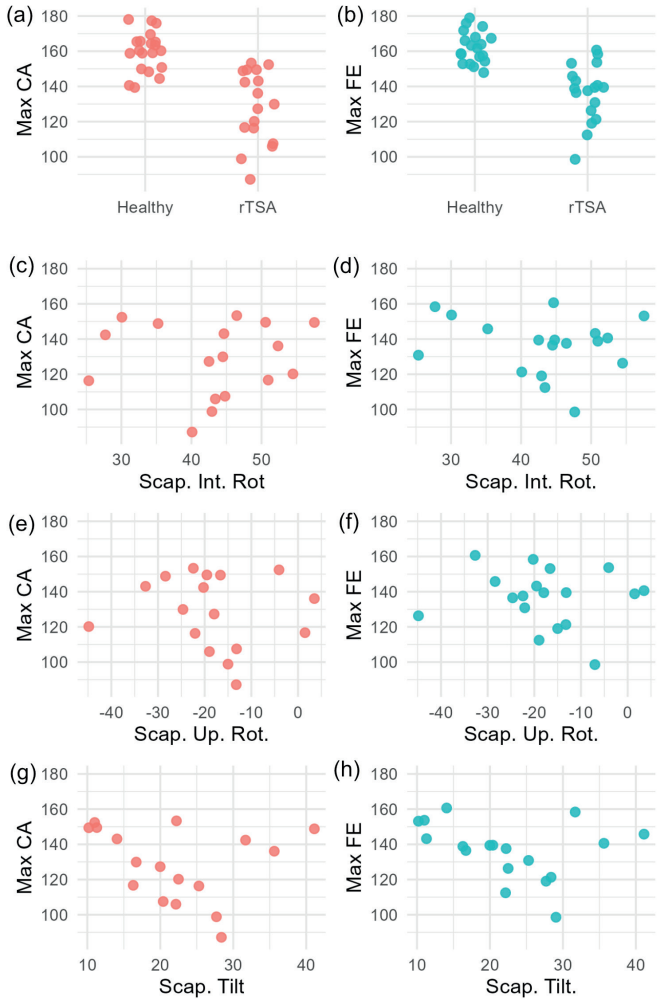

Figure 1. Comparison of max. CA **(a)** and FE **(b)** between healthy and rTSA. In rTSA subjects, no clear linear effects of scapular posture on max CA **(c,e,g)** and FE **(d,f,h)**.

Credit: ECH and MvB.

Table 1, p<0.00001). rTSA patients exhibited higher variability in CA and FE (higher standard deviation (SD), Table 1). Scapular global posture at rest, age, sex, or humeral starting position did not significantly impact maximum CA or FE in rTSA subjects (Fig. 1c-h). However, when excluding the 2-3 outliers at the extremes of ST, there is an apparent visible trend of decreasing CA and FE with ST. Studies with higher sample sizes are needed to investigate this further.

Other studies found that patient posture influences simulated range of motion (ROM) (Lappen et al. 2025), but that study isolated effects of scapular posture on collision-free glenohumeral range of motion, whereas various other factors may affect maximum CA and FE *in vivo*. Additionally, the simulation study did not account for soft tissue limits or active range of motion capacity. Clinical studies have also shown that abduction and flexion clinical ROM differs between posture categories (Moroder et al. 2024), although the effect was small, and may not be detected in a smaller study such as ours. In addition to the small sample size, the healthy – rTSA comparison in our study is limited by lack of age matching, with the rTSA cohort being older and with a narrower age range, although age did not affect maximum humeral CA or FE in the rTSA cohort. We analysed posture in a relaxed starting position, but starting posture for specific trials may differ in anticipation on the movement and affect maximum CA/FE. Finally, we did not investigate humeral rotation, which may also influence CA and FE and should be incorporated into future analyses.

Table 1. Summary statistics and effect of parameters on max CA and FE. SD indicated by (), range indicated by [].

	Healthy	rTSA
Max CA	160 (11) *[139–178]*	129 (21) *[87–153]*
Starting Hum. Elev. CA	12 (6) *[3–25]*	16 (8) *[5–33]*
Max FE	162 (9) *[148–179]*	136 (16) *[99–161]*
Starting Hum. Elev. FE	6 (5) *[1–18]*	9 (8) *[1–26]*
SUR	-14 (11) *[-36–6]*	-18 (12) [-45–4]
SIR	47 (7) *[28–60]*	43 (9) *[25–58]*
ST	16 (10) *[-5–38]*	23 (9) *[10–41]*
Age	42 (17) *[22–66]*	70 (8) *[58 – 85]*
Sex	F 10; M 10	F 6; M 12

Credit: ECH and MvB.

4. Conclusions

rTSA subjects exhibit considerable variability in postoperative maximum CA/FE. Given that humeral CA and FE in global space are a combination of thorax global position, scapulothoracic orientation, and

glenohumeral orientation, further work is needed to elucidate factors influencing post-operative CA and FE capacity in rTSA.

Acknowledgements

We thank the Georg und Bertha Schwyzer-Winiker Foundation for funding this research.

Conflict of Interest Statement

The authors declare no conflict of interest.

Contributor Roles

ECH: Conceptualization, Methodology, Investigation, Data Curation, Writing original draft, Validation, Formal analysis, Visualization, Project administration; MvB: Investigation, Validation, Formal analysis, Visualization Writing- review & editing; HBH: Resources, Writing- review & editing; SJF: Supervision: Writing- review & editing, PM: Supervision, Funding acquisition, Writing- review & editing.

Funding

This work was funded by the Georg und Bertha Schwyzer-Winiker Foundation. Source data collection was supported by the National Institute of Arthritis and Musculoskeletal and Skin Diseases (NIAMS) of the National Institutes of Health under award number R01 AR067196.

Data, software, code availability

Biplane dataset: https://doi.org/10.5281/zenodo.10972004

References

Henninger, H. B. (2025). Shoulder kinematics derived from radiographic and optical motion analysis, (v1.2), [Data set]. Zenodo. https://doi.org/10.5281/zenodo.10972004

Moroder, P., Urvoy, M., Raiss, P., Werthel, J-D., Akgün, D., Chaoui, J., & Siegert, P. (2022). Patient posture affects simulated ROM in reverse total shoulder arthroplasty: A modeling study using preoperative planning software. *Clinical Orthopaedics & Related Research, 480*(3): 619–631. https://doi.org/10.1097/CORR.0000000000002003

Moroder, P., Siegert, P., Coifman, I., Rüttershoff, K., Spagna, G., Scaini, A., Weber, B., Schneller, T., Scheibel, M., & Audigé, L. (2024). Scapulothoracic orientation has a significant influence on the clinical outcome after reverse total shoulder arthroplasty. *Journal of Shoulder and Elbow Surgery, 33*(10): 2159–2170. https://doi.org/10.1016/j.jse.2024.02.018

2026-3 | International Shoulder Group (ISG) Congress 2026
2-3 June 2026, Lyon, France

Multidisciplinary Biomechanics Journal

Trapezius Excitation is Altered without Kinematic Differences in Asymptomatic Scapular Dyskinesis

Sarah Bohunicky[a], Brad Bergen[a], Angelica Lang[b], Trisha Scribbans[a]*

a Integrative Musculoskeletal Research Lab, University of Manitoba, Winnipeg, Canada
b Canadian Centre for Rural and Agricultural Health, University of Saskatchewan, Saskatoon, Canada
* Corresponding author: trisha.scribbans@umanitoba.ca

Received date: 16/01/2026
Accepted date: 16/03/2026
Publication date: 02/06/2026

Keywords: muscle excitation, shoulder, arm elevation, electromyography

1. Introduction

Scapular dyskinesis (SD) is aberrant scapular position and/or movement at rest or during motion and is often implicated in shoulder pathology (Costa e Silva Cabral et al, 2024). However, SD is also common in in asymptomatic individuals, making its clinical significance unclear. Although SD has been shown to alter scapular kinematics (Huang et al, 2015), potentially due to differences in trapezius muscle excitation, most research has focused on pathological shoulders. Therefore, the purpose of this study was to compare scapular kinematics and regional trapezius excitation (upper [UT], middle [MT], and lower [LT]) during arm elevation in asymptomatic individuals with and without SD.

2. Methods

Fifty-three right-handed participants (n=53, 26±8 years, 34 female) completed the scapular dyskinesis test and were classified as SD (n=25; subtle or obvious SD) or control (normal scapular kinesis [CON]; n=28). Participants performed five repetitions each of weighted shoulder flexion and abduction using a dumbbell (1.4 or 2.5 kg for participants <68.1 kg and >68.1 kg, respectively). Scapular kinematics (upward/downward rotation, internal/external rotation, anterior/posterior tilt) and high-density surface electromyography of the UT, MT, and LT and were collected. Muscle excitation for each region during the arm elevation task was normalized to the peak root mean square obtained for that region. Kinematics and excitation were extracted at nine angles during flexion (F) and extension (E; F/E) and abduction (AB) adduction (AD; AB/AD): start of elevation (START), 45°, 75°, 105°, top of elevation (TOP), 105°, 75°, 45°, end of lowering (END). Two-way (group*angle) mixed ANOVAs were conducted on all kinematic and muscle excitation variables, with Tukey's HSD post-hoc testing applied to significant interactions (p<.05). Small, medium and large effect size (ηp^2) were interpreted as .01, .06, and .14, respectively.

3. Results and Discussion

Regional trapezius excitation results can be found in **Table 1**. No significant interactions or main effects were observed for kinematics, UT excitation, or MT excitation during AB/AD (p>.05). However, significant group-by-angle interactions with small-to-moderate effect sizes were observed during F/E for both MT (p= .041, ηp^2=.051) and LT excitation (p= .046, ηp^2=.049), and in LT excitation during AB/AD (p= .045, ηp^2= .049). Pairwise comparisons revealed that these interactions were driven by distinct excitations patterns throughout the movement. Specifically, the SD group demonstrated higher MT excitation during the middle stages of flexion (75°; p=.035) and extension (75°; p=.043), and at peak elevation (TOP; p=.046). For the LT, the SD group exhibited consistently greater excitation than CON during the beginning and end stages of both tasks. In

To cite this article: Sarah Bohunicky, Brad Bergen, Angelica Lang, Trisha Scribbans, Trapezius Excitation is Altered without Kinematic Differences in Asymptomatic Scapular Dyskinesis, *Multidisciplinary Biomechanics Journal*, 2026, vol. 3, p. 35–37, DOI: 10.46298/mbj.17925.

Table 1. Mean and standard deviation of regional trapezius excitation (% of maximal root mean square) for scapular dyskinesis and control during raising and lowering phases of flexion and abduction arm elevation.

	Raising (mean ± standard deviation)					Lowering (mean ± standard deviation)			
	START	45°	75°	105°	TOP	105°	75°	45°	END
Upper Trapezius Flexion and Extension									
SD	24.9 ±8.4	38.8±11.7	52.6±13.8	65.4±10.9	57.4±8.3	44.9±10.9	37.6±9.2	28.2±9.3	16.5±6.7
C	21.9±10.1	33.4±12.5	46.6±15.5	59.7±12.2	59.7±13.2	42.3±9.1	34.2±9.0	25.1±9.1	14.8±7.2
Upper Trapezius Abduction and Adduction									
SD	25.7 ±8.0	46.5±12.4	57.6±11.0	67.1±8.5	56.2±11.3	45.2±6.8	39.0±8.3	29.3±6.9	18.9±6.6
C	21.4±8.3	40.3±16.0	48.0±14.7	58.5±12.5	55.8±13.9	40.2±9.2	33.7±8.3	25.3±8.4	15.4±6.1
Middle Trapezius Flexion and Extension*									
SD	32.3±9.1	49.9±11.9	57.3±9.3	56.4±9.41	48.6±11.3	42.0±9.2	42.7±9.1	37.1±11.3	20.5±7.8
C	27.4±11.3	43.4±15.7	49.5±15.8†	50.8±13.2	54.7±10.3†	36.8±8.8	37.9±9.2†	31.3±9.6	17.8±8.7
Middle Trapezius Abduction and Adduction									
SD	28.9±7.1	48.8±8.9	59.8±9.2	66.3±8.9	53.9±12.3	44.2±7.3	39.6±8.6	28.4±6.4	18.0±6.0
C	26.5±9.7	46.8±14.3	56.0±13.0	65.2±10.3	56.7±9.8	42.2±8.0	37.8±8.5	28.3±9.0	17.2±7.6
Lower Trapezius Flexion and Extension*									
SD	27.7±8.9	45.8±9.4	57.7±11.8	59.2±10.9	58±10.6	51.4±10.4	44.1±8.4	32.8 ±8.6	20.9±11.9
C	19.8±9.1†	37.5±11.2†	50.9±13.0	54.5±11.8	56.6 ±9.3	39.4±10.1†	34.0±11.2†	21.4±10.2†	11.8±9.2†
Lower Trapezius Abduction and Adduction*									
SD	22.6±9.6	35.1±10.3	44.2±12.0	56.3±11.6	67.4±7.8	41.2±9.9	35.8±9.6	28.0±10.4	22.8±12.4
C	14.5±8.5†	29±10.4†	41.4±12.0	55.8 ±9.7	64.2 ±8.9	35.6±8.3†	27.1±9.3†	20.1±10.2†	14±10.4†

C= control; SD= scapular dyskinesis; *p<.05= two-way interaction, †p<.05 pairwise comparison.

F/E, LT excitation was higher in SD at START, 45°F, and throughout the lowering phase (105°E to END; all p<.01). Similarly, the SD group had greater LT excitation during AB/AD at START and during the majority of the adduction phase (p<.05).

These findings deviate from prior reports of reduced MT and LT excitation in individuals with SD (Huang et al, 2015, Costa e Silva Cabral et al, 2024, Cools et al., 2014). In contrast, our results demonstrated that asymptomatic SD is characterized by a moderate increase in MT and LT excitation despite a lack of detectable kinematic differences. This may be explained by the scapular force-couple relationship; the serratus anterior (SA) works synergistically with the trapezius to facilitate upward rotation and posterior tilt. It is possible that the increased MT and LT excitation observed represents a neuromuscular compensation for SA insufficiency. By over-recruiting the trapezius, individuals with SD may successfully maintain kinematics and remain asymptomatic, albeit through altered motor strategies. However, the absence of SD subgrouping by pattern may have obscured more specific kinematic deviations (Huang et al, 2015).

4. Conclusions

In asymptomatic individuals, scapular dyskinesis was not associated with altered scapular kinematics during F/E or AB/AD but was characterized by greater MT and LT excitation across arm raising and lowering. The lack of SD subgrouping may have obscured pattern-specific differences, highlighting the importance of considering SD classification when interpreting neuromuscular and kinematic outcomes.

Acknowledgements

The authors thank Josee Rochon for their contributions to this study and the participants for their time and participation.

Conflict of Interest Statement

The authors have no conflicts of interest to declare.

Contributor Roles

SB: formal analysis, investigation, methodology, visualization, writing-original draft, writing-review & editing; BB: data curation, formal analysis, investigation, methodology, project administration; AL: methodology, software; TS: conceptualization, methodology, resources, supervision, writing-review & editing.

Funding

Thanks to the Manitoba Medical Service Foundation for funding this project.

References

Cools, A. M., Struyf, F., De Mey, K., Maenhout, A., Castelein, B., & Cagnie, B. (2014). Rehabilitaion of scapular dyskinesis: from the office worker to the elite overhead athlete. *British Journal of Sports Medicine, 48*(8), 692–697. https://doi.org/10.1136/bjsports-2013-092148

Costa e Silva Cabral, A. L., de Paula Marques, J., & Dionisio, . C. (2024). Scapular dyskinesis and overhead athletes: A systematic review of electromyography studies. *Journal of Bodywork and Movement Therapies, 39*, 606–614. https://doi.org/10.1016/j.jbmt.2024.03.014

Huang, T. S., Ou, H. L., Huang, C. Y., & Lin, J. J. (2015). Specific kinematics and associated muscle activation in individuals with scapular dyskinesis. *Journal of shoulder and elbow surgery, 24*(8), 1227–1234. https://doi.org/10.1016/j.jse.2014.12.022

2026-3 | International Shoulder Group (ISG) Congress 2026
2-3 June 2026, Lyon, France

Multidisciplinary Biomechanics Journal

Restoring Dynamic Shoulder Stability: Insights from the MoveUS Program

Laura Ramírez-Pérez[a, b*], María del Carmen Martín-Molina[b, c], Antonio Ignacio Cuesta-Vargas[a, b, d]

a Department of Physiotherapy, University of Málaga, Málaga 29071, Spain
b The Institute of Biomedical Research and Nanomedicine Platform in Málaga (IBIMA Plataforma BIONAND), Clinimetric Group F-14, Málaga 29010, Spain
c Traumatology, Rehabilitation and Physiotherapy Unit, Axarquia Hospital, Málaga 29700, Spain
d ARC Centre for Joint Biomechanics, Queensland University of Technology, Brisbane, QLD 4059, Australia
* Corresponding author: lrp@uma.es

Received date: 19/11/2025
Accepted date: 16/03/2026
Publication date: 02/06/2026

Keywords: shoulder, joint instability, exercise, physical endurance, functional status

1. Introduction

Glenohumeral instability affects approximately 1-2% of the general population and 11% of the overhead athletes, generating a wide variety of symptoms, highlighting pain, loss of functionality, mobility limitations, loss of strength, alterations in movement patterns, and multivariable fatigue.

Management of glenohumeral instability includes both conservative and surgical approaches. Surgical interventions, such as Bankart or Latarjet, are indicated for recurrent instability or when conservative treatment fails, but the risk of recurrence is between 7% and 20%. Regarding the conservative approach, physiotherapy programs try to restore function through shoulder strengthening, but existing protocols are not fully satisfactory. Moreover, there is no consensus about the best approach (Kavaja et al., 2018).

For these reasons, the main aim of this study was to evaluate the effect of an original multicomponent exercise protocol, the MoveUS Program, on the improvement of symptoms in patients with glenohumeral instability.

2. Methods

2.1 Study design

A phase 1 prospective cohort study was designed, enrolling 25 patients. Patients were included if they were 18 to 64 years old, had a clinical diagnosis radiographically confirmed of shoulder instability, and had suffered at least one episode of shoulder instability during the last year.

They underwent a 12-week exercise-based intervention, the MoveUS Program, which was divided into four stages of equal duration with three weekly days of training. The approximation phase focused on regaining motor control, the structural phase was based on strengthening the periarticular muscles, the neural stage emphasized the improvement of motor unit recruitment, and the functional readaptation phase was based on returning to sports and daily life activities. As for supervision, 1 weekly session was developed face-to-face with continuous monitoring by the physiotherapist, and 2 weekly sessions were performed at the hospital without presential monitoring but using the dosage prescription provided by the physiotherapist (Ramírez-Pérez & Cuesta-Vargas, 2024).

2.2. Procedure

The patients were followed for 24 weeks, and the improvements were measured using validated questionnaires such as the Western Ontario Shoulder Instability Index (WOSI) for pain, functionality, and quality of life, the Quick-Piper Scale-revised (Quick-Piper) for psychological fatigue, the Questionnaire on the self-perception of the athlete for the return to standardized training after an injury (Return to Play) for the capacity

To cite this article: Laura Ramírez-Pérez, María del Carmen Martín-Molina, Antonio Ignacio Cuesta-Vargas, Restoring Dynamic Shoulder Stability: Insights from the MoveUS Program, *Multidisciplinary Biomechanics Journal*, 2026, vol. 3, p. 39–41, DOI: 10.46298/mbj.17928.

of a safely return to daily life activities and sports, the modified T-Fast Test for endurance, the MoveUS Test for dynamic stability, a handheld dynamometer for force peak, an electromyography for physiological fatigue, and inertial sensors for kinematic fatigue.

2.3. Statistical analysis

Descriptive statistics were performed. Moreover, pre- and post-intervention changes were analyzed using paired t-tests for within-group comparisons, with mean differences, corresponding p-values, and effect sizes. No corrections for multiple comparisons were applied. Subgroup analyses were not performed due imbalance in traumatic and atraumatic instability.

2.4. Ethical approval

The study had ethics approval from the Malaga Clinical Research Ethics Committee (PEIBA: 1311-M1-23).

3. Results and discussion

The sample consisted of 17 males and 8 females, with a mean age of 34.3 ± 12.4 years. Regarding the instability profile, 17 patients (68%) were atraumatic.

After the MoveUS Program, patients showed a significant improvement in WOSI (mean difference = 703 ± 89.1 points; $p < 0.001$; Cohen's d = 1.81), Quick-Piper (mean difference = 2.6 ± 0.45 points; $p < 0.001$; Cohen's d = 1.32), and Return to Play (mean difference = 11.21 ± 2.04 points; $p < 0.001$; Cohen's d = 1.26). These differences regarding the self-reported outcomes were greater than those found by previous authors (Warby et al., 2018), a fact that could be explained by the specificity of the original exercise program in terms of dosage, load, and progression.

Likewise, the MoveUS Program had a significant effect on endurance, including repetitions in the T-Fast Test 30" (mean difference = 11.78 ± 1.87, $p < 0.01$; Cohen's d = 1.48) and the T-Fast Test 120" (mean difference = 37.06 ± 5.72, $p < 0.01$; Cohen's d = 1.53). This finding is consistent with previous studies that reinforced the effect of endurance training through repetitive tasks on shoulder resistance to fatigue (Reinold et al., 2018).

These changes were also observed in the delay of the fatigue appearance measured by inertial sensors, both in the T-Fast Test 30" (mean difference = 4.9 ± 1.6 seconds, $p = 0.03$; Cohen's d = 1.24) and 120" (mean difference = 33.44 ± 4.1 seconds, $p < 0.001$; Cohen's d = 3.3). Furthermore, trends in physiological fatigue measured with electromyography were noted, especially in the middle deltoid muscle in elevation in the scapular plane (mean difference = 7.9 ± 3.6 % of mean frequency change in Hz, $p = 0.04$; Cohen's d = 0.51). These results indicate that this intervention can improve neuromuscular efficiency, thus agreeing with previous researchers who highlighted the great relationship between force and endurance training on fatigue reduction (Rønnestad & Mujika, 2014).

Moreover, the MoveUS Program had a significant effect on isometric force peak (mean difference = 42.65 ± 4.9 Newtons, $p < 0.001$; Cohen's d = 1.1) and on dynamic stability measured with the MoveUS Test adjusted (mean difference = 1160.8 ± 289.6 number of repetitions x pressure in Newtons, $p < 0.001$; Cohen's d = 0.95). These gains in isometric force and unilateral wall-push-up stability indicate that the exercise program effectively enhances both shoulder force production and neuromuscular control, aligning with evidence that targeted strengthening and stability training can promote better periarticular shoulder muscles function and dynamic scapular control, helping to explain the functional changes observed.

All these results are summarized in Fig. 1.

4. Conclusions

The MoveUS Program was associated with increased endurance, reduced multivariable fatigue, improved stability, and enhanced quality of life and safety in returning to sports. Nonetheless, further research is needed to optimize the implementation of the intervention.

Acknowledgements

The authors thank the University of Málaga for providing the necessary material to develop this study and the Axarquia Hospital for providing the space to carry out the evaluations and treatments.

Conflict of Interest Statement

The authors, their immediate families, and any research foundation with which they are affiliated did not receive any financial payments or other benefits from any commercial entity related to the subject of this article.

Contributor Roles

LRP: Conceptualization, Data Curation, Formal analysis, Funding acquisition, Investigation, Methodology, Software, Writing – original draft, Writing – review & editing; MCMM: Data curation, Investigation,

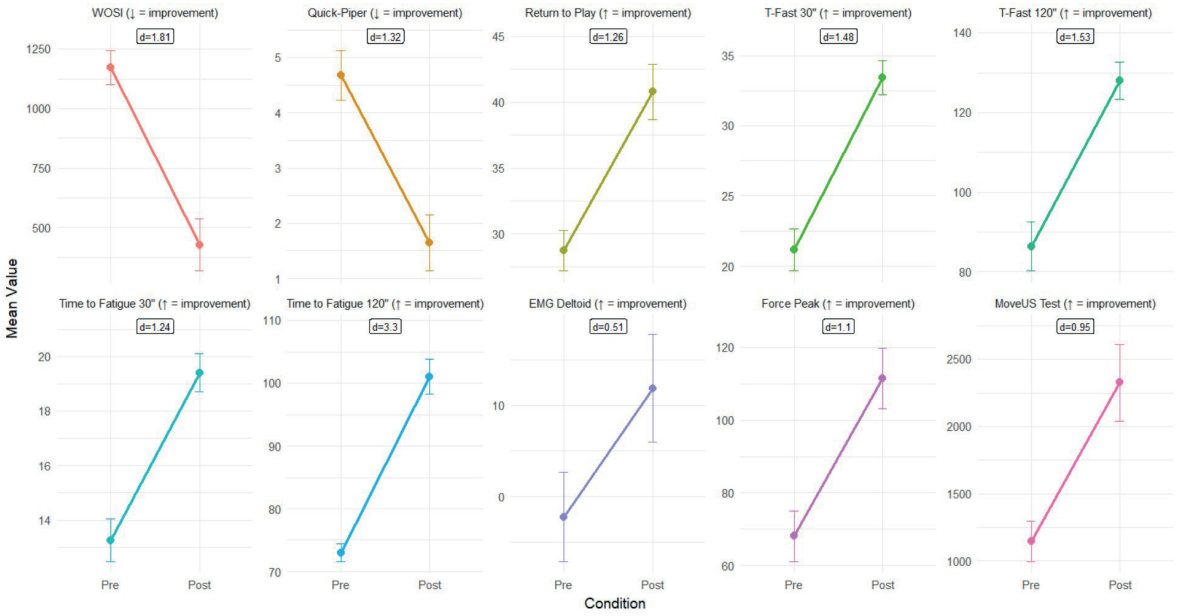

Figure 1. Pre-Post Evolution by Test (± SE) with Cohen's d.

Credit: Laura Ramírez-Pérez.

Resources, Visualization, Writing – review & editing; AICV: Conceptualization, Methodology, Project administration, Supersion, Validation, Visualization, Writing – review & editing.

Funding

This work is part of a government-funded project supported by the University Teaching Training Programme (FPU) of the Ministry of Universities of Spain. Grant number: FPU21/06296.

This work has been co-financed with FEDER funds through the "Financing for applied research projects and/or technological development projects, interdisciplinary and intersectoral for Research Groups, within the framework of the II Own Plan for Research, Transfer and Scientific Dissemination of the University of Málaga". Grant number: CTS-631.

Data, software, code availability

Data are available upon reasonable request to the corresponding author.

References

Kavaja, L., Lähdeoja, T., Malmivaara, A., & Paavola, M. (2018). Treatment after traumatic shoulder dislocation: A systematic review with a network meta-analysis. *British Journal of Sports Medicine*, *52*(23), 1498–1506. https://doi.org/10.1136/bjsports-2017-098539

Ramírez-Pérez, L., & Cuesta-Vargas, A. I. (2024). Effect of a multicomponent exercise program focused on multivariable fatigue improvement versus standard care for glenohumeral instability: MoveUS study protocol. *BMC Musculoskeletal Disorders*, *25*(1), 1013. https://doi.org/10.1186/s12891-024-08193-4

Reinold, M. M., Macrina, L. C., Fleisig, G. S., Aune, K., & Andrews, J. R. (2018). Effect of a 6-week weighted baseball throwing program on pitch velocity, pitching arm biomechanics, passive range of motion, and injury rates. *Sports Health: A Multidisciplinary Approach*, *10*(4), 327–333. https://doi.org/10.1177/1941738118779909

Rønnestad, B. R., & Mujika, I. (2014). Optimizing strength training for running and cycling endurance performance: A review. *Scandinavian Journal of Medicine & Science in Sports*, *24*(4), 603–612. https://doi.org/10.1111/sms.12104

Warby, S. A., Ford, J. J., Hahne, A. J., Watson, L., Balster, S., Lenssen, R., & Pizzari, T. (2018). Comparison of 2 exercise rehabilitation programs for multidirectional instability of the glenohumeral joint: A randomized controlled trial. *The American Journal of Sports Medicine*, *46*(1), 87–97. https://doi.org/10.1177/0363546517734508

2026-3 | International Shoulder Group (ISG) Congress 2026
2-3 June 2026, Lyon, France

Multidisciplinary Biomechanics Journal

Inter- and Intra-rater Reliability of the Shoulder Isometric Force Test (SHIFT) Protocol

Ursina Minder[a, b]*, Claudio Perret[a, b], Wiebe de Vries[a], Sabrina Koch-Borner[a, b, c], Ursina Arnet[a]

a Neuromusculoskeletal Functioning and Mobility Group, Swiss Paraplegic Research, Nottwil, Switzerland
b Faculty of Health Sciences and Medicine, University of Lucerne, Lucerne, Switzerland
c Swiss Paraplegic Centre, Nottwil, Switzerland
* Corresponding author: ursina.minder@paraplegie.ch

Received date: 15/01/2026
Accepted date: 16/03/2026
Publication date: 02/06/2026

Keywords: robustness, measurement error, strength assessment, shoulder pain, wheelchair users

1. Introduction

Assessment of shoulder muscle strength plays a crucial role in clinical practice and research and is frequently applied in both athletic (Fontánez et al., 2023) and pathological (Schrama et al., 2014) contexts. It is used to evaluate intervention effectiveness (Padulo et al., 2020) and quantify impairment. Numerous measurement protocols with varying levels of reliability are available. However, despite the increased risk of shoulder problems in wheelchair users with spinal cord injury (SCI), protocols adapted to this population are rare. As SCI directly affects trunk control, adapted strength assessment protocols with adequate reliability are required. Therefore, our goal was to evaluate a multidirectional shoulder strength assessment protocol adapted specifically for wheelchair users with SCI. Key considerations in the development of the Shoulder Isometric Force Test (SHIFT) protocol included minimizing lever arms, stabilizing the trunk, enabling testing in the individual's personal wheelchair, reducing setup complexity, while ensuring adequate standardization. The purpose of this study is to investigate the intra- and inter-rater reliability of the SHIFT protocol.

2. Methods

This reliability study was conducted in the movement laboratory of Swiss Paraplegic Research in Nottwil, Switzerland between February and April 2025. Healthy volunteers with pain-free shoulders participated in three strength measurement sessions, each separated by 48 h. Two sessions were conducted by tester A and one by tester B. Isometric shoulder abduction (ABD), adduction (ADD), flexion (FLEX), extension (EX), internal rotation (IR), external rotation (ER), and a combined abduction and external rotation task (ABD+ER) were assessed using a dynamometer (LSB350, Futek, USA) fixed to a wall-mounted rail. Each direction of movement (DOM) was tested three times with a 5 s maximal isometric hold followed by 30 s rest. Participants were seated in a wheelchair with their upper body manually fixated. Arm and body position, device placement, instructions, warm-up, familiarization and encouragement were standardized. Testers and participants were blinded to the results. Raw force data were collected and mean isometric torque was calculated over a 2 s window centred within the force application period and averaged across repetitions. Relative inter- and intra-rater reliability were assessed using inter-class correlation coefficients (ICC). Absolute reliability was quantified as minimal detectable change (MDC) and reported as MDC% relative to the mean torque of test and retest. Measurement error was further evaluated using Bland-Altman plots and comparison of limits of agreement (LoA) with the spreads of scores.

3. Results and discussion

A total of 20 participants (mean age: 36 ± 3 y, height: 170.8 ± 10.0 cm, weight: 70.6 ± 10.9 kg; 10 females) were included in the analysis.

To cite this article: Ursina Minder, Claudio Perret, Wiebe de Vries, Sabrina Koch-Borner, Ursina Arnet, Inter- and Intra-rater Reliability of the Shoulder Isometric Force Test (SHIFT) Protocol, *Multidisciplinary Biomechanics Journal*, 2026, vol. 3, p. 43–45, DOI: 10.46298/mbj.17942.

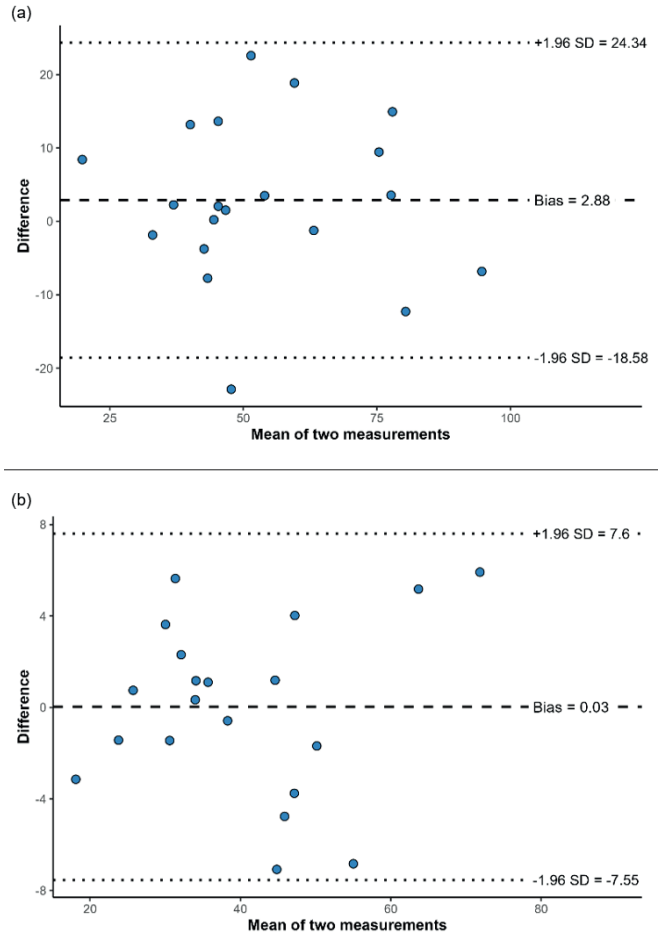

Figure 1: Bland-Altmann plots for intra-rater analysis of (a) shoulder abduction and (b) combined shoulder abduction and external rotation strength. Measurement unit: Nm. SD: standard deviation.

Relative reliability across most DOMs and rater conditions was good to excellent, with ICCs (95% CI) ranging from 0.92 (0.79-0.97) to 0.98 (0.96-0.99). Absolute reliability, expressed as MDC% ranged from 11.6 to 28.9%. Only inter-rater reliability for EX was lower, demonstrating moderate to excellent reliability (ICC of 0.82 (0.54-0.93)) and an MDC% of 41.9%. Ratios between the LoA and the spread of means were lower than 0.50 for ABD+ER, ADD, IR and ER. In contrast, higher ratios were observed for ABD, FLEX and particularly EX. The Bland-Altman plot for intra-rater ABD and ABD+ER is shown in Fig. 1.

Overall, most DOMs demonstrated high relative intra- and inter-rater reliability, except for inter-rater EX. The SHIFT protocol therefore provides a robust framework for multidirectional shoulder strength assessment tailored to wheelchair users and applicable in research and applied contexts. High relative reliability supports group-level comparison and inter-individual ranking. However, as measurement error differed between DOMs, precision at the individual level also varied. DOMs with lower measurement error (ABD+ER, ER, IR, ADD) appear particularly suitable for individual monitoring, whereas others (ABD, FLEX, EX) may be more appropriate for research and group-level comparisons. Consequently, caution is warranted when interpreting small individual changes.

Only ABD+ER and intra-rater ER, demonstrated MDC% values below the predefined 15% threshold. As no established minimal clinically important difference exists for shoulder strength, this threshold was adopted based on previous literature (Sørensen et al., 2021). For context, strength changes reported in intervention studies often exceed this threshold (e.g. ER improvements

ranged from 14.5 to 32.7% across training and surgical interventions), suggesting that the observed reliability thresholds are within a range relevant to clinically meaningful changes.

The potential and clinical relevance of the combined testing of shoulder external rotation and abduction has still to be evaluated.

4. Conclusions

The SHIFT protocol demonstrates robust relative reliability for multidirectional isometric shoulder strength assessment and supports group-level comparisons, supporting its application in wheelchair users with SCI. However, variability in absolute reliability limits sensitivity for detecting small individual changes and requires cautious interpretation in clinical and sports settings. The higher absolute reliability of the ABD+ER measure suggests potential utility for monitoring clinically meaningful strength changes.

Acknowledgements

The authors thank Lara Wasem for her contribution to this study (measurement assistant).

Conflict of Interest Statement

None.

Contributor Roles

UM: Conceptualization, Formal analysis, Investigation, Methodology, Project administration, Writing – original draft; CP: Conceptualization, Supervision, Writing – review & editing; WdV: Formal analysis, Methodology, Writing – review & editing; SKB: Investigation, Methodology, Writing – review & editing; UA: Conceptualization, Methodology, Supervision, Writing – review & editing.

Funding

This research was internally funded by Swiss Paraplegic Research.

References

Fontánez, R., De Jesus, K., Frontera, W. R., & Micheo, W. (2023). Return to sports following shoulder injury: Clinical evaluation, isokinetic, and functional testing. *Current Sports Medicine Reports, 22*(6), 191–198. https://doi.org/10.1249/jsr.0000000000001072

Padulo, J., Trajković, N., Cular, D., Grgantov, Z., Madić, D. M., Di Vico, R., Traficante, A., Alin, L., Ardigò, L. P., & Russo, L. (2020). Validity and reliability of isometric-bench for knee isometric assessment. *International Journal of Environmental Research and Public Health, 17*(12), 4326. https://doi.org/10.3390/ijerph17124326

Schrama, P. P., Stenneberg, M. S., Lucas, C., & Van Trijffel, E. (2014). Intraexaminer reliability of hand-held dynamometry in the upper extremity: a systematic review. *Archives of Physical Medicine and Rehabilitation, 95*(12), 2444–2469. https://doi.org/10.1016/j.apmr.2014.05.019

Sørensen, L., Oestergaard, L. G., van Tulder, M., & Petersen, A. K. (2021). Measurement properties of isokinetic dynamometry for assessment of shoulder muscle strength: A systematic review. *Archives of Physical Medicine and Rehabilitation, 102*(3), 510–520. https://doi.org/10.1016/j.apmr.2020.06.005

2026-3 | International Shoulder Group (ISG) Congress 2026
2-3 June 2026, Lyon, France

Multidisciplinary Biomechanics Journal

Can the Combination of Motion Tracking and Virtual Reality Make Shoulder Rehabilitation Entertaining?

Matteo Mancuso[a*], Alexandre Lädermann[b, c], Yves Schmid Dornbierer[a], Antoine Seurot[d], Caecilia Charbonnier[a, c]

a Artanim Foundation, Meyrin, Switzerland
b Division of Orthopaedics and Trauma Surgery, La Tour Hospital, Meyrin, Switzerland
c Faculty of Medicine, University of Geneva, Geneva, Switzerland
d Service of Physiotherapy, La Tour Hospital, Meyrin, Switzerland
* Corresponding author: matteo.mancuso@artanim.ch

Received date: 16/01/2026
Accepted date: 16/03/2026
Publication date: 02/06/2026

Keywords: shoulder, motion capture, virtual reality, functional assessment, physical rehabilitation

1. Introduction

Patients' adherence to the physiotherapeutic program is challenging, leading often to suboptimal recovery (Kern et al., 2019). Both virtual reality (VR) and gamification have the potential to increase patients' motivation and interest (Marley et al., 2022; Schuermans et al., 2022), shifting their focus of attention to the game instead of the challenging and potentially painful movements that they need to do for their rehabilitation, resulting in improved rehabilitation outcomes (Wulf et al., 2001).

Mostly due to their high prevalence, this study focused on the rehabilitation following three common shoulder treatments or pathologies: i) surgical stabilization of the glenohumeral joint following Latarjet's procedure (*Lat*), ii) frozen shoulders (*FS*), and iii) surgical repair of rotator cuff tears (*RCuff*). Each of these rehabilitations is usually subdivided into three phases. The first phase aims at preserving the patient's mobility while the injuries heal. The second phase aims to restore the articular range of motion (*ROM*). The third phase aims to restore the strength of the articulation.

The goal of this research project was to create a highly motivating and effective rehabilitation experience leveraging a set of high-quality VR games combined with commercially available VR hardware. This paper presents the pilot clinical study performed at La Tour Hospital, evaluating the feasibility, safety and user acceptance of the current games and physical setup on 15 patients.

2. Methods

Five *Lat*, five *FS* and five *RCuff* patients were tested (age: 39 ± 22 y.o.) targeting the timeframe between 2 to 5 weeks post-surgery, by undertaking 4 gamified sessions of 15 minutes each.

We used an HTC Vive Pro as VR headset combined with 2 hand controllers, and 5 Vive trackers 2.0 strapped to the patient's trunk, arms, and forearms to track the patients' upper body motions while immersing them in a custom-built relaxing VR environment developed in Unity. The accuracy of the tracking system for the VR hardware used was previously evaluated in Mancuso & Charbonnier, 2024.

The VR rehabilitation sessions consisted in solving several mazes that the patients controlled using the five or six main upper body exercises present in their rehabilitation protocol (Fig. 1). These movements allowed participants to tilt the virtual environment (pitch and roll) and adjust the elevation of certain platforms within the maze, thereby creating pathways that enabled a small mouse to navigate across it. The target motions of the affected upper limbs for *Lat* and *FS* patients were: i) pushing the shoulder forward, ii) pulling the shoulder backward, iii) pushing the shoulder upward, iv) flexing the elbow, v) wrist pronation, and vi) wrist supination. For the *RCuff* patients, the motions were: i) external rotation of the shoulder, ii) internal rotation of the shoulder, iii) flexion of the elbow, iv) extension of the elbow, v) anterior elevation of the arm. At the

To cite this article: Matteo Mancuso, Alexandre Lädermann, Yves Schmid Dornbierer, Antoine Seurot, Caecilia Charbonnier, Can the Combination of Motion tracking and Virtual Reality Make Shoulder Rehabilitation Entertaining?, *Multidisciplinary Biomechanics Journal*, 2026, vol. 3, p. 47–49, DOI: 10.46298/mbj.17919.

beginning of every session, the articular ROM of the patient was evaluated, and the exercises calibrated to match at least 80% of that range. Moreover, the mazes presented to the patients progressively evolved in complexity both to keep the patients' mind challenged and to increase the frequency of the movements needed to solve them.

Figure 1. User with the headset, and sensors strapped to his upper limbs and waist, solving a maze in VR using his shoulder's movements as input. On the screen in the background, a holographic coach stands ready to re-explain the motor tasks or to correct the user in case of erroneous movements. See also a demo video available at https://youtu.be/BAcPVS4HW40?si=3lIaqle9EZ224Umw.

After each session, the patients filled in a questionnaire aiming to measure the patient's i) cybersickness, ii) motivation (reduced version of the post-experimental Intrinsic Motivation Inventory (*IMI*), and iii) perceived risk during the tasks (3 custom questions). Moreover, the *IMI* questionnaire provided 4 scores to evaluate interest, competence, effort, and pressure. All the questions and subsequent scores were rated on a 1 to 7 scale, with 1 corresponding to "not at all true", 4 "somewhat true" and 7 "very true".

3. Results

All the patients involved were able to successfully complete the gamified protocol without particular difficulties. No patient reported significant amount of discomfort as confirmed by the Cybersickness scale (μ_{Lat}=1.2±0.5, μ_{FS}=1.5±1.1, μ_{RCuff}=1.1±0.3), with the main reported effect being "Ocular fatigue" (μ_{Lat}=1.7, μ_{FS}=2.1, μ_{RCuff}=1.0) and "Difficulty to focus" (μ_{Lat}=1.1, μ_{FS}=1.8, μ_{RCuff}=1.2). The patients did not feel endangered as confirmed by the evaluation of perceived risk (μ_{Lat}=1.0±0.2, μ_{FS}=1.4±1.0, μ_{RCuff}=1.2±0.6). Based on the subscales of the *IMI* questionnaire, the patients did not feel pressured (2.0±1.8), the effort perceived was average (4.2±2.1), but the interest (6.1±1.1) and perceived competence (5.3±1.3) were good.

4. Conclusions

This pilot study showed that patients were all able to perform the requested exercises while playing their rehabilitation games. Overall, within the limits of a small sample size of 60 sessions (15 patients performing 4 sessions each), the patients appeared motivated to perform their rehabilitation sessions without being exposed to risks or discomfort. Those results are promising, but a larger study involving a larger number of patients should be performed and compared with a control group to objectively and reliably measure the clinical validity and effectiveness of this VR approach. More specifically, we aim in a further study at i) validating the clinical effectiveness of the present approach both for the restoration of the patients' mobility and for the recovery of their capacity to perform their daily activities, and ii) extending the current methodology to other rehabilitation phases of the treatments presented.

Acknowledgements

We would like to thank Michelle Drocco and Brian Rochat, the 3D artists who created the game environment; Valérie Juillard for animating the game characters; Marlène Arévalo for the voice-overs as well as Bart Kevelham for his invaluable assistance and insightful comments on this research.

Conflict of Interest Statement

None.

Contributor Roles

MM: Data curation, Formal analysis, Investigation, Software, Writing – original draft; AL: Investigation, Supervision; YSD: Software; AS: Investigation; CC: Formal analysis, Supervision; All: Conceptualization, Methodology, Writing – review & editing.

Funding

This work was entirely funded by Artanim Foundation's internal funds.

References

Kern, F., Winter, C., Gall, D., Kathner, I., Pauli, P., & Latoschik, M. E. (2019). Immersive virtual reality and gamification within procedurally generated environments to increase motivation during gait rehabilitation. *26th IEEE Conference on Virtual Reality and 3D User Interfaces, VR 2019 - Proceedings*, 500–509. https://doi.org/10.1109/VR.2019.8797828

Mancuso, M., & Charbonnier, C. (2024). Technical evaluation of the fidelity of the HTC Vive for upper limb tracking. *42nd International Society of Biomechanics in Sport Conference*, 624–627. https://commons.nmu.edu/isbs/vol42/iss1/188

Marley, W. D., Barratt, A., Pigott, T., Granat, M., Wilson, J. D., & Roy, B. (2022). A multicenter randomized controlled trial comparing gamification with remote monitoring against standard rehabilitation for patients after arthroscopic shoulder surgery. *Journal of Shoulder and Elbow Surgery*, *31*(1), 8–16. https://doi.org/10.1016/j.jse.2021.08.019

Schuermans, J., Van Hootegem, A., Van den Bossche, M., Van Gendt, M., Witvrouw, E., & Wezenbeek, E. (2022). Extended reality in musculoskeletal rehabilitation and injury prevention - A systematic review. *Physical Therapy in Sport*, *55*, 229–240. https://doi.org/10.1016/j.ptsp.2022.04.011

Wulf, G., McNevin, N., & Shea, C. H. (2001). The automaticity of complex motor skill learning as a function of attentional focus. *The Quarterly Journal of Experimental Psychology A*, *54*(4), 1143–1154. https://doi.org/10.1080/02724980143000118

2026-3 | International Shoulder Group (ISG) Congress 2026
2-3 June 2026, Lyon, France

Multidisciplinary Biomechanics Journal

Muscle Activation Synergies and Contributions to Shoulder Torques across Testing Positions

Eleonora Croci[a, b*], Corina Nüesch[a, b, c], Dirk Maier[b], Andreas Marc Müller[a, b, d], Annegret Mündermann[a, b, d, e]

a Department of Biomedical Engineering, University of Basel, Basel, Switzerland
b Department of Orthopaedics and Traumatology, University Hospital Basel, Basel, Switzerland
c Department of Spine Surgery, University Hospital Basel, Basel, Switzerland
d Department of Clinical Research, University of Basel, Basel, Switzerland
e Department of Teaching, Research and Development, Schulthess Clinic, Zurich, Switzerland
* Corresponding author: eleonora.croci@unibas.ch

Received date: 14/01/2026
Accepted date: 16/03/2026
Publication date: 02/06/2026

Keywords: electromyography, torque, positions, rotation, flexion, abduction

1. Introduction

Muscle strength is an important part of the clinical evaluation process to guide therapy and rehabilitation. Shoulder muscle strength can be measured objectively using isokinetic dynamometry, often in various testing positions including standing, supine, and sitting (Edouard et al., 2011). Electromyography (EMG) provides an important complement to these assessments. Previous studies have shown that muscle activity of the deltoid, infraspinatus, trapezius and serratus anterior during isokinetic external rotation at 45° and 90° abduction is position-dependent (Sung et al., 2023). However, it remains unclear whether testing position affects how individual muscle activation pattern contribute to the variation in torque. This study aimed to determine the relative contributions of different muscles to joint torque across multiple shoulder tasks performed in various testing positions, using an EMG-based synergy approach.

2. Methods

Ten men and ten women (mean ± standard deviation, age: 25.4 ± 3.1 years; height: 1.75 ± 0.10 m; body mass: 71.0 ± 11.7 kg; BMI: 23.0 ± 2.3 kg/m^2) performed 8 isokinetic shoulder tasks at 60°/s for each side with the Humac Norm dynamometer (CSMi, each 2 trials with 3 repetitions; tasks: internal/external rotation at 15° abduction in standing and seated position, and at 90° abduction in supine and seated position; flexion/extension in supine and seated position; and abduction/adduction in lateral recumbent and seated position).

EMG signals of the three deltoids, infraspinatus, biceps brachii, latissimus dorsi, pectoralis major and upper trapezius (Criswell, 2011; Hermens et al., 2000) were recorded with surface EMG sensors (Ultium EMG, Noraxon), filtered with a 4th order bandpass filter (40–450 Hz), full-wave rectified, and smoothed using a 100-ms moving average window (De Luca et al., 2010). For each muscle, the EMG trajectories of each trial were normalised to the maximum values across all trials. Peak torques and normalized EMG signals at peak torques were extracted for each repetition, task, side and participant.

Non-negative matrix factorization was applied to EMG data at peak torque to reduce collinearity among muscle activations, and the first three synergies were retained (Moghadam et al., 2013). Peak torques for each task were then modelled using linear mixed-effects models with the synergies and testing positions as fixed effects (with interaction) and a random intercept for each participant. The estimated regression coefficients reflected the mechanical contribution of each synergy in a given position. The group-level percentage of the approximate torque contributions for each muscle was then estimated. Differences in testing positions larger than 10% were outlined.

To cite this article: Eleonora Croci, Corina Nüesch, Dirk Maier, Andreas Marc Müller, Annegret Mündermann, Muscle Activation Synergies and Contributions to Shoulder Torques across Testing Positions, *Multidisciplinary Biomechanics Journal*, 2026, vol. 3, p. 51–53, DOI: 10.46298/mbj.17932.

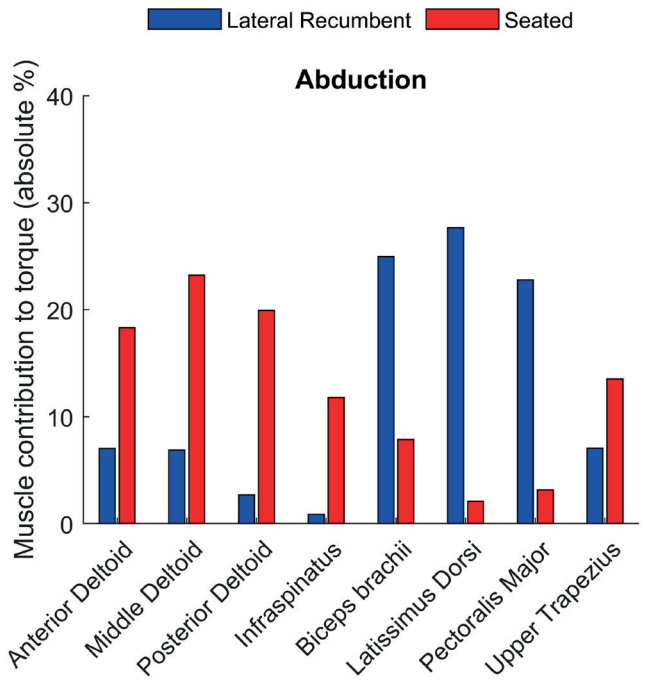

Figure 1. Estimated group-level muscle contribution per torque by position for abduction task.

Credit: EC.

3. Results and discussion

Across all tasks, the first three synergies accounted for 93–95% of the EMG variance at peak torque. The model explained most of the variance in peak joint torque across all tasks (conditional $R^2 \geq 0.963$), while fixed effects accounted for 33.2 to 38.3% of the variance (marginal R^2).

The relative contribution of individual muscles varied across tasks and differed between testing positions, but mostly similar contribution patterns were observed. All comparison described here are comparisons to the seated position. The latissimus dorsi and pectoralis major contributed more to the external rotation torque at 15° abduction when standing (Δ: 10.3 to 11.9%). The middle and posterior deltoids contributed less (Δ: -17.9 to -10.6%) and the upper trapezius contributed more (Δ: 18.0%) to external rotation torque at 90° abduction when supine. The anterior deltoid and latissimus dorsi contributed less to flexion torque when supine (Δ: -14.6 to -12.0%). The infraspinatus and upper trapezius contributed more (Δ: 13.1 to 15.6%) and the latissimus dorsi and pectoralis major less (Δ: -30.1 to -10.6%) to extension torque when supine.

Abduction showed quite different muscle contribution patterns to torque between the lateral recumbent and seated position (Figure 1). The three deltoids, infraspinatus and biceps brachii contributed less (Δ: -17.2 to -10.9%) and the biceps brachii, latissimus dorsi and pectoralis major contributed more (Δ: 17.1 to 25.5%) to abduction when in the lateral recumbent position.

The anterior and middle deltoid and the upper trapezius contributed more (Δ: 11.8 to 12.1%) and the biceps brachii and latissimus dorsi contributed less (Δ: -22.0 to -14.7%) to adduction torque when in the lateral recumbent position.

Similar muscle contributions to torque were observed for internal rotation tasks at both 15° and 90° abduction between the standing or supine and seated positions.

This study acknowledges the limitations of EMG measurements (e.g. crosstalk) and the small number of muscles used for this model.

4. Conclusions

The modest marginal R^2 indicated a considerable between-subject variation influencing torque production. This reflects the complexity of the neuromuscular torque production. Nevertheless, some position-dependent differences in muscle contribution to peak torque were identified for most of the tasks, indicating that differences in postural stability and gravity derived from the testing positions can lead to different muscle coordination strategies. Overall, these findings could support neuromuscular training to promote neuromuscular plasticity.

Acknowledgements

We would like to thank Marie-Louise Karg and Rishi Dilip Soni for their help with the data collection.

Conflict of Interest Statement

The authors declare no conflict of interest.

Contributor Roles

EC: Conceptualization, Methodology, Formal analysis, Data Curation, Writing original draft; CN: Methodology, Writing – review & editing; DM: Conceptualization, Writing – review & editing; AMM: Supervision, Writing – review & editing; AM: Conceptualization, Supervision, Writing – review & editing.

Funding

Funding was mainly provided by departmental means of the Department of Biomedical Engineering of the University of Basel by providing the infrastructure.

Data, software, code availability

Data are available upon reasonable request from the corresponding author.

References

Criswell, E. (2011). *Cram's introduction to surface electromyography*. Sudburry (MA): Jones Bartlett Publ.

De Luca, C.J., Donald Gilmore, L., Kuznetsov, M., & Roy, S.H., (2010). Filtering the surface EMG signal: Movement artifact and baseline noise contamination. *J. Biomech., 43*, 1573–1579. https://doi.org/10.1016/j.jbiomech.2010.01.027

Edouard, P., Samozino, P., Julia, M., Cervera, S.G., Vanbiervliet, W., Calmels, P., & Gremeaux, V. (2011). Reliability of isokinetic assessment of shoulder-rotator strength: A systematic review of the effect of position. *J. Sport Rehabil. 20*, 367–383. https://doi.org/10.1123/jsr.20.3.367

Hermens, H.J., Freriks, B., Disselhorst-Klug, C., & Rau, G. (2000). Development of recommendations for SEMG sensors and sensor placement procedures. *J. Electromyogr. Kinesiol., 10*, 361–374. https://doi.org/10.1016/s1050-6411(00)00027-4

Moghadam, M.N., Aminian, K., Asghari, M., & Parnianpour, M. (2013). How well do the muscular synergies extracted via non-negative matrix factorisation explain the variation of torque at shoulder joint? *Comput. Methods Biomech. Biomed. Engin., 16*, 291–301. https://doi.org/10.1080/10255842.2011.617705

Sung, J., Jung, W., Wang, J., & Kim, J.-H. (2023). The effects of body positions and abduction angles on shoulder muscle activity patterns during external rotation exercises. *Healthcare, 11*(14), 1977, 1–12. https://doi.org/10.3390/healthcare11141977

2026-3 | International Shoulder Group (ISG) Congress 2026
2-3 June 2026, Lyon, France

Multidisciplinary Biomechanics Journal

Effect of Camera Position on the Robustness of a 2D Markerless Motion Capture System for Assessing Shoulder Kinematics

Maxime Perek[a*], Yoann Blache[a], Felix Lefebvre[b], Isabelle Rogowski[a], Brice Guignard[a]

a Universite Claude Bernard Lyon 1, LIBM, Laboratoire Interuniversitaire de Biologie de la Motricité, UR 7424, F-69622 Villeurbanne, France
b Trinoma, Villefort, France
* Corresponding author: maxime.perek@univ-lyon1.fr

Received date: 13/01/2026
Accepted date: 16/03/2026
Publication date: 02/06/2026

Keywords: upper limb, camera angle, deep neural network

1. Introduction

Markerless motion capture has emerged as a promising alternative to marker-based systems for assessing shoulder kinematics, offering accessibility and ecological validity. Monocular 2D approaches are particularly attractive because they require only a single camera and minimal experimental setup. However, these models rely on the visual appearance of the shoulder from a single viewpoint; changes in camera orientation or position may therefore influence neural network predictions (Berlinger et al., 2025). Understanding the sensitivity of a 2D markerless system to such variations is essential for reliable implementation in clinical environments, where camera placement may not be standardized.

The objective of this study was therefore to evaluate the robustness of a 2D deep-learning–based markerless system to changes in camera position when estimating humerothoracic (HT), scapulothoracic (ST), and scapulohumeral (SH) angles.

2. Methods

2.1 Participants

Eighty-eight healthy participants (35 women; age: 23.5 ± 3.7 yrs; height: 173.3 ± 7.2 cm; body mass: 68.0 ± 8.5 kg; body fat: 19.1 ± 5.9%) provided written informed consent. The protocol was approved by the local ethics committee (CER-UdL #2022-10-13-002).

2.2. Procedure

Participants held 12 standardized static postures representative of common upper-limb elevations across three movement planes (scaption, flexion, abduction) and the lateral scapular slide test. For each posture, two iPad 10th-generation devices (4032 × 3024 px) captured two successive images: bare back, back with 10 anatomical markers placed after palpation: the seventh cervical vertebra, the eighth thoracic vertebra, and bilaterally the acromial angle, trigonum spinae, inferior angle of the scapula, and lateral humeral epicondyle. A rigid positioning guide was held by the participants to minimize body motion between images. A 300-mm ruler was placed in the thoracic plane enabling pixel-to-millimeter scaling.

The reference iPad was positioned in the frontal plane, 3 m behind the participant, at a height of 1.5 m. The second iPad was systematically displaced to simulate alternative viewpoints. Relatively to the position of the reference iPad, four orientation changes (up/down tilt and left/right pan of ±10°) and four translations (±20 cm in height or lateral position) were applied alone or in combination in random order, resulting in 20 displaced viewpoints.

2.3. Deep neural network training and evaluation

The network (ResNet-50, DeepLabCut) was trained to identify the location of 10 anatomical landmarks for 150,000 iterations on markerless images labeled

To cite this article: Maxime Perek, Yoann Blache, Felix Lefebvre, Isabelle Rogowski, Brice Guignard, Effect of Camera Position on the Robustness of a 2D Markerless Motion Capture System for Assessing Shoulder Kinematics, *Multidisciplinary Biomechanics Journal*, 2026, vol. 3, p. 61–63, DOI: 10.46298/mbj.17936.

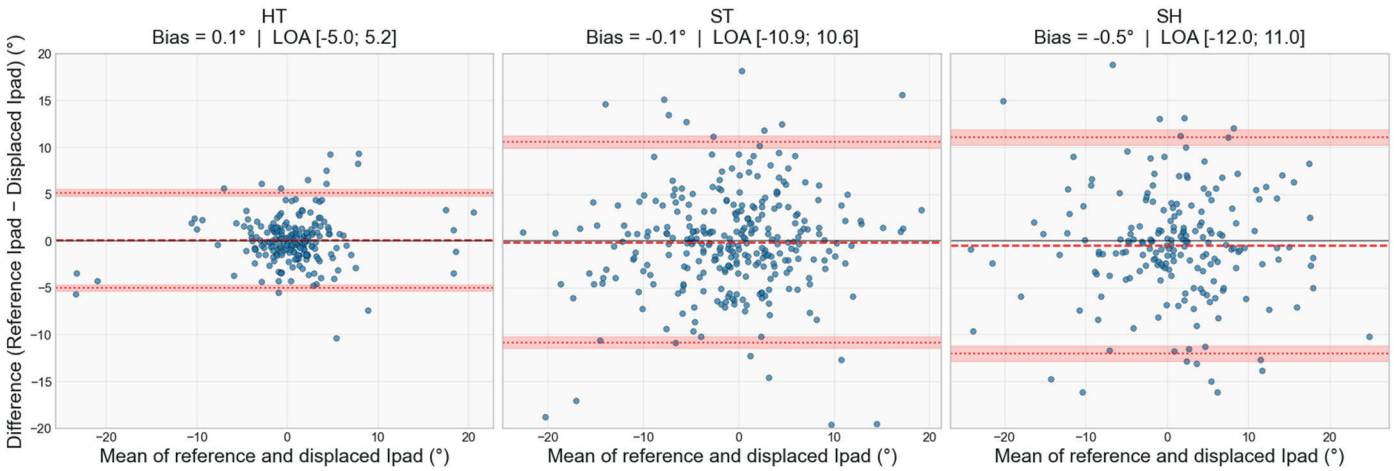

Figure 1. Bland–Altman plots comparing joint-angle errors obtained from the reference and displaced iPads for humerothoracic (HT), scapulothoracic (ST), and scapulohumeral (SH) angles. Each plot displays the mean difference (bias: red dotted line) and the limits of agreement (LOA) with a 95% confidence interval (red transparent area).

Credit: Perek.

via palpation, following a previously described labelling procedure (Perek et al., 2026), using images from 59 participants (reference iPad), and tested on all images (reference and displaced iPads) from an independent set of 29 participants. Joint angles (HT, ST and SH) were computed from anatomical landmark 2D coordinates following ISB recommendations (Wu et al., 2005). Then, joint-angle errors were defined, for each pose and iPad, as the differences between neural-network predictions and palpation. Linear mixed models were used to evaluate the effects of PLANE (flexion vs scaption vs abduction) and iPad POSITION (reference vs. displaced) on joint-angle errors, with participants as random intercept. Level of significance was set at $p < 0.05$, Tukey post-hoc tests and effect sizes (η^2 and Cohen's d) were reported when required. Inter-device agreement across configurations was then assessed using Bland–Altman analyses.

3. Results and discussion

Linear mixed models revealed neither significant interaction nor main effects of PLANE and iPad POSITION ($p > 0.05$, $\eta^2 < 0.003$) on joint angles errors, indicating that camera displacements did not systematically bias HT, ST, or SH angle estimates.

Bland–Altman analyses showed small biases in joint angle errors (from −0.5° to 0.1°), with limits of agreement up to ±5° for HT, ±11° for ST and ±12° for SH (Fig. 1).

Although individual predictions varied across configurations, no systematic directional bias was observed, resulting in comparable overall accuracy. In most cases, absolute error magnitudes remained limited; occasional configuration-specific increases or decreases in error were observed, without a consistent trend favoring either the reference or displaced camera positions. Previous monocular 2D markerless studies have reported view-dependent effects across different populations under markedly different camera viewpoints (>20° error) (Baldinger et al., 2025). In contrast, moderate and controlled camera changes have been shown to preserve kinematic accuracy in human gait analysis (Wang et al., 2024). Consistent with these findings, the magnitude of the overall errors (represented by the x-axis of figure 1) observed in the present study (predominantly within −20° to 20°) is comparable to the errors reported in Perek et al. (2026). These findings suggest that our 2D pose estimation system tolerates natural viewpoint changes without systematic bias, while shoulder joint angle estimates remain sensitive to parallax effects.

4. Conclusions

This study demonstrates that changes in camera position do not systematically degrade 2D neural network predictions. These findings suggest that small adjustments in camera positioning, as typically occur in clinical environments, are unlikely to affect neural

network accuracy. However, joint angle estimation is likely affected by parallax effects; an optimal camera axis perpendicular to the plane of motion should therefore still be preferred. Future studies should further assess the sensitivity of the neural network to environmental variations (e.g., lighting or background changes).

Conflict of Interest Statement

None.

Contributor Roles

MP: Conceptualization, Methodology, writing original draft; YB: Conceptualization, Methodology, Validation, Supervision, Writing – review & editing draft; FL: software, ressources, review & editing draft; IR: Methodology, Validation, Supervision, review & editing draft; BG: Conceptualization, Methodology, Validation, Supervision Writing – review & editing draft.

References

Baldinger, M., Reimer, L. M., & Senner, V. (2025). Influence of the camera viewing angle on OpenPose validity in motion analysis. *Sensors*, *25*(3), 799. https://doi.org/10.3390/s25030799

Mathis, A., Mamidanna, P., Cury, K. M., Abe, T., Murthy, V. N., Mathis, M. W., & Bethge, M. (2018). DeepLabCut: markerless pose estimation of user-defined body parts with deep learning. *Nature Neuroscience*, *21*(9), 1281–1289. https://doi.org/10.1038/s41593-018-0209-y

Perek, M., Guignard, B., Lefebvre, F., Rogowski, I., & Blache, Y. (2026). Automatic identification of shoulder landmarks with a single camera in healthy participants. *Engineering Research Express, 8*(3), 035223. https://doi.org/10.1088/2631-8695/ae3ef7

Wang, H., Su, B., Lu, L., Jung, S., Qing, L., Xie, Z., & Xu, X. (2024). Markerless gait analysis through a single camera and computer vision. *Journal of biomechanics*, *165*, 112027. https://doi.org/10.1016/j.jbiomech.2024.112027

Wu G, van der Helm FC, Veeger HE, et al. (2005). ISB recommendation on definitions of joint coordinate systems—Part II: shoulder, elbow, wrist and hand. *Journal of Biomechanics, 38*(5), 981–992. https://doi.org/10.1016/j.jbiomech.2004.05.042

2026-3 | International Shoulder Group (ISG) Congress 2026
2-3 June 2026, Lyon, France

Multidisciplinary Biomechanics Journal

Patient-Specific Musculoskeletal Model of the Shoulder: Kinematics Comparison of Linear Scaling and Statistical Shape Model Scaling

Jeremy Genter[a*], Eleonora Croci[b, c], Ajay Seth[d], Lisa Mareschal[a], Dominic Gascho[e], Eva Deininger-Czermak[e, f], Andreas M. Müller[b, c], Annegret Mündermann[b, g], Daniel Baumgartner[a]

a Institute of Mechanical Systems, Zürich University of Applied Sciences, Switzerland
b Department of Biomedical Engineering, University of Basel, Switzerland
c Department of Orthopaedics and Traumatology, University Hospital of Basel, Switzerland
d Department of Biomechanical Engineering, TU Delft, Netherlands
e Institute of Forensic Medicine, University of Zurich, Switzerland
f Department of Nuclear Medicine, University Hospital Zurich, Zurich, Switzerland
g Department of Teaching, Research and Development, Schulthess Clinic, Zurich, Switzerland
* Corresponding author: jeremy.genter@zhaw.ch

Received date: 14/01/2026
Accepted date: 16/03/2026
Publication date: 02/06/2026

Keywords: statistical shape modeling (SSM), musculoskeletal modeling, shoulder, patient-specific models

1. Introduction

Musculoskeletal (MSK) models are widely used to study joint and muscle loading during activities of daily living (ADL). In OpenSim, subject-specific morphology is commonly obtained by linear scaling from external markers, which assumes uniform scaling and retains generic bone and joint morphology. Bone morphology and joint center location affect the shoulder complex's kinematics, limiting anatomical fidelity (Lempereur et al., 2019). Statistical shape models (SSMs) provide a data-driven alternative to subject-specific scaling by capturing population-level variability in bone morphology and enabling anatomically consistent morphing of MSK structures, as demonstrated in gait applications (Bakke & Besier, 2020). It remains unclear whether these anatomical refinements lead to measurable differences in kinematics during shoulder movements in ADL. The purpose of this study was to compare the effects of SSM-based against linear scaling on scapulothoracic and glenohumeral (GH) joint kinematics during ADL.

2. Methods

2.1 Activities of daily living

Seven healthy subjects performed hair combing, moving a coffee pot, hammering, placing a 2-kg weight on a shelf at navel height and head height, and lifting 10 kg beside the body. Each ADL was repeated three times and recorded using an optical motion capture system (Vicon, Oxford, UK) at 200 Hz, according to the protocol described by Croci et al. (2022).

2.2 Musculoskeletal model and scaling

The Seth et al. (2019) shoulder model was compared under OpenSim linear scaling and SSM-based morphing using a shoulder SSM from Soltanmohammadi et al. (2020).

Linear scaling was computed from the distances of the static trial markers. For SSM morphing, the shape parameters of the shoulder were optimized to match the radiographic anatomical measures derived from coronal-plane Dixon MRI (e.g., glenoid version and inclination, critical shoulder angle, acromial index and slope, lateral acromial angle).

Joint definitions were updated from the morphed bony landmarks following the Seth et al. (2019) shoulder model, with the scapulothoracic joint defined from Angulus Acromialis, Angulus Inferior and Trigonum Spinae Scapulae, the acromioclavicular joint center from the corresponding landmark, and the GH joint center obtained by sphere fitting the humeral head condyles. The model markers were then adjusted to align with the static trial in both scaling methods. Scapulothoracic and

To cite this article: J. Genter, E. Croci, A. Seth, L. Mareschal, D. Gascho, E. Deininger-Czermak, A. M. Müller, A. Mündermann, D. Baumgartner, Patient-Specific Musculoskeletal Model of the Shoulder: Kinematics Comparison of Linear Scaling and Statistical Shape Model Scaling, *Multidisciplinary Biomechanics Journal*, 2026, vol. 3, p. 65–67, DOI: 10.46298/mbj.17937.

GH joint kinematics were computed using OpenSim's inverse kinematics (IK) tool. Overall tracking performance was summarized using OpenSim's IK root mean square (RMS) marker-tracking error tool. This was applied to all model–experimental marker pairs, and the results were computed per ADL and averaged across repetitions and ADL within each subject.

2.3 Statistics

Paired Wilcoxon signed-rank tests were used to compare overall RMS marker-tracking errors at the subject level between SSM-based and linear scaling across all ADL. Using hair combing as a representative example, we compared scapulothoracic and GH joint kinematics using one-dimensional statistical nonparametric mapping (SnPM) with a repeated-measures design over normalized task duration. To distinguish systematic offsets from shape variations, waveform similarity was quantified using the coefficient of multiple correlation (CMC) on mean-centered waveforms, as well as the RMS difference for each degree of freedom.

3. Results and discussion

RMS marker-tracking error was lower for SSM-based than for linear scaling (11.6 ± 2.7 mm vs 13.6 ± 4.2 mm; $p = 0.031$). SnPM identified systematic differences in scapulothoracic and GH joint kinematics between SSM-based and linear scaling over substantial portions of the task (Figure 1). Waveform shape agreement was high (CMC >= 0.90) with RMS differences ranging from 2.4° to 9.8° (Table 1).

Table 1. Waveform similarity between SSM-based and linear scaling for each scapulothoracic and GH degree of freedom, reported as mean (SD) coefficient of multiple correlation (CMC; mean-centered waveforms) and root-mean-square difference (RMSD) across subjects.

Degree of Freedom	CMC	RMSD (°)
$scapula_{abduction}$	0.97 (0.04)	4.5 (2.5)
$scapula_{elevation}$	0.92 (0.07)	3.7 (1.5)
$scapula_{upward\ rot}$	1.00 (0.00)	3.1 (2.6)
$scapula_{winging}$	0.99 (0.01)	7.3 (2.9)
$plane_{elevation}$	1.00 (0.00)	9.8 (4.8)
$shoulder_{elevation}$	0.90 (0.25)	2.4 (2.5)
$axial_{rotation}$	0.96 (0.10)	8.2 (3.8)

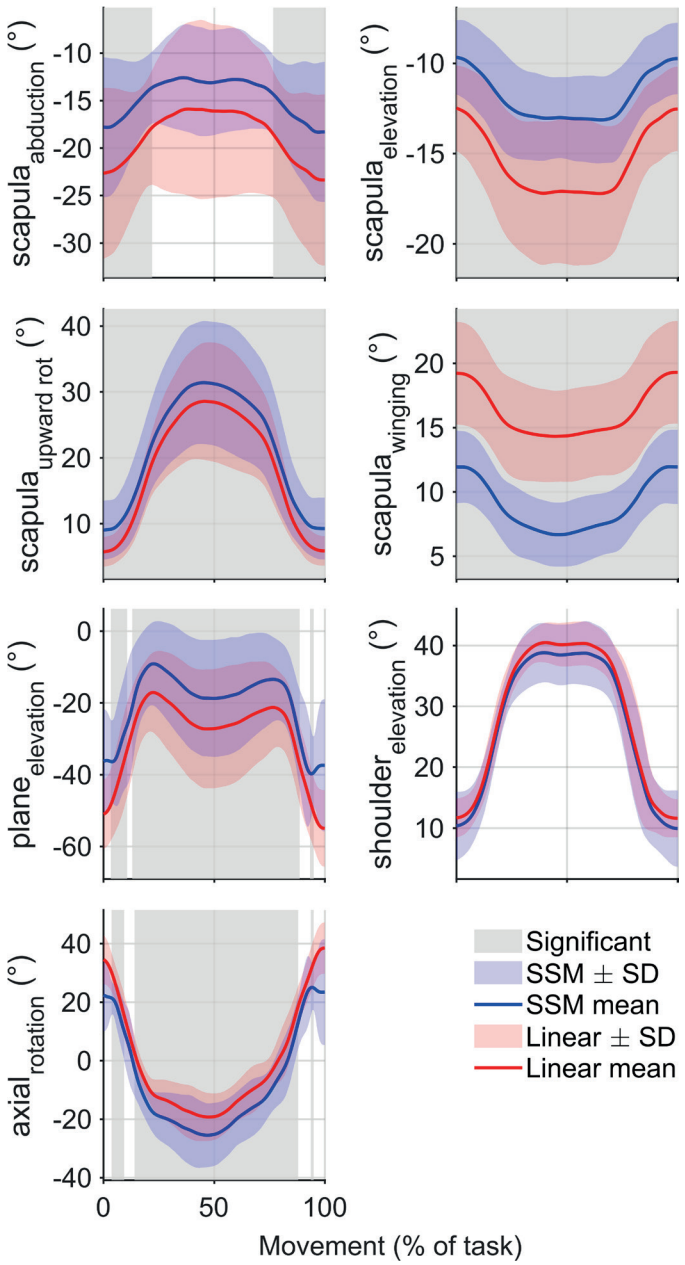

Figure 1. Scapulothoracic and GH joint kinematics during the combing task for SSM-based and linear scaling.

SSM-based scaling produced systematic offsets in scapulothoracic and GH joint kinematics while achieving lower RMS marker-tracking errors than linear scaling. This suggests improved IK accuracy for ADL. This is likely due to SSM-based scaling producing more anatomically consistent scapulothoracic and GH joint definitions than linear scaling. However, SSM morphing is limited to workflows that include subject imaging and radiographic anatomical measures labeling.

4. Conclusions

SSM-based scaling reduced RMS marker-tracking error compared to linear scaling across ADL. As demonstrated by the hair-combing task, SSM-based scaling produced consistent differences in scapulothoracic and GH joint kinematics. These results suggest that anatomically informed SSM scaling is beneficial for creating subject-specific shoulder simulations. Additionally, they demonstrate that the scaling approach can impact kinematics and downstream loading estimates.

Conflict of Interest Statement

None.

Contributor Roles

JG: Conceptualization, Methodology, Formal analysis, Visualization, Funding acquisition, Supervision, Project administration, Writing – review & editing; AM,BD: Conceptualization, Methodology, Funding acquisition, Supervision, Writing – review & editing; EC: Conceptualization, Methodology, Resources, Writing – review & editing; LM&EDC: Methodology, Writing original draft; DG: Conceptualization, Methodology, Funding acquisition, Writing – review & editing; AS&AMM: Conceptualization, Supervision, Writing – review & editing.

Funding

This study used partly data from the liTrans study (Swiss National Science Foundation, SNF 189082) and was funded by the Digitalization Initiative of the Zurich Higher Education Institutions (DIZH).

References

Bakke, D., & Besier, T. (2020). Shape model constrained scaling improves repeatability of gait data. *Journal of Biomechanics, 107*, 109838. https://doi.org/10.1016/j.jbiomech.2020.109838

Croci, E., Eckers, F., Nüesch, C., Aghlmandi, S., Kovacs, B. K., Genter, J., . . . Mündermann, A. (2022). Load-Induced Glenohumeral Translation After Rotator Cuff Tears: Protocol for an In Vivo Study. *JMIR Res Protoc, 11*(12), e43769. https://doi.org/10.2196/43769

Lempereur, M., Brochard, S., Leboucher, J., Leboeuf, F., Rémy-Néris, O., & Borotikar, B. (2019). Effects of gleno-humeral joint centre mislocation on gleno-humeral kinematics and kinetics. *Computer Methods in Biomechanics and Biomedical Engineering, 22*(7), 764–771. https://doi.org/10.1080/10255842.2019.1590822

Seth, A., Dong, M., Matias, R., & Delp, S. (2019). Muscle contributions to upper-extremity movement and work from a musculoskeletal model of the human shoulder. *Frontiers in Neurorobotics, 13*, 90. https://doi.org/10.3389/fnbot.2019.00090

Soltanmohammadi, P., Elwell, J., Veeraraghavan, V., Athwal, G. S., & Willing, R. (2020). Investigating the effects of demographics on shoulder morphology and density using statistical shape and density modeling. *Journal of Biomechanical Engineering, 142*(12). https://doi.org/10.1115/1.4047664

2026-3 | International Shoulder Group (ISG) Congress 2026
2-3 June 2026, Lyon, France

Multidisciplinary Biomechanics Journal

Preliminary Evaluation of the Kinematics of a Shoulder Musculoskeletal Model during Arm Abduction

Sandrine Bousigues, Sonia Duprey*, Sacha Guitteny, Raphael Dumas

Univ Eiffel, Univ Lyon 1, LBMC_UMR_T9406, F-69622 Lyon, France
* Corresponding author: sonia.duprey@univ-lyon1.fr

Received date: 14/01/2026
Accepted date: 16/03/2026
Publication date: 02/06/2026

Keywords: biplane x-rays, inverse kinematics, skin markers, soft tissue artefact, kinematic constraints

1. Introduction

Shoulder musculoskeletal models enable to analyze muscle function during motor tasks (Hasan et al., 2025) and generally rely on accurate kinematics as input data. Shoulder kinematics is often captured using skin markers and optoelectronic cameras. The accuracy of the results is affected by the soft tissue artefact (STA), which is especially large for this joint (Cereatti et al., 2017). STA can be compensated using kinematic constraints and multibody kinematics optimization (MKO). In this optimization, the choice of the kinematic constraints has a direct influence on the calculated joint angles and displacements but evaluating their reliability remains difficult due to the challenges in obtaining reference values. Dumas & Duprey (2022) used biplane X-ray data to evaluate the effect of different kinematic constraints for the gleno-humeral joint on MKO. Promising results were obtained with a sphere-on-sphere kinematic constraint.

Thus, the present study proposes to include a sphere on-sphere glenohumeral constraint to a whole shoulder musculoskeletal model. A preliminary evaluation of the model using the biplane X-ray dataset from Dumas & Duprey (2022) is presented.

2. Methods

2.1 Arm abduction data

Biplane X-rays of one asymptomatic male participant (43 years old, 1.70 m, 65 kg) equipped with 12 radio-opaque skin markers on humerus, scapula, and thorax, were acquired at 0°, 45°, 90°, 120°, 150° and 180° of arm abduction.

2.2 Reference kinematics

Segment coordinate systems, following the ISB recommendations (Wu et al., 2005), were embedded within the 3D reconstructions of the scapula and the humerus using numerical palpation for the landmark definition, and were constructed from skin markers for the thorax. Reference kinematics corresponds to the gleno-humeral angles and displacements and the scapulo-thoracic angles computed using respectively the XZY and YXZ sequences of rotations.

2.3 Model-derived kinematics

After gap filling (using rigid clustering and interpolation) the radio-opaque markers' trajectories, MKO was applied to track the skin markers using a scaled shoulder musculoskeletal model built with the geometry of the OpenSim model (Hasan et al., 2025), initially with 7 degrees of freedoms (DoFs). The glenoid curve formulation for joint stability of Hasan et al., (2025) was reformulated as a sphere-on-sphere glenohumeral kinematic constraint. The humeral head and glenoid radii were 3.5 mm and 10 mm, respectively. Including this sphere-on-sphere kinematic constraint resulted in the addition of two glenohumeral displacements and thus a 9-DoF shoulder musculoskeletal model. The MKO was performed in Matlab using natural coordinates (El Habachi et al., 2015).

To cite this article: Sandrine Bousigues, Sonia Duprey, Sacha Guitteny, Raphael Dumas, Preliminary Evaluation of the Kinematics of a Shoulder Musculoskeletal Model during Arm Abduction, *Multidisciplinary Biomechanics Journal*, 2026, vol. 3, p. 69–71, DOI: 10.46298/mbj.17934.

2.4 Evaluation metrics

Root mean square (RMS) errors and coefficients of determination (R^2) between the reference and model-derived kinematics were calculated for each DoF.

3. Results and discussion

The skin marker tracking RMS residuals was between 9.5 mm and 15.7 mm depending on the arm abduction.

Table 1. Evaluation metrics for some of the degrees of freedom.

	DoF	RMSE	R^2
Gleno-humeral displacements [mm]	Anterior / Posterior	12.2	0.10
	Proximal / Distal	6.4	0.52
Gleno-humeral angles [°]	Adduction / Abduction	9.5	0.98
	Flexion / Extension	8.3	0.76
Scapulo-thoracic angles [°]	Downward / Upward Rotation	12.1	0.98
	Posterior / Anterior tilt	4.6	0.94

The prediction of the gleno-humeral displacements does not seem to be realistic (up to 16 mm of displacement in proximal distal direction, see Figure 1) considering the scapula glenoid size. Indeed, the amplitude for the reference remains around 1 mm, and the RMSE confirms large inconsistencies. This may be explained by the geometric parameters taken from Hasan et al., (2025) to formulate the sphere-to-sphere kinematic constraints. The prediction of the angles (both gleno-humeral and scapula-thoracic) seems to be realistic and the RMSE are in line with the literature (Dumas & Duprey, 2022) especially for a generic scale model. For the main DoFs during the arm movement studied, namely the gleno-humeral adduction / abduction and scapulo-thoracic downward / upward rotation, the R^2 were high (0.98).

The observed errors (Table 1) are related to several factors: the definition of the kinematic constraints (number of DoFs and geometrical parameters) and the effects of STA, as well as the correspondence between the actual placement of skin markers and the definition of the marker positions in the model.

This preliminary study has several limitations. Only one arm movement is studied and at only 6 static postures. It was conducted on one participant, and the statistics and conclusions will need to be corroborated with the addition of other participants from the dataset.

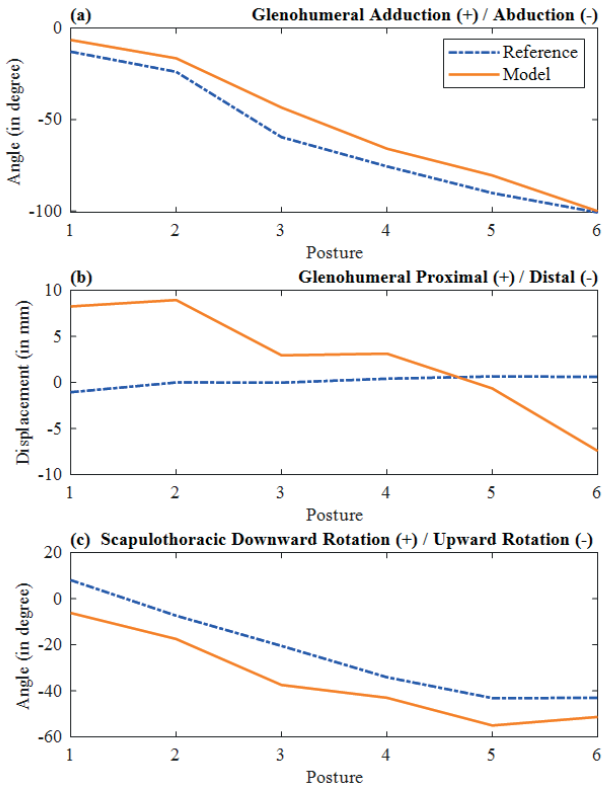

Figure 1. Reference and model-derived kinematics for some of the degrees of freedom.

4. Conclusions

This preliminary study evaluates the results of MKO using a 9-DoF shoulder musculoskeletal model during arm abduction up to 180°. The model-derived kinematics shows some promising results for joint angles but may need some improvements for the geometrical parameters of the sphere-on-sphere gleno-humeral kinematic constraint.

Conflict of Interest Statement

The authors declare no conflict of interest for this study.

Contributor Roles

Sandrine Bousigues: Formal analysis, Investigation, Visualization, Writing – original draft. Sonia Duprey: Data curation, Project administration, Writing – review & editing. Sacha Guitteny: Software, Resources, Writing – review & editing. Raphael Dumas: Conceptualization, Funding acquisition, Methodology, Writing – review & editing.

Funding

This study was funded by the I-Site Future (Feed-Feel-Move project).

References

Cereatti, A., Bonci, T., Akbarshahi, M., Aminian, K., Barré, A., Begon, M., Benoit, D. L., Charbonnier, C., Dal Maso, F., Fantozzi, S., Lin, C.-C., Lu, T.-W., Pandy, M. G., Stagni, R., Van Den Bogert, A. J., & Camomilla, V. (2017). Standardization proposal of soft tissue artefact description for data sharing in human motion measurements. *Journal of Biomechanics, 62*, 5–13. https://doi.org/10.1016/j.jbiomech.2017.02.004

Dumas, R., & Duprey, S. (2022). Subject-specific model-derived kinematics of the shoulder based on skin markers during arm abduction up to 180°—Assessment of 4 gleno-humeral joint models. *Journal of Biomechanics, 136*, 111061. https://doi.org/10.1016/j.jbiomech.2022.111061

El Habachi, A., Duprey, S., Cheze, L., & Dumas, R. (2015). A parallel mechanism of the shoulder—Application to multi-body optimisation. *Multibody System Dynamics, 33*(4), 439–451. https://doi.org/10.1007/s11044-014-9418-7

Hasan, I. M. I., Belli, I., Seth, A., & Gutierrez-Farewik, E. M. (2025). Modeling glenohumeral stability in musculoskeletal simulations: A validation study with in vivo contact forces. *IEEE Transactions on Neural Systems and Rehabilitation Engineering, 33*, 4657–4668. https://doi.org/10.1109/TNSRE.2025.3635012

Wu, G., van der Helm, F. C. T., (DirkJan) Veeger, H. E. J., Makhsous, M., Van Roy, P., Anglin, C., Nagels, J., Karduna, A. R., McQuade, K., Wang, X., Werner, F. W., & Buchholz, B. (2005). ISB recommendation on definitions of joint coordinate systems of various joints for the reporting of human joint motion—Part II: Shoulder, elbow, wrist and hand. *Journal of Biomechanics, 38*(5), Article 5. https://doi.org/10.1016/j.jbiomech.2004.05.042

2026-3 | International Shoulder Group (ISG) Congress 2026
2-3 June 2026, Lyon, France

Multidisciplinary Biomechanics Journal

Inverse Kinematics of the Closed-Loop Shoulder: Quadratic Programming is Faster than Interior-Point Methods with Equivalent Accuracy

Pierre Puchaud[a]*, Mégane Millan[b], Lucas Joseph[a]

a AUCTUS, Inria, Bordeaux, France
b WILLOW, Inria, Paris, France
* Corresponding author: pierre.puchaud@inria.fr

Received date: 16/01/2026
Accepted date: 16/03/2026
Publication date: 02/06/2026

Keywords: quadratic progamming, inverse kinematics, close-loop, constraints, optimization

1. Introduction

Shoulder girdle kinematics reconstruction is special due to the closed-loop nature of the osteoarticular mechanism. While open-loop tree structures can be solved using non-linear least squares, anatomically plausible shoulder models often require holonomic constraints. Current modeling propositions for the scapulothoracic contact vary from single-point contact on ellipsoids (Seth et al. 2019) to multi-point constraints (Naaim et al. 2017). These modeling choices may introduce a kinematic loop, specifically in between three bone-segments the clavicle, scapula, and the thorax, that must be enforced strictly during Inverse Kinematics (IK).

In the presence of holonomic constraints, the IK problem shifts from unconstrained optimization to a constrained non-linear programming (NLP) problem. A common approach is to use robust, general-purpose such as Interior-Point (IP) methods ,such as (Waechter & Biegler, 2006). However, these solvers can be computationally expensive and may be overkill for tracking tasks where the pose changes incrementally. Alternatively, Differential Inverse Kinematics (DIK) allows the problem to be formulated as a Quadratic Program (QP) by linearizing the constraints at the velocity level (Duclusaud et al. 2025). While QP is standard for real-time control in robotics, its suitability for biomechanics remains unproven, particularly regarding its ability to handle inevitable residual errors caused by Soft Tissue Artifact and model scaling mismatches compared to global IP methods. The aim of this study is to compare these two approaches (IP vs. QP) applied to a closed-loop upper limb model.

2. Methods

2.1 Model and data

We utilized experimental data from Seth et al. (2019), consisting of 18 motion capture files (shoulder flexion, abduction, and shrugging). The scaled model representing a 26-year-old healthy female subject (height: 162 cm, weight: 52 kg), had a 6-DOF floating base, a 2-DOF sternoclavicular joint, a 4-DOF thoracoscapular joint including an ellipsoid mobilizer, a 3-DOF glenohumeral joint. The model is defined by generalized coordinates $\mathbf{q}$ and parsed with the Pinocchio library (Carpentier et al., 2019). The loop closure constraint $c_{AC}(\mathbf{q})$ at the acromioclavicular (AC) joint, enforcing that the distal clavicle acromial joint location p_{AC}^{C} coincides with its scapula equivalent p_{AC}^{S} is defined as:

$$c_{AC}(\mathbf{q}) = p_{AC}^{S}(\mathbf{q}) - p_{AC}^{C}(\mathbf{q}) = 0$$

2.2 Non-linear programming (Interior-Point)

Using CasADi SX with the IPOPT solver, we formulated the standard IK problem, as finding the configuration $\mathbf{q}$ that minimizes the weighted squared distance between experimental markers $\mathbf{x}_i^{exp}$ and model markers $\mathbf{x}_i^{model}$, subject to the hard loop closure constraint:

To cite this article: Pierre Puchaud, Mégane Millan, Lucas Joseph, Inverse Kinematics of the Closed-Loop Shoulder: Quadratic Programming is Faster than Interior-Point Methods with Equivalent Accuracy, *Multidisciplinary Biomechanics Journal*, 2026, vol. 3, p. 73–75, DOI: 10.46298/mbj.17921.

$$\min_{\mathbf{q}} \ \frac{1}{2}\sum_{i=1}^{M} w_i \left\| \mathbf{x}_i^{exp} - \mathbf{x}_i^{model}(\mathbf{q}) \right\|^2$$

$$s.t. \ \ c_{AC}(\mathbf{q}) = 0$$

with weights being {100, 100, 100, 10, 10, 10, 2, 2, 2} corresponding to the thoracic landmarks (centpxt8, centijc7, ij), humeral markers (gu, centelbow, EpL), and scapular markers (ts, aa, ai), the same markers weight were used in next section. They were fine-tuned to guarantee the thorax to remain static and to guarantee the scapula visually match its markers.

2.3 Differential Inverse Kinematics

Alternatively, we formulate the problem at the velocity level using DIK. Instead of solving for absolute position $\mathbf{q}$, we solve for a small increment $\Delta\mathbf{q}$ that minimize tracking error while satisfying linearized constraints. We linearize the marker error and constraints with relationship between task space velocity and joint space velocity using well-known analytical jacobians:

$$\mathbf{x}_i^{model}(\mathbf{q}) \approx \mathbf{x}_i^{model}(\mathbf{q_0}) + \mathcal{J}_{i,q}(\mathbf{q_0})\Delta\mathbf{q}$$

and,

$$c_{AC}(\mathbf{q}) \approx p_{AC}^{S}(\mathbf{q_0}) - p_{AC}^{C}(\mathbf{q_0}) + \left(\mathcal{J}_{p_{AC}^{S}}(\mathbf{q_0}) - \mathcal{J}_{p_{AC}^{C}}(\mathbf{q_0})\right)\Delta\mathbf{q}$$

This formulation results in a convex QP which can be solved extremely efficiently compared to the non-linear IP formulation, using proxQP solver. As the constraints are linearized through an initial pose, we allow up to 10 executions of the QP if the nonlinear constraint is not satisfied at 1e-6 mm.

$$\min_{\Delta\mathbf{q}} \ \frac{1}{2}\sum_{i=1}^{M} w_i \left\| \mathbf{x}_i^{exp} - \left(\mathbf{x}_i^{model}(\mathbf{q_0}) + \mathcal{J}_{i,q}(\mathbf{q_0})\Delta\mathbf{q}\right) \right\|^2$$

$$s.t. p_{AC}^{S}(\mathbf{q_0}) - p_{AC}^{C}(\mathbf{q_0}) + \left(\mathcal{J}_{p_{AC}^{S}}(\mathbf{q_0}) - \mathcal{J}_{p_{AC}^{C}}(\mathbf{q_0})\right)\Delta\mathbf{q} = 0$$

3. Results and Discussion

Both solvers were used through Python. The solvers were tested on all 18 trials (Flexion, Abduction, Shrugging). **Computation Time.** The QP solver demonstrated a speedup factor of approximately 83x in average. The average computation time per frame was 0.40 ms (± 0.1 ms) for the QP solver compared to 36.2 ms (± 4.5 ms) for the Interior-Point method. For specific tasks like Abduction (ABD01), the QP solver processed the full 10.9s trial in 0.43s, whereas IPOPT required 35.9s, see Table 1. Despite the linearization, the QP approach maintained high accuracy comparable to the non-linear solver. **Marker Residuals:** For typical trials (e.g., ABD01), the mean marker residual was 22.02 mm for both QP and IP solvers, with differences appearing only at the sub-micrometer level. This residual magnitude can be attributed to both the model minimally pre-scaled and to the marker trajectories are not gold standard data, bu recomputed from digitized locations of bony landmarks. **Constraint Violation:** The kinematic loop constraint error (AC joint gap) was respected below 1e-7 mm by IPOPT. For the QP solver, it remained effectively zero (mean 0.0003 mm, max 0.0015 mm across abduction trials). This confirms that the QP formulation effectively keeps the violation below the optical motion capture noise, with sufficient precision for use in forward dynamics. Despite all the code was written in Python (but interfaced with compiled library), the code was already performant, but we would win additional computation time using IPOPT and proxQP in a compiled language too.

Table 1. Comparison of solver performance on representative trials.

Trial	Frames	QP Time (s)	IP Time (s)	Speedup (x)
ABD01	1091	0.44	35.98	82.5
FLX01	794	0.44	31.87	72.7
SHRUG01	462	0.17	17.44	102.9

Note: Res. = Mean Marker Residual.

4. Conclusion

We compared a Quadratic Programming formulation against a standard Interior-Point method for solving inverse kinematics of a closed-loop shoulder model. Our results indicate that QP is as accurate as Interior-Point methods for this application but is significantly faster (approx. 83 times). The primary challenge with QP in biomechanics is handling the drift associated with linearization; however, our results show the constraint violation remains below sub-millimetric precision. This

finding implies that complex, anatomically realistic shoulder models and other similar joints such as knee, talo-crural joint with multiple holonomic constraints can be solved in real-time. This efficiency opens new avenues for real-time applications and large-scale dataset processing without the computational penalty usually associated with constrained non-linear programming.

Acknowledgements

The author thank J. Carpentier, J. Vaillant for helping on implementing the ellipsoid joint in Pinocchio, and G. Passault, and A. Schortgen for their helpful discussion on Differential Inverse Kinematics.

Contributor Roles

PP: Conceptualization, Methodology, Software, Formal Analysis, Writing – original draft. MM : Methodology, Software. LJ : Software.

References

Carpentier, J., Saurel, G., Buondonno, G., Mirabel, J., Lamiraux, F., Stasse, O., & Mansard, N. (2019). The Pinocchio C++ library: A fast and flexible implementation of rigid body dynamics algorithms and their analytical derivatives. *2019 IEEE/SICE International Symposium on System Integration (SII)* (pp. 614–619). https://doi.org/10.1109/SII.2019.8700380

Duclusaud, M., Passault, G., Padois, V., & Ly, O. (2025). PlaCo: a QP-based robot planning and control framework. arXiv preprint arXiv:2511.06141. https://doi.org/10.48550/arXiv.2511.06141

Naaim, A., Moissenet, F., Duprey, S., Begon, M., & Cheze, L. (2017). Effect of various upper limb multi-body models on soft tissue artefact correction: A case study. *Journal of biomechanics, 62*, 102–109. https://doi.org/10.1016/j.jbiomech.2017.01.031

Seth, A., Dong, M., Matias, R., & Delp, S. (2019). Muscle contributions to upper-extremity movement and work from a musculoskeletal model of the human shoulder. *Frontiers in Neurorobotics, 13*, 90. https://doi.org/10.3389/fnbot.2019.00090

Waechter, A., & Biegler, L. T. (2006). On the implementation of an interior-point filter line-search algorithm for large-scale nonlinear programming. *Mathematical Programming, 106*(1), 25–57. https://doi.org/10.1007/s10107-004-0559-y

2026-3 | International Shoulder Group (ISG) Congress 2026
2-3 June 2026, Lyon, France

Multidisciplinary Biomechanics Journal

Finding the Best Calibration Poses for Shoulder Rhythm Personalization in a Computational Shoulder Model

Jennifer Maier*, Trausti Saevarsson, Lanie Gutierrez Farewik

KTH MoveAbility, Department of Engineering Mechanics, KTH Royal Institute of Technology, Stockholm, Sweden
* Corresponding author: jenmai@kth.se

Received date: 16/01/2026
Accepted date: 16/03/2026
Publication date: 02/06/2026

Keywords: shoulder model, personalization, calibration

1. Introduction

Computational models of the shoulder joint are a valuable tool to analyze and understand shoulder motion. To obtain meaningful results, it is crucial that the models can represent an individual's shoulder biomechanics accurately. One way of modeling the shoulder joint is to implement the scapulohumeral rhythm that describes the dependency of the scapula position and orientation on the glenohumeral joint angles (Holzbaur et al., 2005; Saul et al., 2015).

A recent study has shown that personalizing the shoulder rhythm in a computational model of the shoulder joint using five calibration poses can significantly improve the accuracy of kinematics estimates (Maier, Bianco, et al., 2024). The authors chose calibration poses that span the range of motion of participants (neutral, 180° abduction, 180° flexion, maximal horizontal abduction and adduction at 90° shoulder elevation) but did not analyze if the selected calibration poses lead to the best presentation of an individual's shoulder rhythm.

In this work, we use the mentioned study's publicly available data set to perform shoulder rhythm personalization with a variety of subsets of poses (Maier, Delp, et al., 2024). We investigate which number of poses, and which subset of poses can best represent an individual's shoulder rhythm by evaluating the scapula marker error.

2. Methods

We used the data, model, and code published with the aforementioned contribution (Maier, Bianco, et al., 2024). The data included motion capture data of 10 participants in 13 poses spanning the range of glenohumeral motion in the three body planes (5 in the frontal plane, 5 in the sagittal plane, 3 in the transverse plane) with palpated ground truth scapula measurement. We modified the algorithm to allow using a different and/or reduced subset of poses for shoulder rhythm personalization. The bilinear function describing the shoulder rhythm dependencies is

$$f(x, y) = ax + by + c,$$

where x and y are the glenohumeral elevation plane angle and glenohumeral elevation angle, respectively. As three parameters a, b, and c are fitted, at least three poses are necessary to obtain sufficient information. For this reason, we investigated subsets of 3, 4, and 5 poses for calibration and used the remaining poses for scapula marker error evaluation. The calibration pose subsets included the neutral pose, and additionally all unique combinations of the following poses: extension; 90°, 135°, and 180° abduction; 90°, 135° and 180° flexion; maximal horizontal adduction and abduction at 90° shoulder elevation.

The test set for each calibration subset consisted of all poses that were not included in the calibration subset. For each model, we computed inverse kinematics (IK) for all poses in the test set (not using the palpated scapula markers) and computed the scapula marker error between the model markers and the palpated ground

To cite this article: Jennifer Maier, Trausti Saevarsson, Lanie Gutierrez Farewik, Finding the Best Calibration Poses for Shoulder Rhythm Personalization in a Computational Shoulder Model, *Multidisciplinary Biomechanics Journal*, 2026, vol. 3, p. 77–79, DOI: 10.46298/mbj.17920.

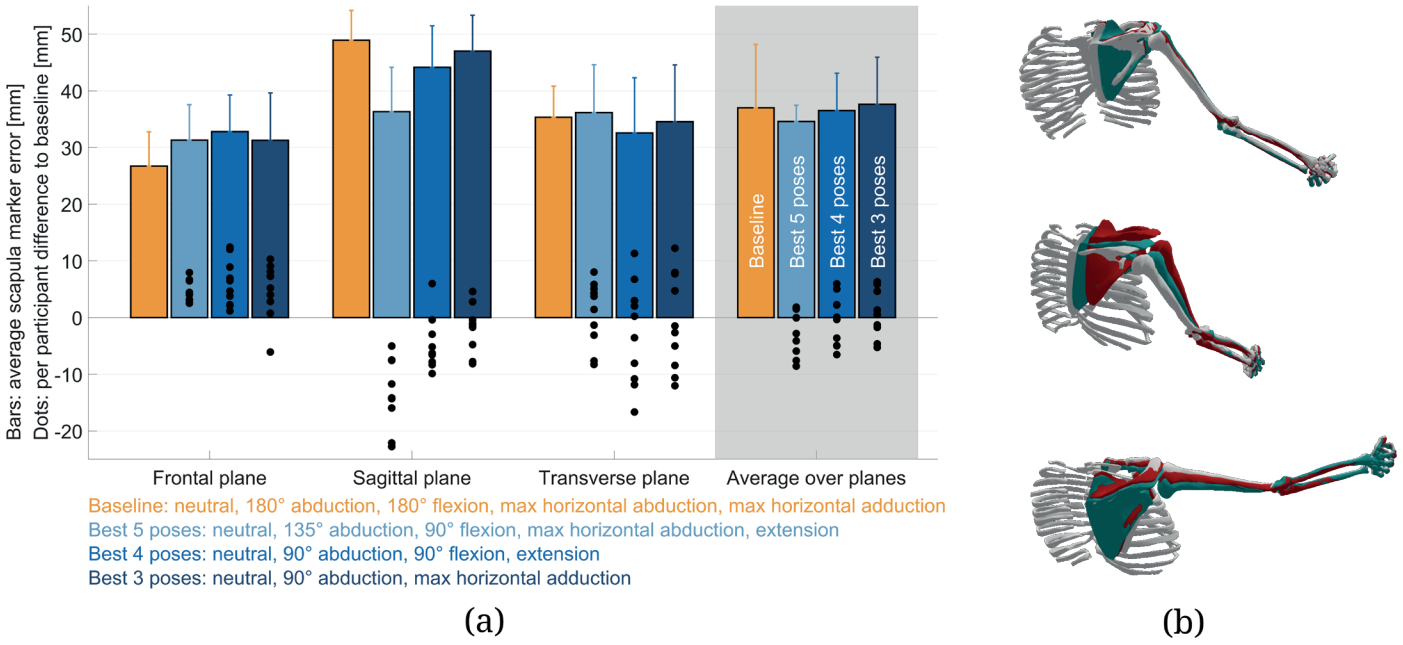

Figure 1. (a) Average scapula marker errors compared with palpated ground truth measurement. The baseline is plotted in yellow, the best 5, 4, and 3 pose combinations in shades of blue. The groups of bars show the error in the body planes and the average error over all planes (shaded in gray). Black dots represent the per participant difference compared with the baseline. (b) Exemplary models of the same participant in three poses; top to bottom: 45° abduction (frontal plane), 45° flexion (sagittal plane), 45° horizontal abduction (transverse plane). The white, red and teal models represent ground truth, baseline, and best 5 poses models, respectively.

Credit: Jennifer Maier

truth markers. The amount of test poses and their distribution over the body planes varied depending on how many and which poses were used for calibration. To avoid a bias toward one of the body planes, we grouped the test set poses per body plane and computed the average scapula marker error per body plane for each participant. We then averaged over all participants resulting in the error per body plane and computed the final error measure as the average error over all body planes. We compared the results for all pose subsets with the baseline calibration poses from the original publication (Maier, Bianco, et al., 2024).

3. Results and discussion

The pose combinations that result in the lowest average scapula marker error use 5 poses for calibration. No combination of 3 poses achieves a lower error than baseline, and only two combinations of 4 poses achieve a marginally lower error than baseline. Figure 1(a) shows the average scapula marker errors of the best subsets of 5, 4, and 3 calibration poses compared to the baseline calibration per body plane, and the average over all body planes (baseline: 37.0 ± 11.2 mm, best 5 poses: 34.6 ± 2.9 mm, best 4 poses: 36.5 ± 6.6 mm, best 3 poses: 37.6 ± 8.3 mm). The best 5 pose subset achieves a lower average error compared to baseline and is notably more uniform between the body planes, with a significantly lower error in the sagittal plane (paired t-test, $p < 0.001$) and an only slightly higher error in the frontal plane (paired t-test, $p = 0.11$) for all participants compared with baseline. This is confirmed visually by an example model in Figure 1(b), where both the baseline model (red) and the best 5 poses model (teal) match similarly well with the ground truth (white) in the frontal and transverse plane poses, but the best 5 poses model matches the ground truth better than the baseline model in the sagittal plane pose. Both best 4 and 3 poses combinations show a higher variance between planes than the best 5 poses combination. These results suggests that it might be beneficial to use certain subsets of poses depending on the investigated motion. If motion performed in all body planes is analyzed,

the best 5 calibration poses should be used, whereas for analyses in certain planes of motion, a calibration focusing on these planes might be sufficient. The results also show that high accuracy can be achieved with lower range of motion poses than required for baseline calibration, as all best pose combinations require a maximal shoulder elevation of 135° (best 5 poses) or only 90° (best 4 and 3 poses). This can be beneficial if the ability of participants does not allow them to raise their arms to higher elevations.

4. Conclusions

Our work showed that there might be better poses for personalizing the shoulder rhythm than the ones proposed in the original research. Certain clinical studies can benefit from the use of fewer and lower range of motion poses, especially when individuals with limited shoulder mobility are investigated. Future work should include more participants to allow for a thorough statistical analysis of the results.

Conflict of Interest Statement

None.

Contributor Roles

JM: Conceptualization, Methodology, Formal analysis, Writing original draft, Visualization; TS: Methodology, Formal analysis, Writing- review & editing; LGF: Funding acquisition, Conceptualization, Supervision, Writing – review & editing.

Funding

10.13039/100006639-Promobilia Foundation (Grant Number 23027, 18200, 23300, 22060 and 21034)

References

Holzbaur, K. R. S., Murray, W. M., & Delp, S. L. (2005). A model of the upper extremity for simulating musculoskeletal surgery and analyzing neuromuscular control. *Annals of Biomedical Engineering*, *33*(6), 829–840. https://doi.org/10.1007/s10439-005-3320-7

Maier, J. N., Bianco, N. A., Ong, C. F., Muccini, J., Kuhl, E., & Delp, S. L. (2024). Personalizing the shoulder rhythm in a computational upper body model improves kinematic tracking in high range-of-motion arm movements. *Journal of Biomechanics*, *176*, 112365. https://doi.org/10.1016/j.jbiomech.2024.112365

Maier, J. N., Delp, S. L., Ong, C. F., & Bianco, N. A. (2024). *Shoulder model personalization* [Data set]. Retrieved from https://simtk.org/projects/shoulder-perso

Saul, K. R., Hu, X., Goehler, C. M., Vidt, M. E., Daly, M., Velisar, A., & Murray, W. M. (2015). Benchmarking of dynamic simulation predictions in two software platforms using an upper limb musculoskeletal model. *Computer Methods in Biomechanics and Biomedical Engineering*, *18*(13), 1445–1458. https://doi.org/10.1080/10255842.2014.916698

2026-3 | International Shoulder Group (ISG) Congress 2026
2-3 June 2026, Lyon, France

Multidisciplinary Biomechanics Journal

A novel Workflow for in Vivo Assessment of Glenohumeral Contact Patterns Following Anatomic Total Shoulder Arthroplasty Using Biplanar Radiography

Nazanin Daneshvarhashjin[a*†], Laurens Jansen[a†], Philippe Debeer[b], Filip Verhaegen[b], Lennart Scheys[a]

a KU Leuven, Leuven, Belgium
b UZ Leuven, Leuven, Belgium
† Shared first authorship
* Corresponding author: nazanin.daneshvarhashjin@kuleuven.be

Received date: 16/01/2026
Accepted date: 16/03/2026
Publication date: 02/06/2026

Keywords: anatomic total shoulder arthroplasty, glenoid component loosening, in vivo contact patterns, automated workflow

1. Introduction

Glenoid component loosening remains a relevant complication after anatomic total shoulder arthroplasty (aTSA). Glenohumeral contact patterns govern load transfer and bone-implant mechanics, making their accurate estimation critical for patient-specific biomechanical models aiming to predict loosening. Yet, their inter- and intra-subject variability across different functional arm poses remains poorly documented and hence rarely accounted for in such models. Therefore, this study presents a workflow to assess in vivo glenohumeral contact patterns across multiple arm poses after aTSA.

2. Methods

2.1 Data collection

Input data were collected as part of a prospective clinical study approved by the Ethics Committee of the University Hospitals Leuven (S64986) and included postoperative supine CT scans and low-dose biplanar radiographs (EOS imaging) from aTSA patients implanted with a Comprehensive® glenoid component (Zimmer Biomet). Biplanar radiographs were acquired in six upright functional arm poses: relaxed standing (RS), 45° extension (45EX), 45° and 90° flexion (45F, 90F), and 45° and 90° abduction (45AB, 90AB).

2.2 Workflow definition

The workflow comprises four main stages (Fig. 1):
1) *3D model creation and coordinate system definition:* Patient-specific 3D models of the scapula and humerus, including humeral implant, were created from postoperative CT scans using threshold-based segmentation in Mimics (Materialise), with manual refinement applied to the humeral model (Fig. 1a). To reconstruct the postoperative scapula, a preoperative model was registered to the rough postoperative segmentation using 3-matic (Materialise) and further refined manually (Fig. 1b). Patient-specific coordinate systems were defined for both bones as in our previous work (Daneshvarhashjin et al., 2025).
2) *Glenoid component registration:* The manufacturer-provided glenoid component 3D model was semi-automatically registered to the postoperative CT scan using landmark-based alignment and manual adjustment, guided by peg-related contours and radiolucent zones (Fig. 1c).
3) *Pose-specific joint reconstruction:* For each pose, the scapula and humerus were segmented as 2D contours from the biplanar radiographs. Custom MATLAB code (Dzialo et al., 2018) then iteratively repositioned the 3D bone models until their projected contours matched the segmented ones (Fig. 1d). All bone models and the registered glenoid component were transformed into a unified patient-specific coordinate system in 3-matic (Fig. 1e).

To cite this article: Nazanin Daneshvarhashjin, Laurens Jansen, Philippe Debeer, Filip Verhaegen, Lennart Scheys, A novel Workflow for in Vivo Assessment of Glenohumeral Contact Patterns Following Anatomic Total Shoulder Arthroplasty Using Biplanar Radiography, *Multidisciplinary Biomechanics Journal*, 2026, vol. 3, p. 81–83, DOI: 10.46298/mbj.17930.

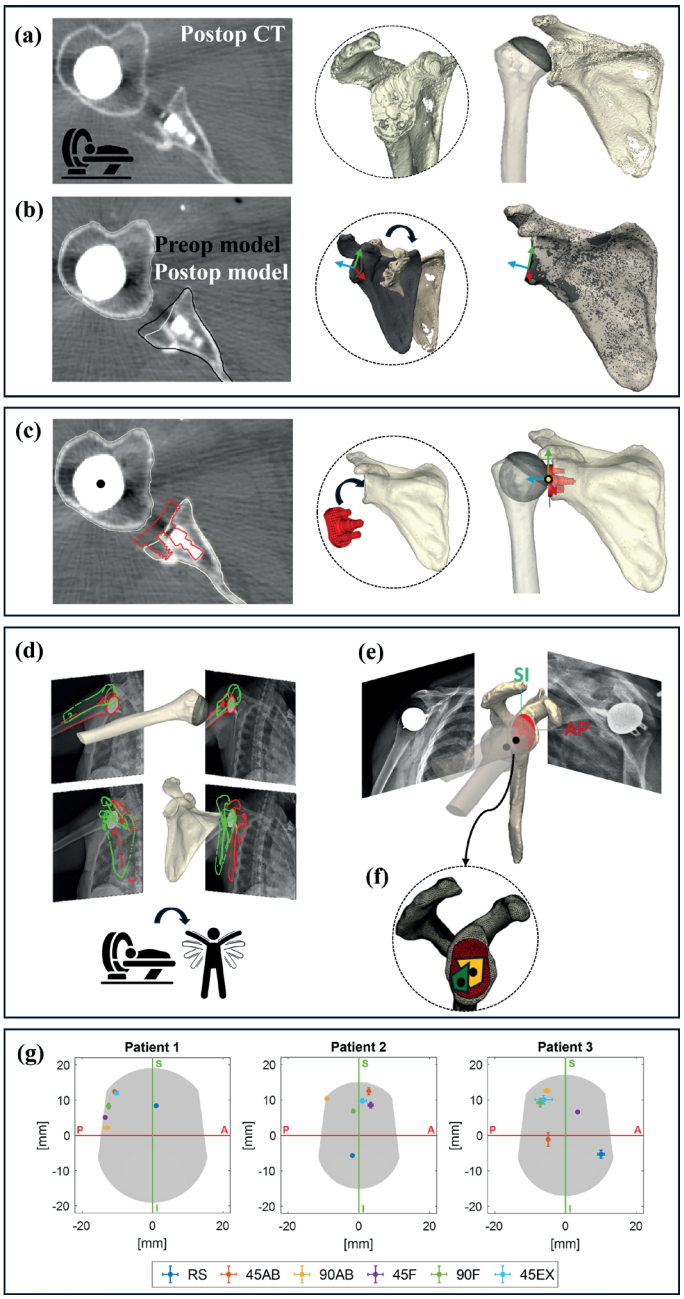

Figure 1. The proposed workflow (a-f) and proof-of-concept application to three patients (g).

4) *Contact calculation:* For each pose, the glenohumeral contact area and center were automatically computed using a custom Python script in 3-matic. The algorithm first generates triangular meshes for the humeral and glenoid components (0.1 mm edge length) and defines the contact area as the region of the glenoid component closest to the humeral component, using a threshold equal to 50% of the minimum intra-articular distance, similar to Massimini et al. (2014). The contact center is then calculated as the centroid of the resulting contact area (Fig. 1f), and expressed in the local glenoid component coordinate system.

2.3 Proof-of-Concept Application

The workflow was applied to three aTSA patients with different glenoid component sizes, using one-year postoperative imaging. The computed contact centers across the six arm poses were projected onto a 2D representation of the component, and displayed in a right-sided configuration to allow visual comparison in MATLAB. Sensitivity to the distance threshold was assessed by repeating the analyses across thresholds ranging from 25% to 75% in 5% increments.

3. Results and discussion

Figure 1g shows the computed contact centers across the six arm poses for the three patients, with ranges reflecting distance threshold sensitivity. Although the small sample size precludes clinical conclusions, the effect of the threshold seems limited and a superior trend is observed (average contact location 20.2% of the component height above its midpoint), suggesting persistent humeral head subluxation after aTSA, consistent with Massimini et al. (2010). The results indicate that the workflow captures patient-specific glenohumeral contact locations across different functional arm poses, and that sensitivity analyses can be readily incorporated. We are currently applying the workflow to 25 patients from the same clinical study, and plan to analyze both contact location and area, include additional predictors such as scapular anatomy and implant placement, and perform sensitivity analyses on key parameters (e.g., segmentation and registration accuracy, mesh size and smoothness), where the most influential parameters will be investigated further. Registration accuracy is expected to be the most critical and can be addressed using multi-operator tracking, as in our previous work (Daneshvarhashjin et al., 2025). Validation against population-level data from the OrthoLoad database may be considered after further model refinements.

4. Conclusions

We developed a workflow to quantify *in vivo* glenohumeral contact patterns after aTSA using postoperative CT scans and biplanar radiography across multiple arm poses. Proof-of-concept application demonstrates feasibility and highlights the potential to analyze larger

cohorts, ultimately supporting predictive biomechanical modeling of glenoid component loosening.

Acknowledgements

The authors wish to acknowledge Anna Tarasiuk for her assistance in coordinating the clinical trial, and Line Ven for her support in acquiring the biplanar radiographs.

Conflict of Interest Statement

The authors declare no conflicts of interest relevant to the content of this work.

Contributor Roles

ND: Conceptualization, Data curation, Methodology, Software, Visualization, Writing – original draft; **LJ**: Data curation, Methodology, Software, Visualization, Writing – original draft; **PD**: Conceptualization, Project administration, Resources, Supervision, Funding acquisition, Writing – review & editing; **FV**: Conceptualization, Project administration, Resources, Supervision, Funding acquisition, Writing – review & editing; **LS**: Conceptualization, Project administration, Resources, Supervision, Funding acquisition, Writing-review & editing.

Funding

This work was supported by a research project from KU Leuven (C2M/25/061) and by the PRosPERoS II project funded through the Interreg VA Flanders-The Netherlands program (2021TC16RFCB041).

Data, software, code availability

The Python code developed in this work for automated calculation of contact locations and areas will be made available upon reasonable request.

References

Daneshvarhashjin, N., Debeer, P., Andersen, M. S., Verhaegen, F., & Scheys, L. (2025). Biplanar radiography for in-vivo assessment of six degrees of freedom glenohumeral kinematics in shoulder osteoarthritis: an intra- and inter-observer reliability study. *Journal of Biomechanics*, *189*. https://doi.org/10.1016/j.jbiomech.2025.112845

Dzialo, C. M., Pedersen, P. H., Simonsen, C. W., Jensen, K. K., de Zee, M., & Andersen, M. S. (2018). Development and validation of a subject-specific moving-axis tibiofemoral joint model using MRI and EOS imaging during a quasi-static lunge. *Journal of Biomechanics*, *72*, 71–80. https://doi.org/10.1016/j.jbiomech.2018.02.032

Massimini, D. F., Li, G., & Warner, J. J. P. (2010). Glenohumeral contact kinematics in patients after total shoulder arthroplasty. *Journal of Bone and Joint Surgery*, *92*(4), 916–926. https://doi.org/10.2106/JBJS.H.01610

Massimini, D. F., Warner, J. J. P., & Li, G. (2014). Glenohumeral joint cartilage contact in the healthy adult during scapular plane elevation depression with external humeral rotation. *Journal of Biomechanics*, *47*(12), 3100–3106. https://doi.org/10.1016/j.jbiomech.2014.06.034

2026-3 | International Shoulder Group (ISG) Congress 2026
2-3 June 2026, Lyon, France

Multidisciplinary Biomechanics Journal

Cost Function Choice Matters in Functional Electrical Stimulation Hand-Cycling Exercise Duration

Kevin Co[a*], Pierre Puchaud[b], Florent Moissenet[a, c], Mickaël Begon[a, d]

a Laboratoire de Simulation et Modélisation du Mouvement, Université de Montréal, Montréal (Qc), Canada
b AUCTUS, Inria Centre de l'Université de Bordeaux, Talence, France
c Laboratoires de Biomécanique et de Cinésiologie, Hôpitaux Universitaires de Genève et Université de Genève, Genève, Suisse
d Centre de recherche Azrieli du CHU Sainte-Justine, Montréal (Qc) Canada
* Corresponding author: kevin.co@umontreal.ca

Received date: 12/12/2025
Accepted date: 16/03/2026
Publication date: 02/06/2026

Keywords: predictive simulation, musculoskeletal shoulder modeling, muscle fatigue

1. Introduction

Functional electrical stimulation (FES) is a rehabilitation technique used to assist and restore motor function after neuro-musculoskeletal disorders. Repetitive motions (e.g., hand cycling) are known to enhance recovery. However, FES induces premature muscle fatigue, which reduces its benefits. To mitigate its apparition, advanced algorithms have been proposed such as FES-driven optimal control problems (OCPs) with muscle dynamics models. To improve the method's clinical efficiency, we showed that further investigation is needed, particularly regarding the cost function (Co et al. 2025). In this study, we investigated how the cost function choice affects the FES hand-cycling exercise duration. We hypothesize that directly minimizing muscle fatigue predicted by FES models will be more effective than indirectly minimizing related variables, such as FES pulses or muscle forces.

2. Methods

We conducted an *in-silico* study using an open-loop receding-horizon optimal control framework to compare 17 cost functions.

2.1 System dynamics – Upper limb and FES

We simplified the upper-limb model of Wu et al. (2016) to keep two degrees of freedom (shoulder and elbow flexion) in the sagittal plane and four muscles (biceps, triceps, anterior and posterior deltoids). We added a third degree of freedom for the hand-crank joint q_c and a holonomic constraint at the center of the crank to close the kinematic chain. The equations of motion were coupled with two models, controlled through stimulation pulse widths, designed to estimate muscle forces (Ding et al. 2007) and muscle fatigue (Ding et al. 2003). The four muscles were scaled based on their physiological cross-section area (for force production) and their fiber type II proportion (for muscle fatigue). Force / passive-length-velocity relationships were used to transform the isometric forces given by the FES models into dynamic forces.

2.2 Optimal control problem

In all simulations, each pulse width $\boldsymbol{u}$ was optimized between 0 and 600 µs, with a constant FES frequency set at 30 Hz. The pedaling task was performed at 60 rpm with a 0.20 N.m pedal resistance. Four cost function archetypes (ϕ^1: average, ϕ^2: root-mean-square, ϕ^3: cubic average, and ϕ^m: peak) were compared (Bečanović et al. 2025), each built from five variables V_m, namely: FES pulse width, muscle force, muscle stress, muscle fatigue and muscle power:

To cite this article: Kevin Co, Pierre Puchaud, Florent Moissenet, Mickaël Begon, Cost Function Choice Matters in Functional Electrical Stimulation Hand-Cycling Exercise Duration, *Multidisciplinary Biomechanics Journal*, 2026, vol. 3, p. 85–87, DOI: 10.46298/mbj.17923.

$$\underset{\boldsymbol{x}(.),\,\boldsymbol{u}(.)}{\text{minimize}} \quad \phi^1 = \int_0^T \left(\frac{1}{4} \sum_{m=1}^{4} V_m \left(\boldsymbol{x}(t), \boldsymbol{u}(t) \right) \right) dt$$

$$\phi^2 = \int_0^T \left(\frac{1}{4} \sum_{m=1}^{4} V_m \left(\boldsymbol{x}(t), \boldsymbol{u}(t) \right)^2 \right)^{\frac{1}{2}} dt$$

$$\phi^3 = \int_0^T \left(\frac{1}{4} \sum_{m=1}^{4} V_m \left(\boldsymbol{x}(t), \boldsymbol{u}(t) \right)^3 \right)^{\frac{1}{3}} dt$$

$$\phi^m = \int_0^T \left(\max_{m=1,\ldots,4} V_m \left(\boldsymbol{x}(t), \boldsymbol{u}(t) \right) \right) dt$$

subject to:

$$\forall t \in]0, T[, \mathbf{x}_{\min} \leq \mathbf{x}(t) \leq \mathbf{x}_{\max} \qquad \textit{State bounds}$$

$$\mathrm{q}_c(0) = 0, \qquad \textit{Task constraints}$$

$$2\pi - 0.05 \leq \mathrm{q}_c(T) \leq 2\pi + 0.05$$

$$\forall t, 0 \leq \mathbf{u}(t) \leq 600\ \mu s \qquad \textit{Control bounds}$$

$$\dot{\mathbf{x}}(t) = \mathbf{f}(\mathbf{x}, \mathbf{u}, t) \qquad \textit{Dynamic constraints}$$

As muscle power can be positive and negative, only the cost function archetype ϕ^2 was calculated for this variable.

2.3 Optimization framework

To reduce computational complexity, a few cycles of the hand cycling task were simulated using a receding-horizon approach. We iteratively solved a finite-horizon OCP using the updated initial state at each step, then advanced the prediction window by one cycle until exhaustion, i.e., when the pedaling motion could no longer be achieved. Simulations were run for different window sizes ranging from 2 to 5 cycles (68 simulations in total). The OCPs were transcribed in Bioptim using a direct collocation scheme (3rd order Radau method, with 33 ms per shooting interval) and solved with IPOPT.

2.4 Data analysis

The number of cycles completed before failure was compared across cost function archetypes and variables. The influence of the window size and the solver convergence time were also investigated.

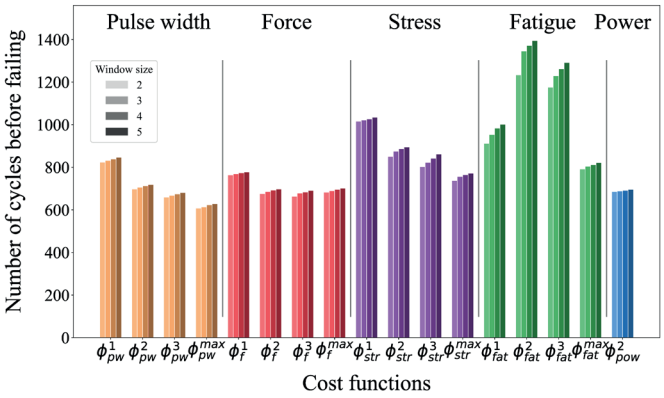

Figure 1. Number of cycles completed before failure for each cost function archetypes (φ^1): average, $\varphi 2$: root-mean-square, $\varphi 3$: cubic average, and φm: peak) and each variables (pw: pulse width, f: force, str: stress, fat: fatigue, pow: power).

Credit: Co].

3. Results and discussion

As hypothesized, more cycles were completed before failure when minimizing muscle fatigue (Fig 1).

Minimizing muscle fatigue resulted in a major 70.4% increase of the number of cycles completed before failure (computation time: +9 min 51 s) compared to minimizing FES pulse width, i.e., the most used cost function in FES-driven OCPs (Co et al. 2025), and a 35% increase compared to the second most efficient variable, i.e., muscle stress. Increasing the window size from 2 to 5 increased linearly the number of cycles from 3 to 11%.

The OCP solving time, critical for real-time applications, was also influenced by the cost function choice. On average, solving a single pedal cycle required 7.14 s with ϕ^2_{fat} and 2.62 s. with ϕ^2_{pw}.

Except for the muscle fatigue variable, mean-based cost function outperformed quadratic, cubic, and min–max archetypes. This may be because the fatigue rate was not directly accessible to the other cost functions, leading to a suboptimal distribution of muscle control (pulse width) for maximizing endurance. In this study, no weights were individually applied to the muscles, a further tuning of those weights may prolong the task duration. The limitation of this study is the use of scaled FES models rather than identifying subject-specific models. A follow-up study should include an in vivo identification and experimental validation.

4. Conclusions

Incorporating a muscle-fatigue-aware FES model into the OCP may help prolong hand-cycling pedaling tasks. We ultimately aim to use these cost functions to generate functional electrical stimulation patterns that extend rehabilitation sessions, and future work will validate their effectiveness in vivo.

Conflict of Interest Statement

None.

Contributor Roles

KC: Conceptualization, Methodology, Software, Formal analysis, Writing – original draft; PP: Conceptualization, Methodology, Software, Writing – review & editing; FM: Supervision, Resources, Writing – review & editing; MB: Supervision, Resources, Funding acquisition, Writing – review & editing.

Funding

This work was supported by the Fonds de recherche du Québec – Nature et technologies (FRQNT), grant number: 2024-PR-341023.

Data, software, code availability

The optimal control problem was set and solved using Bioptim: github.com/pyomeca/bioptim, and the simulations were run using CocoFest, two open-source libraries: github.com/pyomeca/cocofest.

References

Bečanović, F., Bonnet, V., Jovanović, K., Mohammed, S., & Dumas, R. (2025). Inverse optimal control of muscle force sharing during pathological gait. *arXiv preprint*. https://doi.org/10.48550/arXiv.2510.17456

Co, K., Begon, M., Bailly, F., & Moissenet, F. (2025). Optimal control-driven functional electrical stimulation: A PRISMA-ScR scoping review. *Computers in Biology and Medicine, 199*, 111311. https://doi.org/10.1016/j.compbiomed.2025.111311

Ding, J., Wexler, A. S., & Binder-Macleod, S. A. (2003). Mathematical models for fatigue minimization during functional electrical stimulation. *Journal of Electromyography and Kinesiology, 13*(6), 575–588. https://doi.org/10.1016/s1050-6411(03)00102-0

Ding, J., Chou, L., Kesar, T. M., Lee, S. C., Johnston, T. E., Wexler, A. S., & Binder-Macleod, S. A. (2007). Mathematical model that predicts the force–intensity and force–frequency relationships after spinal cord injuries. *Muscle & Nerve, 36*(2), 214–222. https://doi.org/10.1002/mus.20806

Wu, W., Lee, P. V., Bryant, A. L., Galea, M., & Ackland, D. C. (2016). Subject-specific musculoskeletal modeling in the evaluation of shoulder muscle and joint function. *Journal of biomechanics, 49*(15), 3626-3634. https://doi.org/10.1016/j.jbiomech.2016.09.025

2026-3 | International Shoulder Group (ISG) Congress 2026
2-3 June 2026, Lyon, France

Multidisciplinary Biomechanics Journal

Prediction of Deltoid Muscle Force in Reverse Total Shoulder Arthroplasty Using a Deep Learning Model

Léa Pistorius*, Dominique P. Pioletti, Alexandre Terrier

Laboratory of Biomechanical Orthopedics, École Polytechnique Fédérale de Lausanne, Institute of Bioengineering, Lausanne, Switzerland
* Corresponding author: lea.pistorius@epfl.ch

Received date: 15/01/2026
Accepted date: 16/03/2026
Publication date: 02/06/2026

Keywords: reverse total shoulder arthroplasty, deltoid muscle force, musculoskeletal model, deep learning model

1. Introduction

Reverse total shoulder arthroplasty (rTSA) has seen a substantial increase in clinical use over the past decade to treat osteoarthritis, rotator cuff tears, and complex shoulder fractures. Despite its effectiveness in restoring joint stability and function, roughly 9% of patients experience complications within two years postoperatively, including joint instability, fractures, implant loosening, and reduced mobility (Parada et al. 2021). Understanding the mechanical factors underlying these complications is essential for improving implant design and surgical planning.

The deltoid muscle is a primary contributor to shoulder joint force and stability, potentially contributing to bone fractures after rTSA (Khwaja et al. 2020). Since internal muscle forces cannot be measured in vivo, computationally expensive musculoskeletal models (MSM) are commonly used for their estimation. Deep learning models (DLM) offer an efficient alternative, approximating the MSM forces with acceptable accuracy and reduced computation time (Eghbali et al. 2024).

The objective of this study was to develop a DLM to predict the clavicular, acromial, and spinal deltoid forces after rTSA.

2. Methods

2.1 Data

The dataset comprises 998 virtual patients reconstructed from CT-scan–derived data from 495 real patients collected at the Centre Hospitalier Universitaire de Vaud (CHUV), Switzerland. The virtual patients were generated using a Metropolis Markov Chain Monte Carlo (MCMC) algorithm, sampling patient-specific parameters from Bayesian distributions fitted to the real patient (Velikova et al. 2024). The parameters include sex, height, weight, physiological cross-sectional area (PCSA) of the four rotator cuff muscles, and glenoid positional factors (lateralization, anteriorization, distalization). Male and female data distributions were analyzed separately to ensure anatomically consistent virtual data.

2.2 MSM

Muscle forces were estimated with a MSM (Sarshari et al. 2021). Each virtual patient performed one of three simulated activities: scapular-plane abduction, scapular-plane abduction with a 2 kg load, or frontal-plane abduction with a 2 kg load. Each activity was performed with an angular velocity around $20°s^{-1}$. MSM outputs include muscle forces dependent on the shoulder abduction angle produced by each patient, from which the clavicular, acromial, and spinal deltoid force amplitudes were extracted at 60° of abduction and used as DLM targets.

2.2 DLM Optimization

A fully connected DLM was trained to map patient-specific inputs to MSM-predicted deltoid forces at 60° of abduction. Bayesian optimization was conducted

To cite this article: Léa Pistorius, Dominique P. Pioletti, Alexandre Terrier, Prediction of Deltoid Muscle Force in Reverse Total Shoulder Arthroplasty Using a Deep Learning Model, *Multidisciplinary Biomechanics Journal*, 2026, vol. 3, p. 89–91, DOI: 10.46298/mbj.17939.

over 100 iterations, tuning the number of hidden layers (3–10), neurons per layer (16–128), activation functions (ReLU, ELU), dropout rates (0.1–0.3), and optimizers (Adam, Nadam). Learning rates of 10^{-4} and 10^{-3} and loss weights for each deltoid part were explored.

The dataset was split into 85% training and 15% testing, with 15% of the training data used for validation. Model performance was evaluated using the coefficient of determination (R^2) and mean absolute error (MAE).

3. Results and discussion

The optimized DLM consists of 5 fully connected hidden layers with 128, 112, 48, 80, and 128 neurons, respectively, each followed by Batch Normalization and using ELU activation. The Adam optimizer selected has a learning rate of . Regularization is achieved exclusively through Batch Normalization. Additionally, the best loss weights are 2.2, 4.8, and 9.6 for the clavicular, acromial, and spinal deltoid forces.

There is a strong agreement between MSM and DLM forces for the acromial and spinal deltoids, while the clavicular deltoid shows weaker performance due to its lower force contribution (Fig. 1 and Table 1). The MAE represent approximately 3.4%, 2.6%, and 3.3% of the MSM-derived force amplitudes at 60° of abduction for the clavicular (49N), acromial (265N), and spinal (71N) deltoids, respectively.

Table 1. Performance of DLM with coefficient of determination (R^2) and mean absolute error (MAE).

Deltoid part	R^2	MAE (N)
Clavicular	0.419	1.669
Acromial	0.911	6.969
Spinal	0.867	2.339

Overall, DLM predictions fall within the uncertainty bounds of MSM estimates and exhibit a low risk of overfitting, while achieving substantial gains in computational efficiency, reducing runtime from approximately 30 minutes to less than 1 second. Notably, while the clavicular deltoid shows reduced predictive accuracy, the dominant force contribution is captured effectively despite moderate R^2 values, and its influence on total deltoid force calculations remains minimal due to the balanced weighting scheme. This enables straightforward integration into clinical and research workflows and scalable prediction of additional muscle forces.

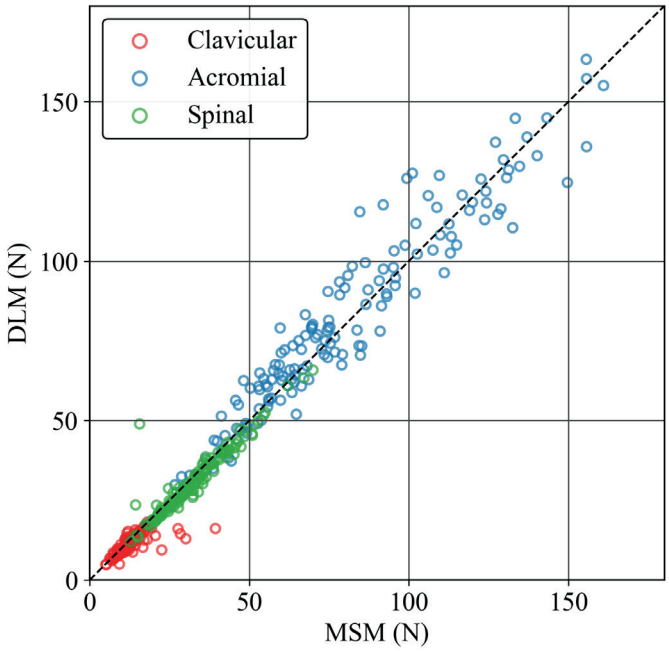

Figure 1. DLM vs. MSM predictions of clavicular, acromial, and spinal deltoid forces after rTSA for the test dataset.

This study is limited by the restricted set of simulated movements and the exclusive use of virtual patients generated. The lack of real patient data limits generalizability and motivates future experimental and clinical validation.

4. Conclusions

This study demonstrates the efficacy of DLM for patient-specific prediction of the clavicular, acromial, and spinal deltoid muscle forces. The proposed DLM achieves acceptable accuracy with dramatically reduced computation time, supporting its integration into an automated workflow of finite element modeling for the statistical analysis of fracture risk assessment.

Contributor Roles

LP: Conceptualization, Methodology, Analysis, Writing original draft; **DPP:** Supervision, Writing – review & editing; **AT**: Conceptualization, Methodology, Resources, Project administration, Funding acquisition, Data curation, Supervision, Writing – review & editing.

Funding

This study was supported by the Swiss National Science Foundation (SNF 10004515) and the "Lausanne Orthopedic Research Foundation" (LORF).

References

Parada, S. A., Flurin, P.-H., Wright, T. W., Zuckerman, J. D., Elwell, J. A., Roche, C. P., & Friedman, R. J. (2021). Comparison of complication types and rates associated with anatomic and reverse total shoulder arthroplasty. *Journal of Shoulder and Elbow Surgery*, *30*(4), 811–818. https://doi.org/10.1016/j.jse.2020.07.028

Khwaja, A., Sherman, N., Knox, A., & Mahoney, A. (2020). Late presentation of acromial base fracture after reverse shoulder arthroplasty: A case report. *JSES International*, *5*(2), 266–269. https://doi.org/10.1016/j.jseint.2020.10.024

Sarshari, E., Boulanaache, Y., Terrier, A., Farron, A., Mullhaupt, P., & Pioletti, D. (2021). A Matlab toolbox for scaled-generic modeling of shoulder and elbow. *Scientific Reports*, *11*(1), 20806. https://doi.org/10.1038/s41598-021-99856-y

Eghbali, P., Becce, F., Goetti, P., Büchler, P., Pioletti, D. P., & Terrier, A. (2024). Glenohumeral joint force prediction with deep learning. *Journal of Biomechanics*, *163*, 111952. https://doi.org/10.1016/j.jbiomech.2024.111952

Velikova, T., Mileva, N., & Naseva, E. (2024). Method "Monte Carlo" in healthcare. *World Journal of Methodology*, *14*(3), 93930. https://doi.org/10.5662/wjm.v14.i3.93930

2026-3 | International Shoulder Group (ISG) Congress 2026
2-3 June 2026, Lyon, France

Multidisciplinary Biomechanics Journal

A Novel Workflow for Personalized Shoulder Modeling to Compute Glenohumeral Joint Loading in Shoulder Osteoarthritis and Anatomic Total Shoulder Arthroplasty Cohorts

Line Ven[a*], Nazanin Daneshvarhashjin[a], Philippe Debeer[b], Filip Verhaegen[b], Lennart Scheys[a, b]

a Institute for Orthopaedic Research and Training, KU Leuven, Leuven, Belgium
b Division of Orthopaedics, University Hospitals Leuven, Leuven, Belgium
* Corresponding author: line.ven@kuleuven.be

Received date: 16/01/2026
Accepted date: 16/03/2026
Publication date: 02/06/2026

Keywords: personalized musculoskeletal shoulder modeling, glenohumeral joint reaction loads, humeral head translations, glenohumeral osteoarthritis, anatomic total shoulder arthroplasty

1. Introduction

Glenoid component loosening is a major complication following anatomic total shoulder arthroplasty (aTSA), with reported rates up to 44% (Gabriel et al. 2023). The rocking-horse phenomenon is considered the primary loosening mechanism, highlighting the value of investigating glenohumeral (GH) joint loading and shear forces to reduce loosening rates. Musculoskeletal modeling and simulations provide a valuable framework to analyze these loadings, which cannot be directly measured *in vivo*. Yet, models for GH osteoarthritis (OA) and post-aTSA patients remain limited, especially in terms of personalization.

This study introduces a workflow for personalized shoulder modeling that uniquely integrates humeral head (HH) translations to compute GH joint loading. The aim is to provide clinically relevant insights into how anatomical variations influence pre-aTSA loading and how surgical correction of glenoid version/inclination could reduce post-aTSA loosening risk.

2. Methods

2.1 Clinical dataset

Six OA patients scheduled for aTSA, with varying glenoid version and inclination, were selected from our prospective study. Within this study, we acquired pre-aTSA computed tomography (CT) scans and biplanar radiographs (EOS) in multiple arm poses—relaxed standing (RS) and 45/90° abduction (AB). CT-based bone models were registered to EOS images to determine 3D GH rotations and translations (Daneshvarhashjin et al. 2025).

2.2 Personalization pipeline

First, the generic thoracoscapular model (Seth et al. 2016) in OpenSim4.0 was adapted to include EOS-based GH translational degrees of freedom (DOF), and a refined scapular mesh, enabling personalization of muscle insertions and wrapping surfaces based on bone-morphing.

Second, this model was personalized through an automated pipeline which:

1. Scales the generic model based on each patient's HH diameter, while preserving the generic model mass.
2. Performs non-rigid morphing of the generic scapular mesh to the patient-specific geometry (MeshMonk, Matlab2023a).
3. Updates muscle insertions based on corresponding morphed scapular nodes.
4. Fits personalized wrapping surfaces to corresponding scapular nodes using Gauss-Newton optimization.

To cite this article: Line Ven, Nazanin Daneshvarhashjin, Philippe Debeer, Filip Verhaegen, Lennart Scheys, A Novel Workflow for Personalized Shoulder Modeling to Compute Glenohumeral Joint Loading in Shoulder Osteoarthritis and Anatomic Total Shoulder Arthroplasty Cohorts, *Multidisciplinary Biomechanics Journal*, 2026, vol. 3, p. 93–96, DOI: 10.46298/mbj.17924.

This pipeline was used to create an average OA model (based on a statistical shape model of 64 OA scapulae), and 6 pre-aTSA personalized models with patient-specific geometries.

2.3 Joint reaction analysis

Following personalization, generic and EOS-derived patient-specific GH rotations and translations were applied to the average and personalized models, respectively. All models incorporated OA-based scapulohumeral rhythms to ensure correct scapular positioning (Spranz et al. 2019).

Next, muscle forces were computed using static optimization with reserve actuators for translational DOFs. GH joint reaction loads were obtained with OpenSim's JointReactionTool.

Spearman's rank correlation was used to assess relationships between glenoid version/inclination and GH loading direction.

3. Results and discussion

Pre-aTSA personalized total GH reaction forces increased with arm abduction (Fig.1C). This association was primarily driven by increasing muscle activity to counteract gravity and stabilize the joint.

Superior shear forces also increased with abduction (Fig.1B), likely reflecting additional muscle contributions to resist downward gravitational pull, consistent with previous findings (Bergmann et al. 2011). In contrast, horizontal shear forces showed large directional variability across patients and arm poses (Fig.1A).

Posterior shear force directions correlated with glenoid retroversion across all poses, while superior force directions correlated with superior inclination (Table 1). These relationships suggest that increased version/inclination reduces GH stability and increases eccentric loading, confirming that centralizing GH loading is a critical aim in aTSA planning to lower loosening risk. However, all results should be interpreted cautiously given our small sample size.

Table 1. Spearman's rank correlations (R) between glenoid version/inclination and force direction.

Arm pose	R(version~ horizontal shear)	R(inclination~ vertical shear)
RS	0.71 (p=0.09)	0.36 (p=0.44)
45AB	0.39 (p=0.4)	0.43 (p=0.35)
90AB	0.6 (p=0.35)	0.9 (p=0.08)

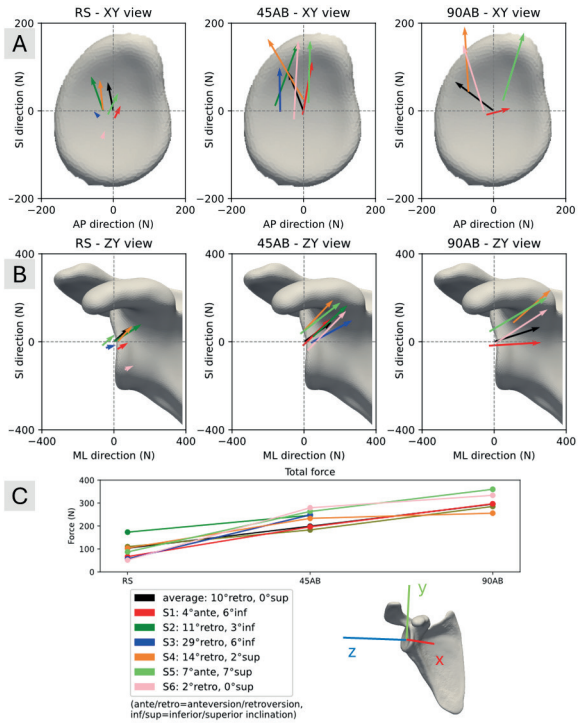

Figure 1. Total GH reaction forces in abduction poses (C), visualized in glenoid (A) and perpendicular (B) planes. Contact locations, considered equal to HH translations, are normalized to patient-specific HH radii. Scapular coordinate frames: X- and Y-axes orthogonal to scapular and transverse plane, respectively; Z-axis mutually orthogonal. AP:anteroposterior/horizontal shear, SI:superior-inferior/vertical shear, ML:mediolateral/compression.

4. Conclusions

These preliminary findings demonstrate feasibility and clinical potential of a novel workflow for personalized shoulder modeling and GH loading estimation. By incorporating patient-specific geometry and HH translations, this workflow enables personalized loading predictions, as reflected in force pattern variability.

The link between glenoid version/inclination and loading direction highlights the need for accurate aTSA implant positioning to reduce postoperative subluxation risk and prevent excessive eccentric loading—a key contributor to glenoid loosening. Future work will analyze our available cohort of 33 patients in pre- and post-aTSA configurations up to 120° abduction, assessing whether the rocking-horse phenomenon occurs post-aTSA and can be predicted preoperatively.

Conflict of Interest Statement

None.

Contributor Roles

LV: Data curation, Formal analysis, Funding acquisition, Investigation, Methodology, Project administration, Software, Validation, Visualization, Writing original draft, Writing – review & editing; ND: Conceptualization, Data curation, Funding acquisition, Investigation, Methodology, Project administration, Writing – review & editing; PD: Conceptualization, Data curation, Funding acquisition, Investigation, Project administration, Resources, Supervision, Writing – review & editing; FV: Conceptualization, Data curation, Funding acquisition, Investigation, Project administration, Resources, Supervision, Writing – review & editing; LS: Conceptualization, Funding acquisition, Methodology, Project administration, Resources, Supervision, Writing – review & editing.

Funding

The authors thank Flanders' Fund for Scientific Research (1SA9026N) and PRosPERoS-II Interreg VA Flanders–The Netherlands (2021TC16RFCB041) for financial support.

References

Bergmann, G., Graichen, F., Bender, A., Rohlmann, A., Halder, A., Beier, A., & Westerhoff, P. (2011). *In vivo* gleno-humeral joint loads during forward flexion and abduction. *J Biomech, 44*(8), 1543–1552. https://doi.org/10.1016/j.jbiomech.2011.02.142

Daneshvarhashjin, N., Debeer, P., Andersen, M. S., Verhaegen, F., & Scheys, L. (2025). Biplanar radiography for in-vivo assessment of six degrees of freedom glenohumeral kinematics in shoulder osteoarthritis: an intra- and inter-observer reliability study. *J Biomech, 189*. https://doi.org/10.1016/j.jbiomech.2025.112845

Gabriel, S., Tucker, T., & Boin, M. A. (2023). A narrative review of non-infected painful total shoulder arthroplasty: evaluation and treatment. *Ann Jt, 8*(16). https://doi.org/10.21037/aoj-22-43

Seth, A., Matias, R., Veloso, A. P., & Delp, S. L. (2016). A biomechanical model of the scapulothoracic joint to accurately capture scapular kinematics during shoulder movements. *PLOS One*. https://doi.org/10.1371/journal.pone.0141028

Spranz, D. M., Bruttel, H., Eckerle, J. M., Wolf, S. I., Berrsche, G., & Maier, M. W. (2019). Variation of the glenohumeral and scapulothoracic motion in progressive severity of glenohumeral osteoarthritis. *OTSR, 105*(8), 1503–1507, https://doi.org/10.1016/j.otsr.2019.07.010

2026-3 | International Shoulder Group (ISG) Congress 2026
2-3 June 2026, Lyon, France

Multidisciplinary Biomechanics Journal

Robustness of a Five-Landmark Predictive Model for the Glenohumeral Rotation Center to Simulate Ultrasound Localization Errors: a Monte-Carlo and Individual Perturbation Analysis

Marc-Olivier St-Pierre[a*], Philippe Paquette[b], Guillaume Desroches[b], Rachid Aissaoui[a]

a Laboratoire de Recherche en Innovation Ouverte en technologie de la santé, École de technologie supérieure, Montréal, Canada
b Institut national d'anatomie, Université du Québec à Trois-Rivières, Trois-Rivières, Canada
* Corresponding author: marc-olivier.st-pierre@etsmtl.ca

Received date: 08/01/2026
Accepted date: 16/03/2026
Publication date: 02/06/2026

Keywords: shoulder, center of rotation, glenohumeral, regression

1. Introduction

Accurate estimation of the center of the humeral head is critical in shoulder biomechanical research, as it defines the glenohumeral joint center of rotation. Moreover, accurate estimation of the center of rotation is of critical importance, as it underpins reliable goniometry, torque assessment, and the design of prostheses. Three-dimensional ultrasound-imaging (US) has shown promising results, outperforming functional methods (Lempereur et al., 2013). The reported 14 mm error using sphere fitting on the humeral head contour is likely due to acoustic attenuation and greater depth. In contrast, superficial landmarks such as the greater and lesser tubercles are more easily visualized (Bustamante & Cheruku, 2016) and reliably identified during post-processing. The aim of this study was to evaluate the robustness of a previously validated five-landmark regression model for glenohumeral center estimation when subjected to simulated localization error on dry humeri (St-Pierre M-O. et al., 2025). Specifically, we quantified the effect of global landmark noise via Monte-Carlo simulation and identified the most error-sensitive landmark through individual perturbation analysis.

2. Methods

Fifty-five dry humeri (n = 55) were scanned using an Artec Eva 3D scanner (± 0.1 mm). Specimens presenting large deformities on one of the anatomical landmarks were excluded. The specimens were scanned and imported as *.STL* files into Meshlab. Each anatomical landmark was then individually segmented (Figure 1).

2.1 Landmark definition

All landmarks coordinates were transformed to the body-fixed reference frame for each humerus based on ISB recommendations to provide a consistent local coordinate system across all specimens. The humeral head was defined as proximal to the anatomical neck of the humerus and its center was estimated using a sphere-fitting technique in MATLAB, representing the dependant variable in the regression model. Lateral and medial epicondyles were segmented as the entire bony protrusions on the distal epiphysis. Greater and lesser tubercles were defined in transverse view as the bony prominences arising from the anatomical neck. More specifically, the greater tubercule was defined laterally by the infraspinatus footprint and medially by the intertubercular groove. The lesser tubercule was defined by its limits in a frontal view (Figure 1). The deltoid tuberosity was segmented along the deltoid muscle insertion, retaining a 2-cm proximal portion (Figure 1). Each landmark centroid was defined as the geometric centroid of its entire bony region in MATLAB.

To cite this article: Marc-Olivier St-Pierre, Philippe Paquette, Guillaume Desroches, Rachid Aissaoui, Robustness of a Five-Landmark Predictive Model for the Glenohumeral Rotation Center to Simulate Ultrasound Localization Errors, *Multidisciplinary Biomechanics Journal*, 2026, vol. 3, p. 57–59, DOI: 10.46298/mbj.17935.

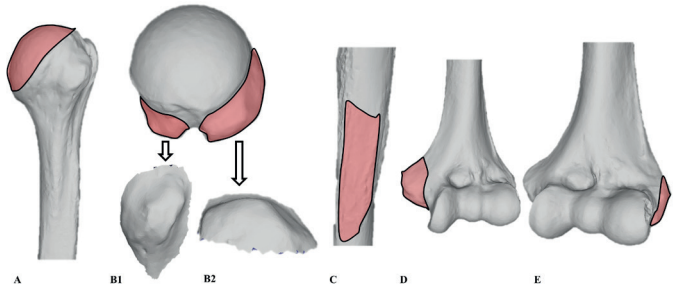

Figure 1. Anatomical landmarks identification. (A) Humeral head (B1) lesser tubercule, (B2) greater tubercule, (C) deltoid tuberosity, (D) medial epicondyle (E) lateral epicondyle. Based on ISB recommendations.

Credit: Marc-Olivier St-Pierre.

2.2 Sensitivity analysis to landmark localization error

A Ridge regularization multiple linear regression model was implemented to enhance numerical stability and prevent overfitting when using the 15 coordinates of the five landmarks (St-Pierre M-O. et al., 2025). To assess robustness against expected US localization errors, two sensitivity analyses were performed: (1) a Monte-Carlo simulation (10,000 iterations) adding independent Gaussian noise (σ = 0-6 mm, 1 mm increment) (Moriguchi et al., 2009) simultaneously to all 15 landmark coordinates; (2) an individual landmark perturbation analysis (1,000 iterations per landmark) adding Gaussian noise (±4 mm) (Hacihaliloglu, 2017) to the three coordinates of one landmark at a time while keeping the others unchanged.

3. Results and discussion

3.1 Simulated landmark error

The simulated landmark localization error (Gaussian noise, 1 to 6 mm) increased the 3D RMSE between the reference and predicted glenohumeral rotation center from 4.3 ± 2.1 (1 mm) to 13.8 ± 6.0 mm (6 mm) (Table 1). A previous study comparing 3D US and computerized tomography (CT) reconstructions of lumbar vertebrae reported highly similar volumes, with US slightly overestimating by only 0.44 mm (Effatparvar et al., 2022). This close agreement suggests that US can accurately capture bony geometry when volumes are reconstructed. Given that the high-precision 3D surface scanner used in the present study serves as a comparable gold standard for osseous morphology, similar volumetric fidelity can be expected with US.

Table 1. Effect of landmark localisation error on predicted humeral head center accuracy.

Simulated error (mm)	3D RMSE	95% PI (mm)
1	4.3 ± 2.1	1.0-9.5
2	5.4 ± 2.8	1.4-12.0
3	7.1 ± 3.5	1.9-15.2
4	8.7 ± 4.3	2.3-18.8
5	10.5 ± 5.2	2.7-22.9
6	13.8 ± 6.0	3.3-26.4

Data expressed in mm, RMSE: root mean square error, PI: prediction interval.

Credit: Marc-Olivier St-Pierre.

3.2 Individual landmark perturbations

The largest increases in 3D RMSE of the predicted glenohumeral rotation center were observed when Gaussian noise (±4 mm) was applied individually to the lesser tubercle (5.8 ± 2.7 mm) and greater tubercle (7.7 ± 3.5 mm). Although individual landmark perturbation revealed the greatest RMSE impact from the greater and lesser tubercles, these superficial landmarks are easy to observe and delineate (Bustamante & Cheruku, 2016).

4. Conclusions

This approach could enhance non-invasive estimation of the glenohumeral rotation center using 3D ultrasound, offering potential applications in personalized biomechanical modeling, preoperative surgical planning, and reducing dependence on ionizing imaging modalities such as CT, lowering the associated costs. Future in vivo validation that incorporates soft tissue effects will be essential for clinical translation.

Conflict of Interest Statement

None.

Contributor Roles

MOSP: Conceptualization, Methodology, Acquisition, Writing original draft; PP: Writing – review & editing, Supervision; GD: Writing – review & editing, Supervision; RA: Writing – review & editing, Supervision.

Funding

The first author (Marc-Olivier St-Pierre) is financially supported by the Natural Science and Engineering Research Council (NSERC).

References

Bustamante, S., & Cheruku, S. (2016). Ultrasound to improve target site identification for proximal humerus intraosseous vascular access. *Anesth Analg, 123*(5), 1335–1337. https://doi.org/10.1213/ane.0000000000001543

Effatparvar, M. R., St-Pierre, M.-O., & Sobczak, S. (2022). Assessment and improvement of a novel ultrasound-based 3D reconstruction method: Registered for lumbar spine. *Journal of Medical and Biological Engineering, 42*(6), 790–799. https://doi.org/10.1007/s40846-022-00764-x

Hacihaliloglu, I. (2017). Ultrasound imaging and segmentation of bone surfaces: A review. *Technology, 5*(02), 74–80. https://doi.org/10.1142/S2339547817300049

Lempereur, M., Kostur, L., Leboucher, J., Brochard, S., & Rémy-Néris, O. (2013). 3D freehand ultrasound to estimate the glenohumeral rotation centre. *Comput Methods Biomech Biomed Engin, 16*(sup1), 214–215. https://doi.org/10.1080/10255842.2013.815854

Moriguchi, C. S., Carnaz, L., Silva, L. C. C. B., Salasar, L. E. B., Carregaro, R. L., Sato, T. d. O., & Coury, H. J. C. G. (2009). Reliability of intra- and inter-rater palpation discrepancy and estimation of its effects on joint angle measurements. *Man Ther, 14*(3), 299–305. https://doi.org/10.1016/j.math.2008.04.002

St-Pierre M-O., Paquette P., Desroches G., & Aissaoui R. (2025). *Estimation of the Humeral Head Center Using Five Bony Landmarks [Unpublished data] Submitted to 10th World Congress of Biomechanics*.

2026-3 | International Shoulder Group (ISG) Congress 2026
2-3 June 2026, Lyon, France

Multidisciplinary Biomechanics Journal

Volumetric Muscle Modelling for Physiological Testing of the Glenohumeral Joint

Molly Abraham[a*], Jeremy Genter[a], Maria Grazia Polizzotto[b], Federico Andrei[b], Linda Paternò[b], Daniel Baumgartner[a]

[a] Institute of Mechanical Systems (IMES), Zurich University of Applied Sciences (ZHAW), Winterthur, Switzerland
[b] The BioRobotics Institute, Sant'Anna School of Advanced Studies, Pisa, Italy
* Corresponding author: abra@zhaw.ch

Received date: 16/01/2026
Accepted date: 16/03/2026
Publication date: 02/06/2026

Keywords: biomechanics, glenohumeral joint, muscle forces

1. Introduction

Accurate Glenohumeral (GH) simulation is challenging because the glenoid covers a small portion of the much larger humeral head, hence stability depends strongly on soft tissue and fine coordinated action of an over-actuated muscle system. As highlighted in the review by Genter et al. (2023), there is scope for improvement of existing GH joint simulators.

A key limitation is the modelling of the deltoid. Most simulators implement cable-based actuation, which either neglect the deltoid volume or run cables over the entire volume of cadaveric deltoids, as seen in the review by Genter et al. (2023).

Modelling deltoid volume improves physiological moment arm accuracy, enhancing GH simulation fidelity with easier testing than with cadaveric deltoids, advancing shoulder mechanics understanding.

This study developed a volumetric deltoid muscle model for a GH joint simulator and assessed its influence by comparing the forces required to achieve predefined abduction angles with a conventional cable-based actuation approach.

2. Methods

2.1 Mechanical system

2.1.1 Deltoid model

The deltoid model was manufactured from silicone cast into a custom 3D printed mould, with the geometry derived from one MRI scan (Genter et al., 2024). The deltoid was modelled with seven muscle portions grouped into anterior, middle, and posterior groups. The anterior and posterior groups each comprised two portions, while the middle group comprised three portions. The muscle path of each portion was achieved by positioning a Bowden cable along the midline of the corresponding muscle segment, with the hollow outer cable housing embedded within the silicone.

2.1.2 Scapula and Humerus model

The geometry of the scapula and humerus was derived from a CT scan corresponding to the MRI data used for the deltoid (Genter et al., 2024). The bone models were modified to incorporate insertion points for the actuation cables of each muscle portion, as well as adapters for integration with the GH simulator and prosthetic components, and were subsequently 3D printed. A prosthetic GH joint with CoCr surface was used to minimise friction within the experimental setup.

2.1.3 Integration of the model on a GH Simulator

The deltoid, scapula, and humerus models were implemented in an in-house GH simulator (Genter et al., 2023), which uses motor-actuated cables to simulate muscle-driven joint motion. EC motors (Maxon, Switzerland) tensioned muscle groups, with forces measured via load cells (Interfaceforce, Germany), abduction angles measured with an IMU (Tinkerforge, Germany), and joint reaction force (JRF) recorded using a six-degree-of-freedom load

To cite this article: Molly Abraham, Jeremy Genter, Maria Grazia Polizzotto, Federico Andrei, Linda Paternò, Daniel Baumgartner, Volumetric Muscle Modelling for Physiological Testing of the Glenohumeral Joint, *Multidisciplinary Biomechanics Journal*, 2026, vol. 3, p. 97–99, DOI: 10.46298/mbj.17940.

cell (Transmetra, Switzerland). To model arm inertia, a 2.8 kg mass was attached to the humerus at 23 cm from the humeral head centre.

Each EC motor was connected to a pulley system distributing force equally to the muscle portions. From the pulleys, cables ran through scapular insertion points, wrapping over the humerus and through the volumetric deltoid model when applicable, to the humeral insertion points (Figure 1).

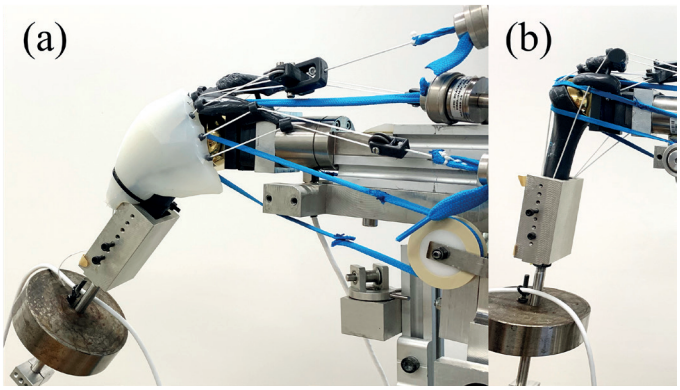

Figure 1. (a) Posterior view of abducted shoulder with volumetric deltoid model. **(b)** Anterior view of relaxed shoulder with cables wrapping over humerus.

2.2 Proof of concept testing

To validate the developed deltoid muscle model, forces in the middle and anterior deltoid muscle groups were measured under static conditions at predefined shoulder abduction angles, 15°, 30°, 45° and 60°, achieved by first increasing the force to achieve 60° and slowly reducing to achieve the specified abduction angles. As only abduction was of interest, the posterior deltoid was not tensioned. Equal forces were applied to both actuating deltoid muscle groups.

The measurements were replicated without the volumetric deltoid model, with the actuation cables wrapped directly over the bone. Three repeats were done for each setup.

3. Results and discussion

Integration of the volumetric deltoid model in the GH simulator altered the force–abduction relationship (Table 1), with muscle forces and JRFs required for a given abduction up to 75% lower than in the wrapped cable configuration. Without stabilisation from the volumetric deltoid, full abduction was not reached.

Table 1. Force applied in the middle/anterior deltoid and corresponding JRF to achieve abduction angle, n=3.

Angle (°)	Average Muscle Force (N)		Average Joint Reaction Force (N)	
	Silicone	Wrapped cables	Silicone	Wrapped cables
15	39±3	82±8	55±6	142±21
30	77±4	117±5	142±8	207±11
45	107±3	148±2	193±5	257±3
60	143±5	-	239±7	-

Measured JRFs were comparable to in vivo measurements of 207 (60) N at 30° (Bergmann et al., 2011). Our muscle force measurements were in a similar range to the ex vivo measurements from Ackland et al. (2011), of 104 (21) N at 30° in the middle deltoid and 11 (2) N in the anterior deltoid, where actuating cables ran over cadaveric deltoids.

4. Conclusions

Incorporating a volumetric deltoid model in a GH joint simulator improves accuracy by replicating physiological muscle moment arms in comparison to cable over bone or cadaveric deltoid setups. 3D printed components allow for personalisation of the experiment. It is seen that by increasing the deltoid moment arms, forces required for abduction can be reduced, therefore, cable-driven simulators wrapping over the humerus or deltoid might over or underestimate deltoid forces. Further tests could include the effect on rotator cuff contribution and incorporation of a more refined muscle force solver.

Acknowledgements

This work was done in collaboration between the Institute of Mechanical Systems (IMES) at Zurich University of Applied Sciences (ZHAW) and the BioRobotics Institute at Sant'Anna School of Advanced Studies in Pisa, Italy. We would like to thank the EELISA network for the collaboration opportunity.

Conflict of Interest Statement

None.

Funding

ZHAW internal funding with additional support of the EELISA alliance for travelling & exchange.

References

Ackland, D.C., Roshan-Zamir, S., Richardson, M., &Pandy, M.G. (2011). Muscle and joint-contact loading at the glenohumeral joint after reverse total shoulder arthroplasty. *J. Orthop. Res., 29*, 1850–1858. https://doi.org/10.1002/jor.21437

Bergmann, G., Graichen, F., Bender, A., Rohlmann, A., Halder, A., Beier, A., & Westerhoff, P. (2011). *In vivo* gleno-humeral joint loads during forward flexion and abduction. *Journal of biomechanics*, *44*(8), 1543–1552. https://doi.org/10.1016/j.jbiomech.2011.02.142

Genter, J., Rauter, G., Müller, A., Mündermann, A., & Baumgartner, D. (2023). Musculoskeletal model-based control strategy of an over-actuated glenohumeral simulator to assess joint biomechanics. *at - Automatisierungstechnik*, *71*(7), 505–514. https://doi.org/10.1515/auto-2023-0064

Genter, J., Croci, E., Ewald, H., Müller, A. M., Annegret Mündermann, & Baumgartner, D. (2023). *Ex vivo* experimental strategies for assessing unconstrained shoulder biomechanics: A scoping review. *Medical Engineering & Physics*, *117*, 104003–104003. https://doi.org/10.1016/j.medengphy.2023.104003

Genter, J., Croci, E., Oberreiter, B., Franziska Eckers, Dominik Bühler, Gascho, D., Müller, A. M., Annegret Mündermann, & Baumgartner, D. (2024). The influence of rotator cuff tear type and weight bearing on shoulder biomechanics in an ex vivo simulator experiment. *Journal of Biomechanics*, *166*, 112055–112055. https://doi.org/10.1016/j.jbiomech.2024.112055

2026-3 | International Shoulder Group (ISG) Congress 2026
2-3 June 2026, Lyon, France

Multidisciplinary Biomechanics Journal

Impact of the Posture – Standing or Sitting – on the Kinematics of the Violinist's Right Upper Limb

Amélie Roy[a*], Alexandre Naaim[a], Thomas Hoegy[a], Felipe Verdugo[b], Sonia Duprey[a]

a Univ Eiffel, Univ Lyon 1, LBMC UMR_T 9406, F-69622 Lyon, France
b S2M, Montréal, Canada
* Corresponding author: amelie.roy@univ-lyon1.fr

Received date: 16/01/2026
Accepted date: 16/03/2026
Publication date: 02/06/2026

Keywords: violin, kinematics, motion analysis

1. Introduction

Professional musicians spend several hours every day practicing their instrument. Among professional violinists, 86.8% reported pain-related musculoskeletal disorders (PRMD) mainly located in the upper body in the last twelve months, for 8.1% of them, it led to activity interruption (Kochem and al., 2017).

Violinists tend to practice both sitting down and standing up respectively for orchestral playing and for individual lessons. These different playing postures may have an influence on upper limb kinematics (Spahn and al., 2014), since modifying the spine curvatures can modify the scapula orientation and thus the whole upper limb kinematic chain.

Since kinematic variations can be beneficial in terms of PRMD prevention, it would be interesting to quantify the upper limb kinematics difference generated by different postures. The aim of this study is to investigate how the posture conditions influence this kinematics on professional violinists.

2. Methods

2.1 Protocol

Eight professional violinists played long notes on the four strings in two postural conditions: sitting upright and standing up. Fifty markers were positioned on their body. Participants all played the same violin and bow. Five and six additional markers were placed respectively on the bow and the violin. Ten Qualisys cameras were used to record the markers' coordinates (240 Hz). A metronome set to 80 bpm in an earpiece was used to control the tempo.

2.2 Data processing

Kinematics of each upper limb joint were extracted according to Wu and al. (2005), using a multi-segment open-loop model. In this model, the gleno-humeral (GH) joint has three degrees of freedom (DOF): flexion-extension, abduction-adduction and intern-extern rotation. The elbow and wrist have 2 DOF. The elbow has flexion-extension and intern-extern rotation whereas the wrist has flexion-extension and abduction-adduction. The multibody optimizations were performed with Bionc an open source library.

Data from all participants were aligned using the lateral movement of the bow relative to the violin using an Amerced Dynamic Time Warping (aeon toolbox, Hermann and al., 2023). ADTW were used to divide the music piece depending on the string played. For each string and for the full piece of music the range of motion (ROM (max − min)), the maximum, the minimum and the mean of the joint angles were computed.

2.2 Statistics

Parameters of each joint were compared for the 2 conditions using Wilcoxon tests. A difference was considered statistically significant when the p-value was below 0.02.

3. Results and discussion

Data from seven participants were finally used since one participant had too many markers' trajectories losses.

Between sitting straight and standing up, 4 DOF showed significative differences on at least one parameter.

To cite this article: Amélie Roy, Alexandre Naaim, Thomas Hoegy, Felipe Verdugo, Sonia Duprey, Impact of the Posture – Standing or Sitting – on the Kinematics of the Violinist's Right Upper Limb, *Multidisciplinary Biomechanics Journal*, 2026, vol. 3, p. 107–108, DOI: 10.46298/mbj.17941.

These discrepancies were always observed on the two lowest strings of the violin (Table 1).

Table 1. Confidence interval (CI) of parameters for each joint DOF showing a significant difference (p<0.02).

Joint	DOF	Parameters	Sitting straight (CI in °)	Standing (CI in °)
Wrist	Abd/Add	Max	[17.3 ; 27.1]	[16.5 ; 23.3]
		ROM	[5.5 ; 12.6]	[3.6 ; 9.9]
Elbow	Flex/Ext	Max	[99.9 ; 112.9]	[94.5 ; 111.7]
GH	Flex/Ext	Min	[-165.4 ; -145.8]	[-161.0 ; -144.5]
	Abd/Add	Max	[41.2 ; 64.5]	[47.5 ; 73.7]
	Abd/Add	Mean	[30.5 ; 56.4]	[37.9 ; 65.6]

On the shoulder, the maximum and mean abduction-adduction were greater when standing whereas the minimum flexion-extension was smaller when standing versus sitting.

For the elbow, the maximum flexion-extension was greater when sitting versus standing.

For the wrist, the maximum abduction-adduction and its ROM were greater when sitting compared to standing.

The largest influence on the CI was on the shoulder joint. No differences were shown on the two highest strings of the violin.

Spahn et al. (2014) showed differences on the maximum lordosis angle between standing and sitting positions. This could explain why these different postures could generate different scapula postures. The kinematics differences at the shoulder were then compensated at the elbow and wrist levels.

The present results are consistent with those from Tomezzoli et al. (2022) who revealed proximal upper limb kinematics differences during technical tasks performed with two different spine postures. The distal wrist's differences may be explained by the nature of the tasks in this study: its kinematics having a direct effect on the produced sound, it is paramount to adapt it to maintain a similar sound. Violinists would therefore compensate for the different postures by adapting their kinematic chain proximally and even distally to maintain a similar sound in various positions.

4. Conclusions

In conclusion, this study demonstrated an influence on the upper limb kinematics, especially the proximal shoulder kinematics between sitting and standing postures in violinists, on the two lowest strings played. A larger cohort would be required to increase statistical power and expand the present conclusions.

Conflict of Interest Statement

None.

Contributor Roles

A Roy: Formal analysis, Investigation, Writing-original draft. A Naaim: Supervision, Writing – review & editing. T Hoegy: Investigation. F Verdugo: Supervision. S Duprey: Funding acquisition, Conceptualization, Project administration, Writing – review & editing.

References

Kochem, F.B., & Silva, J.G. (2017). Prevalence and associated factors of playing-related musculoskeletal disorders in Brazilian violin players. *Medical Problems of Performing Artists, 32*(1), 27-32. https://doi.org/10.21091/mppa.2017.1006.

Spahn, C. et al. (2014). Comparing violinists' body movements while standing, sitting, and in sitting orientations to the right or left of a music stand. *Medical Problems of Performing Artists, 29*(2), 86-93. https://doi.org/10.21091/mppa.2014.2019.

Wu, G. et al. (2005). ISB recommendation on definitions of joint coordinate systems of various joints for the reporting of human joint motion—Part II: shoulder, elbow, wrist and hand. *Journal of Biomechanics, 38*(5), 981–992. https://doi.org/10.1016/j.jbiomech.2004.05.042.

Herrmann, M., & Webb, G.I. (2023). Amercing: an intuitive and effective constraint for dynamic time warping. *Pattern Recognition, 137*, 109333. https://doi.org/10.1016/j.patcog.2023.109333.

Tomezzoli, A., Fréchède, B., & Duprey, S. (2022). Slouched and erect sitting postures affect upper limb maximum voluntary force levels and fatiguability: A randomized experimental study. *IISE Transactions on Occupational Ergonomics and Human Factors*, *10*(3), 142–150. https://doi.org/10.1080/24725838.2022.2110544

2026-3 | International Shoulder Group (ISG) Congress 2026
2-3 June 2026, Lyon, France

Multidisciplinary Biomechanics Journal

Effects of Perceived Shoulder Dysfunction on Shoulder Biomechanics during Upper Quarter Y-Balance Test (YBT)

Robin Loiseau[a, b*], Yoann Blache[a], Théo Arnould[a], Mélick Filliard[a], Isabelle Rogowski[a]

a Université Claude Bernard Lyon 1, Laboratoire Interuniversitaire de Biologie de la Motricité- UR 7424, Lyon, France
b Université Lyon 1, Graduate Initiative MuSkLE, Lyon, France
* Corresponding author: robin.loiseau@univ-lyon1.fr

Received date: 14/01/2026
Accepted date: 16/03/2026
Publication date: 02/06/2026

Keywords: physical performance testing, Western Ontario shoulder instability questionnaire, upper limb

1. Introduction

Physical tests are used by clinicians to assess shoulder functions and risk for injury. Especially, YBT is designed to assess joint stability and mobility of the body upper quarter at the limit of stability (Bauer et al., 2023). While frequent physical screening may be time-consuming and fail to detect early injury markers, self-reported functional perception scales emerge as an alternative (Partner et al., 2022). However, it remains to establish whether the athletes with perceived shoulder dysfunction (DYS) present shoulder biomechanical impairments when performing YBT.

This study aimed to assess the effects of DYS on the ground reaction forces (GRF), muscle activity and scapular kinematics of the support upper extremity during YBT.

2. Methods

2.1 Participants

Twelve overhead sport athletes with dominant side DYS and twelve non-dysfunctional (NDYS) matched-controls (Table 1) participated in this study (Ethical Committee #2024121201). DYS was defined by a score above 250 pts for the Western Ontario Shoulder Instability questionnaire (Kirkley et al., 1998).

2.2 Testing procedure

Each athlete was equipped with four surface electromyography (EMG) electrodes on dominant Upper (UT), Middle (MT) and Lower Trapezius (LT), and Serratus Anterior (SA) and with 29 markers placed on the thorax (8), and dominant scapula (5), clavicle (2), arm (7) forearm (3) and hand (4).

After a standardized warm up, four isometric maximal contractions were repeated twice to record the UT, MT, LT and SA maximal activity (2000 Hz; Trigno Avanti Sensor, Delsys, Boston, US). A custom kinematic model with subject-specific ellipsoid, defining the scapulothoracic joint, was used from 5 static poses for which the trigonum spinae and inferior angle markers were relocated after palpation (Lefebvre et al., 2025). The marker trajectories were recorded using 14 cameras (200 Hz; Miqus M3, Qualisys AB, Goeteborg, Sweden).

For YBT, the athlete was in one hand push up position with dominant hand on a force plate (2000 Hz; FP5060-06-PT-2000, Bertec Corporation, Columbus, US) and feet spaced at shoulder width on a second force plate. Then, with the free hand, the athlete was instructed to move a reach indicator as far as possible, in medial, inferolateral and superolateral directions successively. After a familiarization trial, three maximal trials were performed. Maximal distance per direction was normalized by the limb length, i.e. distance between the 7th cervical and 3rd finger when the nondominant upper limb abducted at 90°, elbow, wrist and fingers fully extended, and thumb pointed upward.

2.3 Outcome measures

GRF data were filtered (low-pass 4th-order Butterworth filter, 20-Hz cut-off frequency) and expressed relative

To cite this article: Robin Loiseau, Yoann Blache, Théo Arnould, Mélick Filliard, Isabelle Rogowski, Effects of Perceived Shoulder Dysfunction on Shoulder Biomechanics during Upper Quarter Y-Balance Test (YBT), *Multidisciplinary Biomechanics Journal*, 2026, vol. 3, p. 103–106, DOI: 10.46298/mbj.17918.

to body mass. For each reach direction, the X-axis of the GRF local reference system was aligned with the direction of motion, the Z-axis, perpendicular to motion (GRF_P), and Y-axis with gravitational direction (GRF_G). EMG data were filtered (4th-order Butterworth filter, pass-band 15-450 Hz), rectified, smoothed (4th-order Butterworth filter, low-pass 20-Hz), and expressed relative to maximal activity of maximal contractions. Scapular rotations were defined as internal/external, downward/upward rotations and anterior/posterior tilt.

For each YBT direction. GRF_M, GRF_P, and GRF_G for hand and feet and EMG per muscle were averaged between 70% and 100% of the reach distance during both the reach and return phases. Ranges of motion per scapular rotation were computed for the same phase portions. Finally, for GRF_G, mean hand values were divided by mean feet values (GRF_{Prop}).

Independent t-tests were used to compare demographic and dominant-side biomechanical parameters between DYS and NDYS groups, with significant level set at $p \leq 0.05$. Hedges' g effect sizes were computed and interpreted as $g \approx 0.2$ for small, $g \approx 0.5$ for medium and $g \approx 0.8$ for large effect.

3. Results and discussion

Table 1 shows participants' characteristics and mean outcome measures. Both groups had similar demographic and anthropometric characteristics, and DYS group had WOSI scores 10 times higher than NDYS group, validating the perception of altered shoulder functions. Athletes with perceived shoulder instability achieved similar YBT distances as controls, confirming the limited YBT ability to screen for shoulder injury risk (Bauer et al., 2023).

Perceived shoulder instability of the support upper extremity resulted in no periscapular muscle nor scapular range of motion adaptations when compared to healthy shoulder. For mediolateral reach direction, the perceived shoulder instability led to reduced vertical loading on the hand and a compensatory increase in loading through the feet. These adaptations in GRF distribution would involve changes in reaction force orientation and intensity at the glenohumeral joint and/or changes in force couples of the deep muscles, such as the rotator cuff muscles (Ishikawa et al., 2023). To better understand the underpinning biomechanics, further studies should enroll larger sample size and integrate musculoskeletal simulations to explore the glenohumeral joint loading related to the perceived shoulder dysfunction.

4. Conclusions

Maintaining physical performance despite the perceived shoulder instability did not appear related to adaptations in underlying neuromuscular strategies. These preliminary findings suggest that monitoring athlete's self-reported dysfunction may be relevant for detecting early-stage shoulder pathology.

Conflict of Interest Statement

None.

Contributor Roles

RL: Conceptualization, Methodology, Writing original draft, Data collection and treatment; YB: Conceptualization, Methodology, Data treatment, Supervision, Funding acquisition, Writing – review & editing; TA: Methodology, Data collection and treatment; MF: Methodology, Data collection; IR: Conceptualization, Methodology, Writing – review & editing, Supervision, Funding acquisition.

Funding

This study was supported by the 'Région Auvergne-Rhône-Alpes' (#2101788201).

References

Bauer, J., Panzer, S., Gruber, M., & Muehlbauer, T. (2023). Associations between upper quarter Y-balance test performance and sport-related injuries in adolescent handball players. *Frontiers in Sports and Active Living, 5*, 1076373. https://doi.org/10.3389/fspor.2023.1076373

Partner, R., Jones, B., Tee, J., & Francis, P. (2022). Playing through the pain: The prevalence of perceived shoulder dysfunction in uninjured rugby players using the Rugby Shoulder Score. *Physical Therapy in Sport, 54*, 53–57. https://doi.org/10.1016/j.ptsp.2022.01.001

Kirkley, A., Griffin, S., McLintock, H., & Ng, L. (1998). The development and evaluation of a disease-specific quality of life measurement tool for shoulder instability. *The American Journal of Sports Medicine, 26*, 764–772. https://doi.org/10.1177/03635465980260060501

Lefebvre, F., Rogowski, I., Long, N., & Blache, Y. (2025). Three-dimensional markerless pose estimation for anatomical landmarks of the shoulder and upper limb. *J Electromyogr Kinesiol, 85*, 103067. https://doi.org/10.1016/j.jelekin.2025.103067

Ishikawa, H., Smith, K. M., Wheelwright, J. C., Christensen, G. V., Henninger, H. B., Tashjian, R. Z., & Chalmers, P. N. (2023). Rotator cuff muscle imbalance associates with shoulder instability direction. *Journal of Shoulder and Elbow Surgery, 32*(1), 33–40. https://doi.org/10.1016/j.jse.2022.06.022

Table 1. Mean (± standard deviation) anthropometric and demographic characteristics, YBT distances (% limb length), muscle activity (% IMVC) of upper (UT), middle (MT) and lower trapezius (LT) and serratus anterior (SA), ground reaction forces ($N.kg^{-1}$) in moving direction (GRF_M), perpendicular motion direction (GRF_P), and vertical direction (GRF_G), scapular ranges of motion (°) in internal/external (IER), downward/upward (DUR) rotations and anterior/posterior tilt for athletes with (DYS) and without perceived dysfunction (NDYS); effect sizes (g) and p-value.

			DYS	NDYS	g	p
Age (years)			20.9 ± 2.3	21.1 ± 4.3	0.05	0.46
Sex (M/F)			10/2	10/2		
Height (m)			1.77 ± 0.06	1.76 ± 0.10	0.11	0.30
Weight (kg)			70.2 ± 4.8	69.3 ± 10.5	0.22	0.40
Weekly training (hr)			5 ± 1	5 ± 2	0.00	0.50
WOSI Score			546 ± 232	45 ± 57	2.96	<0.001[a]
YBT Medio-Lateral		Distance	1.09 ± 0.09	1.11 ± 0.04	0.30	0.24
		LT	0.22 ± 0.22	0.19 ± 0.14	0.08	0.35
		MT	0.05 ± 0.03	0.07 ± 0.10	0.29	0.24
		UT	0.19 ± 0.14	0.16 ± 0.11	0.17	0.34
		SA	0.38 ± 0.15	0.37 ± 0.1	0.04	0.46
	Hand	GRF_M	0.43 ± 0.09	0.42 ± 0.14	0.10	0.41
		GRF_G	5.79 ± 0.32	5.98 ± 0.23	0.66	0.06
		GRF_P	1.60 ± 0.35	1.51 ± 0.33	0.29	0.25
	Feet	GRF_M	-0.27 ± 0.39	-0.33 ± 0.32	0.18	0.34
		GRF_G	4.21 ± 0.30	3.99 ± 0.29	0.76	0.04
		GRF_P	1.50 ± 0.33	1.35 ± 0.36	0.44	0.15
	Hand/feet	GRFG	0.58 ± 0.03	0.60 ± 0.02	0.85	0.03
		IER	12.66 ± 13.74	11.84 ± 6.99	0.07	0.43
		DUR	14.71 ± 11.68	16.20 ± 11.76	0.13	0.38
		APT	4.62 ± 5.92	3.41 ± 3.79	0.24	0.28
YBT Infero-Lateral		Distance	0.96 ± 0.17	0.93 ± 0.10	0.27	0.26
	EMG	LT	0.07 ± 0.09	0.06 ± 0.07	0.17	0.35
		MT	0.06 ± 0.06	0.03 ± 0.02	0.63	0.08
		UT	0.28 ± 0.14	0.24 ± 0.13	0.28	0.26
		SA	0.47 ± 0.23	0.50 ± 0.22	0.15	0.36
	Hand	GRF_M	0.21 ± 0.14	0.23 ± 0.07	0.23	0.30
		GRF_G	5.37 ± 0.55	5.37 ± 0.36	0.00	0.50
		GRF_P	1.28 ± 0.48	1.49 ± 0.46	0.44	0.15
	Feet	GRF_M	-0.10 ± 0.23	-0.15 ± 0.21	0.22	0.30
		GRF_G	4.60 ± 0.49	4.55 ± 0.38	0.10	0.42
		GRF_P	1.21 ± 0.57	1.33 ± 0.47	0.23	0.29
	Hand/feet	GRFG	0.54 ± 0.05	0.54 ± 0.04	0.06	0.45
		IER	26.31 ± 12.81	20.48 ± 8.77	0.25	0.27
		DUR	30.97 ± 9.69	26.37 ± 13.25	0.36	0.20
		APT	10.80 ± 10.76	7.41 ± 6.02	0.36	0.19
YBT Supero-Lateral		Distance	0.81 ± 0.10	0.82 ± 0.09	0.10	0.42
		LT	0.07 ± 0.05	0.09 ± 0.05	0.36	0.20
		MT	0.04 ± 0.03	0.03 ± 0.02	0.36	0.20
		UT	0.24 ± 0.16	0.17 ± 0.10	0.48	0.14
		SA	0.21 ± 0.09	0.17 ± 0.08	0.44	0.16
	Hand	GRF_M	0.04 ± 0.14	0.04 ± 0.14	0.03	0.48
		GRF_G	6.88 ± 0.59	7.11 ± 0.34	0.48	0.13
		GRF_P	0.46 ± 0.60	0.32 ± 0.33	0.27	0.26
	Feet	GRF_M	-0.01 ± 0.18	-0.01 ± 0.10	0.01	0.49
		GRF_G	3.07 ± 0.65	2.80 ± 0.27	0.55	0.10
		GRF_P	0.32 ± 0.56	0.14 ± 0.33	0.40	0.17
	Hand/feet	GRFG	0.69 ± 0.06	0.72 ± 0.03	0.53	0.11
		IER	24.45 ± 13.60	30.37 ± 13.40	0.33	0.22
		DUR	34.07 ± 10.49	36.72 ± 14.77	0.63	0.12
		APT	9.17 ± 5.05	10.40 ± 4.66	0.55	0.13

[a] p was obtained from non-parametrical Mann-Whitney test.

Credit: Loiseau.

2026-3 | International Shoulder Group (ISG) Congress 2026
2-3 June 2026, Lyon, France

Multidisciplinary Biomechanics Journal

Greater Shoulder Elevation Variability During Arm Cocking Is Associated with Decreased Elbow Varus Torque in NCAA Division I Baseball Pitchers

Gretchen D. Oliver*, Kai-Jen Cheng, Ian Jump, Ryan Zappa, Kevin Rodriguez Chavarria

Sports Medicine & Movement Laboratory, Auburn University, Auburn, AL, USA
* Corresponding author: goliver@auburn.edu

Received date: 16/01/2026
Accepted date: 16/03/2026
Publication date: 02/06/2026

Keywords: shoulder elevation, UCL, shoulder elevation, RMS deviation

1. Introduction

Ulnar collateral ligament (UCL) injuries are the most common and significant injuries in baseball pitchers. UCL injury is strongly linked to peak elbow varus torque (pEVT), which represents the mechanical loading experienced at the medial elbow (Petty et al., 2004). Considerable effort has been devoted to identifying pitching mechanics that contribute to elbow loading, with a focus on peak shoulder external rotation (MER) and shoulder elevation (Slowik et al., 2019). Previous studies have emphasized the importance of maintaining approximately 90° of shoulder elevation during the pitching cycle, particularly around peak shoulder external rotation (MER) (Matsuo et al., 2002; Sabick et al., 2005). However, shoulder elevation has primarily been assessed using isolated measurements rather than continuous pitching motion, and it is considered that maintaining 90° during the pitching cycle is important (Matsuo et al., 2002; Sabick et al., 2005).

Discrete measures provide only single time-point representations of shoulder elevation and do not reflect how consistently the arm is maintained near the mechanically preferred 90° elevation throughout the pitching phase. As a result, they may fail to characterize the magnitude of deviation from this position across time, potentially limiting interpretation of its relationship with joint loading. This study introduced a biomechanical variable to characterize shoulder elevation. Shoulder elevation control was quantified as the root mean square (RMS) deviation from 90° relative to the trunk–upper arm angle during the arm-cocking phase. The primary objective was to examine the relationship between shoulder elevation RMS deviation pEVT.

2. Methods

Data were collected during NCAA Division I baseball games (2023-2025 seasons). Inclusion criteria were: (1) Only fastballs; (2) Trials without pose-tracking errors; (3) Pitchers with a minimum of 5 pitches; and (4) minimum speed threshold of 35.76 m/s (80mph). 362 pitchers met the criteria (91.12±10.14 kg; 1.88±0.06 m; ball velocity: 40.58±1.32 m/s). Procedures were approved by the Institutional Review Board of the University. Data were collected at 300 Hz using an 8-camera KinaTrax markerless motion-capture system. Data were processed from C3D files using Butterworth low-pass filters (trunk and pelvis: 10 Hz; legs: 6 Hz; arms: 20 Hz) following KinaTrax procedures. Variables were extracted during the arm-cocking phase (foot contact (FC) to MER) and included shoulder elevation and pEVT. Shoulder elevation was defined as the angle between the thorax and throwing upper arm (**Figure 1**), and RMS deviation was calculated as the square root of the mean squared deviation from 90° across time points.

A two-level linear mixed model was used to examine whether RMS deviation of shoulder elevation predicted pEVT, with pitches nested within pitchers. An unconditional model partitioned within- and between-pitcher

To cite this article: Gretchen D. Oliver, Kai-Jen Cheng, Ian Jump, Ryan Zappa, Kevin Rodriguez Chavarria, Greater Shoulder Elevation Variability During Arm Cocking Is Associated with Decreased Elbow Varus Torque in NCAA Division I Baseball Pitchers, *Multidisciplinary Biomechanics Journal*, 2026, vol. 3, p. 109–111, DOI: 10.46298/mbj.17931.

variance, followed by random intercept models estimating both between- and within-pitcher effects utilizing fixed (Model 1) and random slopes (Model 2) to account for individual differences. Analyses were conducted in R, with significance set at $p<.05$.

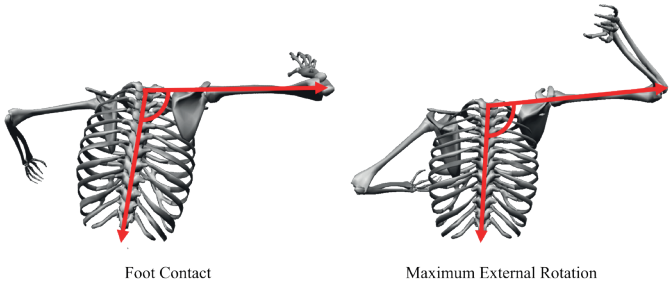

Figure 1. Shoulder Elevation Angle at FC and MER.

3. Results and discussion

Model comparison revealed Model 2 ($\chi^2(2)=381.02$, $p<.001$) showed superior fit. While Model 2 revealed an insignificant within-pitcher effect, the between-pitcher effect indicated that a 1° increase in RMS deviation led to a .3 N.m decrease in pEVT. Fixed and random effects are in Table 1. Pitchers with higher shoulder elevation RMS deviation during the arm-cocking phase exhibited lower average pEVT, suggesting that the variable reflects differences in mechanical loading rather than a discrete positional effect. Although the estimated change in pEVT per 1° increase in RMS deviation appears small (≈0.3 N·m), it should be interpreted in the context of how RMS deviation is defined. RMS deviation summarizes the magnitude of deviation from 90° across all frames of the arm-cocking phase rather than reflecting a single time-point. Accordingly, the practical relevance may be more apparent when considering realistic between-pitcher differences (e.g., several degrees of RMS deviation), which scales to larger N·m differences in pEVT. Given that EVT is associated with pitching intensity and ball velocity (Slowik et al., 2019), these differences may represent meaningful variation in mechanical loading. A measurement-related limitation should be noted. The KinaTrax system has demonstrated reliability in human movement analyses (Schoenwether et al., 2025), but direct validation against marker-based motion capture has not been established for high-velocity throwing.

Table 1. Effects from Random Slopes and Intercepts Model (Model 2).

Parameters	Est	SE	95%	*df*	*t*	*p*
Fixed effects						
Intercept	125.09	1.47	[122.4, 128.17]	219.43	84.87	0.00
RMS (degree)(BS)	-0.30	0.14	[-0.67, 0.02]	176.77	-2.19	0.03
RMS (degree)(WS)	-0.11	0.29	[-0.81, 0.2]	219.16	-0.37	0.71
Random effects						
Intercept variance (level 2: person)	464.34					
RMS (degree)(WS)	1.43					
Residual variance Fixed effects	67.55					

RMS: Root Mean Square of deviation of shoulder elevation from 90° from FC to BR; Est. = estimate; SE = standard error; BS = between-subject; WS = within-subject.

4. Conclusions

This study employed shoulder elevation RMS deviation during arm-cocking as a continuous indicator of shoulder control in competitive pitching. Using in-game markerless motion capture from NCAA Division I pitchers, greater deviation from approximately 90° between FC and MER was associated with lower pEVT. These findings suggest that shoulder elevation RMS deviation was not associated with pEVT at the within-pitcher level. Although a near 90° angle is commonly regarded as biomechanically advantageous, the observed association with pEVT was small, indicating only a modest influence on elbow loading. Shoulder elevation patterns may instead affect pEVT indirectly via pitch velocity, which was not measured in this study. Accordingly, RMS deviation in shoulder elevation appears to be a limited standalone metric, warranting further investigation into its relationship with pitch velocity.

Conflict of Interest Statement

The authors have no conflicts of interest to disclose.

Contributor Roles

GO: Validation, supervision, writing review, editing; KJC: Conceptualization, methodology, analysis, review; IJ: writing, review, editing; RZ: writing, review, editing; KRC: writing, review, editing.

References

Matsuo, T., Matsumoto, T., Mochizuki, Y., Takada, Y., & Saito, K. (2002). Optimal shoulder abduction angles during baseball pitching from maximal wrist velocity and minimal kinetics viewpoints. *Journal of Applied Biomechanics, 18*(4), 306–320. https://doi.org/10.1123/jab.18.4.306

Petty, D. H., Andrews, J. R., Fleisig, G. S., & Cain, E. L. (2004). Ulnar collateral ligament reconstruction in high school baseball players: clinical results and injury risk factors. *American Journal of Sports Medicine, 32*(5), 1158–1164. https://doi.org/10.1177/0363546503262166

Sabick, M. B., Kim, Y. K., Torry, M. R., Keirns, M. A., & Hawkins, R. J. (2005). Biomechanics of the shoulder in youth baseball pitchers: implications for the development of proximal humeral epiphysiolysis and humeral retrotorsion. *American Journal of Sports Medicine, 33*(11), 1716–1722. https://doi.org/10.1177/0363546505275347

Slowik, J. S., Aune, K. T., Diffendaffer, A. Z., Cain, E. L., Dugas, J. R., & Fleisig, G. S. (2019). Fastball velocity and elbow-varus torque in professional baseball pitchers. *J Athl Train, 54*(3), 296–301. https://doi.org/10.4085/1062-6050-558-17

Schoenwether, B., Ripic, Z., Nienhuis, M., Signorile, J. F., Best, T. M., et al. (2025). Reliability of artificial intelligence-driven markerless motion capture in gait analyses of healthy adults. *PLOS ONE, 20*(1), e0316119. https://doi.org/10.1371/journal.pone.0316119

2026-3 | International Shoulder Group (ISG) Congress 2026
2-3 June 2026, Lyon, France

Multidisciplinary Biomechanics Journal

The Relationship Between Biceps Activity and Shoulder Eccentric External Rotation Torque

Jonathan Washatka, PT, DPT[a, b], Mara-Paige Rincher, AT, DAT[b], Alec Banuach, PT, DPT[b], Olivia Roe, PT, DPT[b], Justin L. Staker, PT, PhD[a, b*]

a University of Minnesota Rehabilitation Biomechanics Lab, Minneapolis, MN
b University of Minnesota Department of Intercollegiate Athletics
* Corresponding author: stak@umn.edu

Received date: 16/01/2026
Accepted date: 16/03/2026
Publication date: 02/06/2026

Keywords: electromyography, biceps, torque, eccentric

1. Introduction

Electromyography (EMG) and handheld dynamometry (HHD) are increasingly accessible clinical tools, and clinicians are beginning to use them to assess eccentric shoulder loading for individual-level decision-making such as return-to-play (Johansson et al., 2015). For example, Cools et al. (2016) published HHD strength reference values for overhead athletes, enabling clinical assessment of how an individual compares to normative data. However, the biceps' contribution during eccentric external rotation, thought to help decelerate the arm after throwing, remains unclear, and little is known about the feasibility of pairing EMG with HHD during a standardized shoulder eccentric external rotator test or how to interpret results without reference values. Therefore, the primary aim of this study is to quantify the association between mean and peak biceps EMG activity and eccentric shoulder external rotation torque using clinically available instrumentation.

2. Methods

A convenience sample of nineteen Division 1 softball players were enrolled for this study. Participants were free from shoulder injury and actively participating in team activities. The participants were seated with their shoulder at 90° abduction and external rotation, and their elbow at 90°. Their elbow was placed on a pad to ensure proper positioning and a therapist lightly placed their hand on the participant's shoulder as a cue to maintain proper shoulder positioning. T performed maximal eccentric external rotation against a handheld dynamometer, moving from 90° external rotation to 0° over three seconds, timed with a metronome. This method has been shown to be reliable, result in valid angular velocity (Johansson et al., 2015) and has subsequently been used in research (Cools et al., 2016; Johansson et al., 2025). A practice trial was performed, followed by two recorded trials. Testing was then repeated on the contralateral arm, with limb order randomized by a coin flip. Forearm length was used to derive torque, which was normalized to body mass (kg).

During testing, surface EMG was recorded from the biceps and using wireless Ultium EMG sensors (Noraxon USA Inc., Scottsdale, AZ; MR4.0 software). The skin was cleaned with an alcohol wipe, and the electrodes were placed parallel to the muscle fibers on the mid-belly (Delagi, 1980). The participants performed a two to three-second maximal voluntary isometric contraction (MVIC) of the biceps by exerting maximum effort against an immovable object with the elbow at approximately 90° in a seated position. The biceps signal was normalized to the MVIC signal. EMG was sampled at 2000 Hz, band-pass filtered (4^{th}-order Butterworth, 10 and 500 Hz), rectified, and smoothed using a 50 ms root-mean-square moving window (Gurney et al., 2016). Onset and offset were identified from video-recorded visible motion, with synchronized inertial measurement unit plots from the EMG sensors used to inform the best estimate of movement start and end.

To cite this article: Jonathan Washatka, Mara-Paige Rincher, Alec Banuach, Olivia Roe, Justin L. Staker, The Relationship Between Biceps Activity and Shoulder Eccentric External Rotation Torque, *Multidisciplinary Biomechanics Journal*, 2026, vol. 3, p. 113–115, DOI: 10.46298/mbj.17943.

3. Results and discussion

Two separate linear mixed regression models included mean EMG and maximum EMG on normalized torque (Nm/kg) and side from each trial. An interaction between the predictors was considered, and a random intercepts model was used to account for repeated measures. The outcome was log-transformed, and model diagnostics were performed to account for model fit. Partial Eta^2 is reported for the effect size (ES) for the interaction term. In contrast, ES for the beta coefficients is reported as the percent EMG change for a positive 1-standard-deviation change in torque.

For both models, there was a significant interaction between normalized torque and side tested (mean EMG: $p < 0.01$, ES = 0.13; max EMG: $p < 0.01$, ES = 0.14). For the dominant arm, as torque increased by .1 Nm/kg, mean normalized EMG decreased by 3.0% ($p = 0.88$, ES = decrease by 3.2%) and maximum normalized EMG decreased by 7.3% ($p = 0.70$, ES = decrease by 7.9%). For the non-dominant arm, as torque increased by 0.1 Nm/kg, mean normalized EMG increased by 55% ($p < 0.01$, ES = increase by 62%) and max normalized EMG increased by 50% ($p = 0.01$, ES = increase by 56%).

For mean and maximum EMG, the rate of change in the non-dominant arm compared to the dominant arm is 1.60 ($p < 0.01$) and 1.62 ($p < 0.01$), respectively.

Biceps activation during eccentric external rotation was side-dependent. In the dominant arm, greater eccentric rotation torque was not associated with higher biceps EMG, whereas in the non-dominant arm, biceps EMG increased with torque. While the reason for the difference in sides is unknown, perhaps the dominant arm has better motor control than the non-dominant arm and can therefore better isolate activation of the external rotators, minimzing recruitment of the biceps. These findings provide an initial, clinically feasible approach for assessing biceps co-activation during eccentric shoulder loading.

4. Conclusions

These results help clinicians interpret EMG and HHD eccentric external rotation by showing that higher torque does not necessarily imply greater biceps activation in the dominant throwing arm, and that side-specific references may be needed. Further, while clinical assumptions that the biceps muscle is active during the follow-through of the throwing motion may be true, it is not necessarily a function of high shoulder eccentric external rotation torque production.

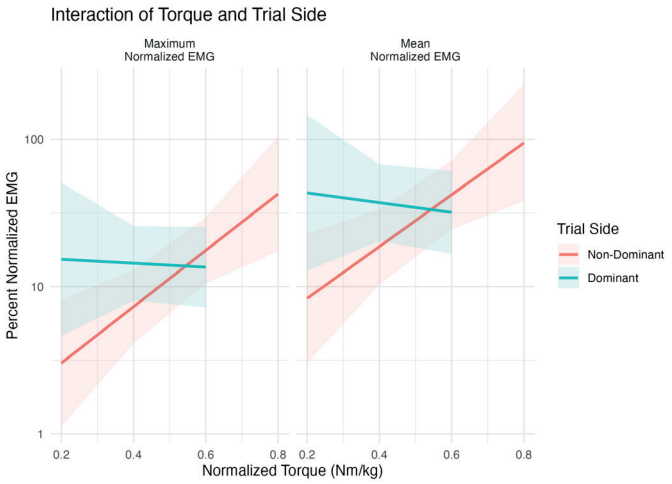

Figure1. Relationship between normalized torque and biceps EMG. EMG is on a log-scale.

Acknowledgements

We appreciate the time commitment of the volunteer participants.

Conflict of Interest Statement

None.

Contributor Roles

JW: Conceptualization, methodology, Data collection and analysis writing original draft; AB, OR: conceptualization; MR: conceptualization, data collection; JS data collection, methodology, supervision, writing – review & editing.

Funding

NIH/NIAMS T32 AR050938 "Interdisciplinary Musculoskeletal Research Training Program".

References

Cools, A. M., Vanderstukken, F., Vereecken, F., Duprez, M., Heyman, K., Goethals, N., & Johansson, F. (2016). Eccentric and isometric shoulder rotator cuff strength testing using a hand-held dynamometer: Reference values for overhead athletes. *Knee Surgery, Sports Traumatology, Arthroscopy, 24*(12), 3838–3847. https://doi.org/10.1007/s00167-015-3755-9

Delagi, E. F. (1980). *Anatomic guide for the electromyographer—The limbs* (3rd ed.). Springfiel, IL: Thomas.

Gurney, A. B., Mermier, C., LaPlante, M., McMahon, J., Schneider, R., & Croy, T. (2016). Shoulder electromyography measurements during activities of daily living and routine rehabilitation exercises. *Journal of Orthopaedic & Sports Physical Therapy, 46*(5), 375–383. https://doi.org/10.2519/jospt.2016.6090

Johansson, F. R., Skillgate, E., Lapauw, M. L., Clijmans, D., Deneulin, V. P., Palmans, T., Engineer, H. K., & Cools, A. M. (2015). Measuring eccentric strength of the shoulder external rotators using a handheld dynamometer: Reliability and validity. *Journal of Athletic Training, 50*(7), 719–725. https://doi.org/10.4085/1062-6050-49.3.72

Johansson, F., Batt, M., Ellenbecker, T., & Skillgate, E. (2026). Association between eccentric and isometric shoulder rotation strength, shoulder range of motion and injury incidence in the shoulder in adolescent competitive tennis players: The SMASH cohort study. *Sports Health, 18*(1), 14–21. https://doi.org/10.1177/19417381251396149

2026-3 | International Shoulder Group (ISG) Congress 2026
2-3 June 2026, Lyon, France

Multidisciplinary Biomechanics Journal

Interest of the Upper Quarter Y-Balance Test for Assessing Upper-Extremity Force Capacity in Multisport Athletes

Thomas De Sousa[a, b*], Isabelle Rogowski[b], Yoann Blache[b]

a TRINOMA, Villefort, France
b Univ Lyon, Université Claude Bernard Lyon 1, Laboratoire Interuniversitaire de Biologie de la Motricité, EA 7424, F-69622 Villeurbanne, France
* Corresponding author: thomas@trinoma.fr

Received date: 15/01/2026
Accepted date: 16/03/2026
Publication date: 02/06/2026

Keywords: physical performance test, assessment, athletes

1. Introduction

Proposed to assess joint stability and mobility of the entire upper quarter and trunk at the limit of stability (Gorman et al., 2012), the Upper Quarter Y-Balance Test (UQYBT) is a physical performance test used in performance and return to sport contexts to improve athlete management (Schwank et al., 2022). While it is suggested that similar performance are reached by the dominant and non-dominant upper extremities (Steele & Valentin, 2024), these performances may result from different motor strategies. Consequently, assessing the biomechanical strategies of the dominant and non-dominant upper extremities may improve understanding of the role of dominance during the test.

To perform the UQYBT, participant must be able to sustain a large portion of his body weight on the support Upper Extremity (UE) (Gorman et al., 2012). However, the role of the forces sustained by the support UE in UQYBT performance remains to be investigated. Therefore, examining the relationship between the force produced by the support UE may improve athlete management by enhancing understanding of the factors influencing UQYBT performance. This study aimed to assess the influence of the dominance and ground reaction forces level on the UQYBT performances.

2. Methods

Twenty-five male athletes (age: 26.0 ± 11.3 yrs; height: 179.0 ± 6.5 cm; mass: 77.8 ± 23; right-handed: 22; dominant limb length: 91.0 ± 3.9; non-dominant limb length: 91.0 ± 3.8) participated in the study (ethical committee #2022-10-13-002). Inclusion criteria were being aged from 18 to 35 years and practicing sport activity involving at least one UE. Exclusion criteria were injured in the 6-months before the study or undergone surgery at one UE.

Ground reaction force signals of the support UE were collected using a force plate (2000 Hz, Kistler, Switzerland). Four reflective markers were fitted on each participant's hand to compute the hand barycenter, calculated as the average of the 3D positions of the markers, using an optoelectronic system (200 Hz, Qualisys, Gothenburg, Sweden). For the UQYBT, three graduated pipes were placed beyond the force plate, to define the medial (ML), inferolateral (IL), and superolateral (SL) directions (Gorman et al., 2012). From a unilateral push-up position, the task consisted of pushing boxes as far as possible in the ML, IL and SL directions, successively. After completing one familiarization trial, three maximal trials were performed per UE, with 30-s recovery between trials.

UQYBT performances were normalized to the moving limb length (MLL). For each UQYBT direction, local reference systems were computed with the origin defined as the barycenter of the support hand with the x-axis pointing towards the box direction, z-axis orthogonal to the box direction and y-axis vertical (Figure 1). Ground reaction force signals were normalized to body

To cite this article: Thomas De Sousa, Isabelle Rogowski, Yoann Blache, Interest of the Upper Quarter Y-Balance Test for Assessing Upper-Extremity Force Capacity in Multisport Athletes, *Multidisciplinary Biomechanics Journal*, 2026, vol. 3, p. 117–119, DOI: 10.46298/mbj.17927.

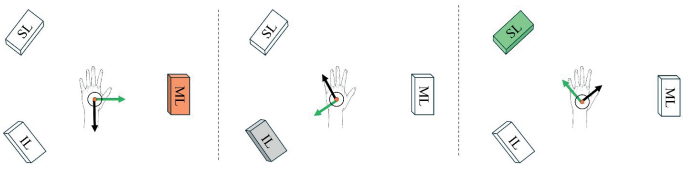

Figure 1. Local reference systems used for the mediolateral direction (ML) (left), inferolateral (IL) direction (center) and superolateral (SL) direction (right). Green arrow: propulsive force; black arrow: orthogonal force; circle: vertical force.

weight and the propulsive force (x-axis), orthogonal force (y-axis) and the body weight supported (vertical axis) were averaged for each direction. Linear mixed models were used to determine the effect of dominance and the force produced by the support hand on the UQYBT performance.

3. Results and discussion

For the ML direction, similar performances were observed (DOM: 106.1 ± 5.9 %MLL *vs.* NDOM: 106.8 ± 5.6 %MLL). In the IL direction, performances were lower on the dominant UE (DOM: 82.3 ± 7.0 %MLL *vs.* NDOM: 90.2 ± 7.7 %MLL) which may highlight diminished mobility of the dominant upper quarter side due to its involvement in the activity. In the SL direction, performances were higher on the dominant UE (DOM: 90.2 ± 7.7 %MLL *vs.* NDOM: 82.3 ± 7.0 %MLL).

For all UQYBT directions, the performance was explained by the participant capacity to produce propulsive force (Table 1). These results highlight that UQYBT is a useful test to assess participant ability to produce propulsive force in different directions. Surprisingly, none of the orthogonal force were discriminating for UQYBT performances. Executing the UQYBT require to sustain higher proportion of the body weight in the SL direction (Degot et al., 2020) Our results confirmed that for the SL direction by showing that being able to increase the amount of body weight sustained on the support UE was associated with increased performance. Therefore, the SL performance may be an indicator of the stability level of the support UE. Overall, these results highlighted that moderate-to-high variation of the UQYBT performances were explained by the force applied by the stance UE (Table 1).

Table 1. bi and βi coefficients of optimized mixed models explaining the mediolateral, inferolateral and superolateral performances of the UQYBT by the average forces of the supprt upper extremity in the direction of movement (FDM), vertical (FDV) and orthogonal (FDO) and Dominance. R^2 for conditional coefficient of determination; AIC for Akaike information criterion.

	Mediolateral		Inferolateral		Superolateral	
	b_i	β_i	b_i	β_i	b_i	β_i
Intercept	102.14	107.97	77.96	83.76	18.96	73.47
FDM	1.03	5.14	1.40	9.47	1.23	9.32
FDV					0.95	8.43
FDO						
DOM			-3.80	-3.80		
R^2	0.70		0.57		0.71	
AIC	305.03		331.60		338.97	

4. Conclusions

In conclusion, this work has shown that the UQYBT assesses the ability of the support UE to produce propulsive forces to move the boxes, but also to sustain high proportion of the body weight in the superolateral direction. Further work is needed to better understand the role of the lower limb on the upper quarter motor strategies.

Acknowledgements

The authors thank Elise Martin for her participation in data collection.

Conflict of Interest Statement

The authors report no conflict of interest.

Contributor Roles

TDS performed data collection, data analysis and wrote the manuscript.
YB participated in the study design and data analysis and contributed to manuscript writing.
IR contributed to the data analysis, study design and manuscript writing.

Funding

This study was supported by "Région Auvergne-Rhône-Alpes" (#21 017882 01).

References

Degot, M., Rogowski, I., & Blache, Y. (2020). Ground reaction force during the Upper Quarter Y-Balance Test. *Computer Methods in Biomechanics and Biomedical Engineering*, *23*, S69–S70. https://doi.org/10.1080/10255842.2020.1812162

Gorman, P. P., Butler, R. J., Plisky, P. J., & Kiesel, K. B. (2012). Upper Quarter Y Balance Test : Reliability and performance comparison between genders in active adults. *Journal of Strength and Conditioning Research*, *26*(11), 3043–3048. https://doi.org/10.1519/JSC.0b013e3182472fdb

Schwank, et al. (2022). 2022 Bern consensus statement on shoulder Injury prevention, rehabilitation, and return to sport for athletes at all participation levels. *The Journal of Orthopaedic and Sports Physical Therapy*, *52*(1), 11–28. https://doi.org/10.2519/jospt.2022.10952

Steele, C., & Valentin, S. (2024). Intrinsic and extrinsic variables impacting upper quarter Y-balance test scores in sporting cohorts : A systematic review. *Journal of Bodywork and Movement Therapies*, *39*, 183–194. https://doi.org/10.1016/j.jbmt.2024.02.043